Doctoral Dissertation

Modification of hexameric tyrosine-coordinated hemoprotein: Construction of an artificial light harvesting system by substitution of the heme cofactor and conversion to peroxidase by mutation of the cofactor-ligated amino acid

Tsuyoshi Mashima

January 2018

Department of Applied Chemistry,
Graduate School of Engineering
Osaka University

Contents

General Introduction

Hemoprotein

Proteins play various important roles in biological events. Especially, hemoproteins having iron-porphyrin (heme) as a cofactor have attracted special interests because they have various functions such as transporting/storing oxygen molecule and mediating electron transfer, and catalytic properties as an enzyme in nature (Figure 1).[1] For examples, myoglobin (Mb) is an oxygen-binding protein located in muscle tissue that accepts and stores dioxygen,[2] catalase is an enzyme to catalyze the disproportionation of hydrogen peroxide to water and dioxygen for protecting the cell from oxidative damage by reactive oxygen species,[3] cytochrome *c* is a hemoprotein to carry an electron and control apoptosis,[4] nitric oxide synthase (NOS) is a family of enzymes that produce nitric oxide (NO) from L-arginine,[5] and cytochrome P450 is one of the most powerful enzymes that oxidize various substrates.[6]

An amino acid residue, which acts as an axial heme-ligand dramatically, affects physicochemical performance and reactivity of heme. Three amino acids, histidine, cysteine, and tyrosine are typical axial ligands to the iron atom of the heme cofactor:[7] Histidine is a common axial ligand often used for Mb, HRP and so on, the sulfur atom of the cysteine coordinates to the iron atom of cytochrome P450 and NOS, and tyrosine is found for the axial position of the heme cofactor of catalase. These examples demonstrate that the amino acid residues are capable of switching the function of hemoproteins, although those hemoproteins have same iron porphyrin. Furthermore, it is known that the surrounding amino acid residues which form the heme pocket also have an influence on the physicochemical properties and reactivities of the hemoproteins. The heme pocket provides not only the substrate binding site but also the second coordination share which assists the enzymatic reactions.

Another notable feature of hemoproteins is self-assembly to provide their quaternary structure or protein–protein binding. In the former, some representative examples are catalase and NOS, which form tetramer and dimer structures, respectively. Another well-known quaternary structure is shown in hemoglobin where the formation of the tetramer of the hemoproteins is essential to show

its efficient allosteric function to bind and release dioxygen.[9] By contrast, the latter example is cytochrome *c* that not only transports the electron in mitochondria through intrinsic assembling structure with cytochrome *c* oxidase[8] but also binds to any appropriate domains for forming apoptosome to induce apoptosis. In the following sections, the author briefly reviews the recent advances in the rapidly developing research fields in hemoprotein engineering, and then summarizes the outline of his achievements.

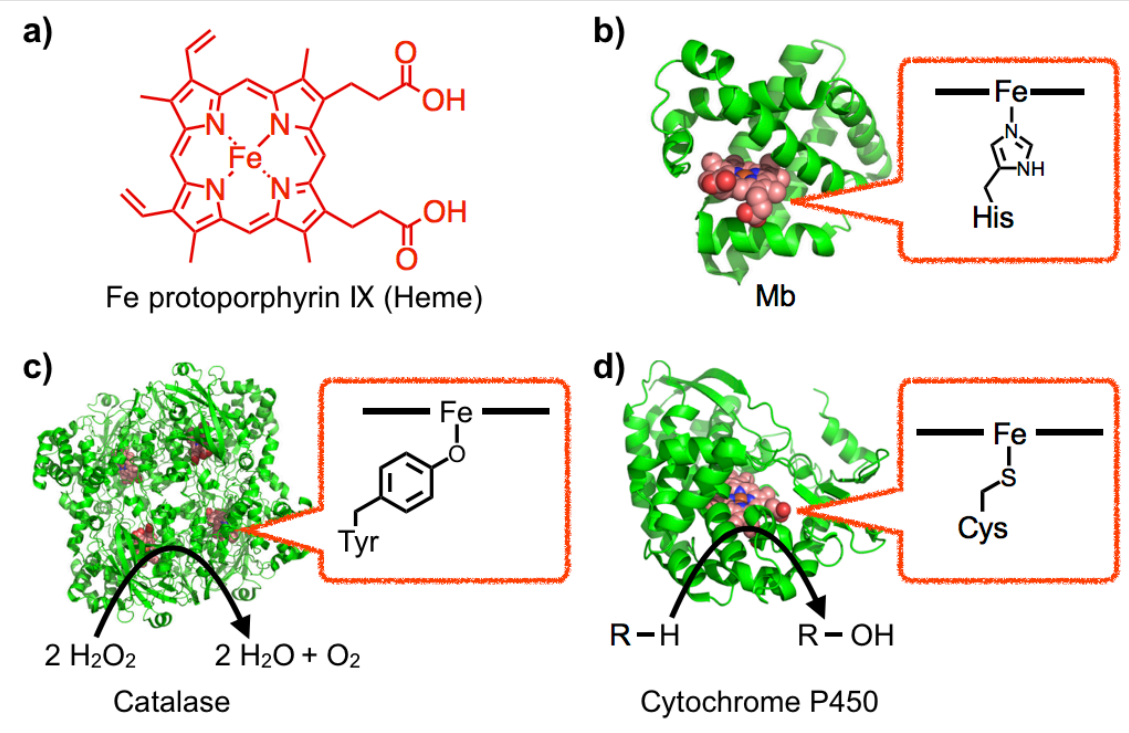

Figure 1. (a) Molecular structure of heme. Crystal structures and schematic representations of heme molecules and the axial ligands of (b) Mb, (c) catalase, and (d) cytochrome P450.

Modification of hemoproteins by reconstitution and mutagenesis

It has been classified into two approaches to modify the hemoproteins for improving performance of the original function of hemoproteins (Figure 2): one is "*the reconstitution method*", in which artificially-designed and synthesized cofactors are inserted into the heme pocket of the apo-hemoproteins, while the other is "*the mutagenesis method*", where some specific amino acid

residues of the native enzymes are replaced by other suitable amino acid residues via a genetic technology.

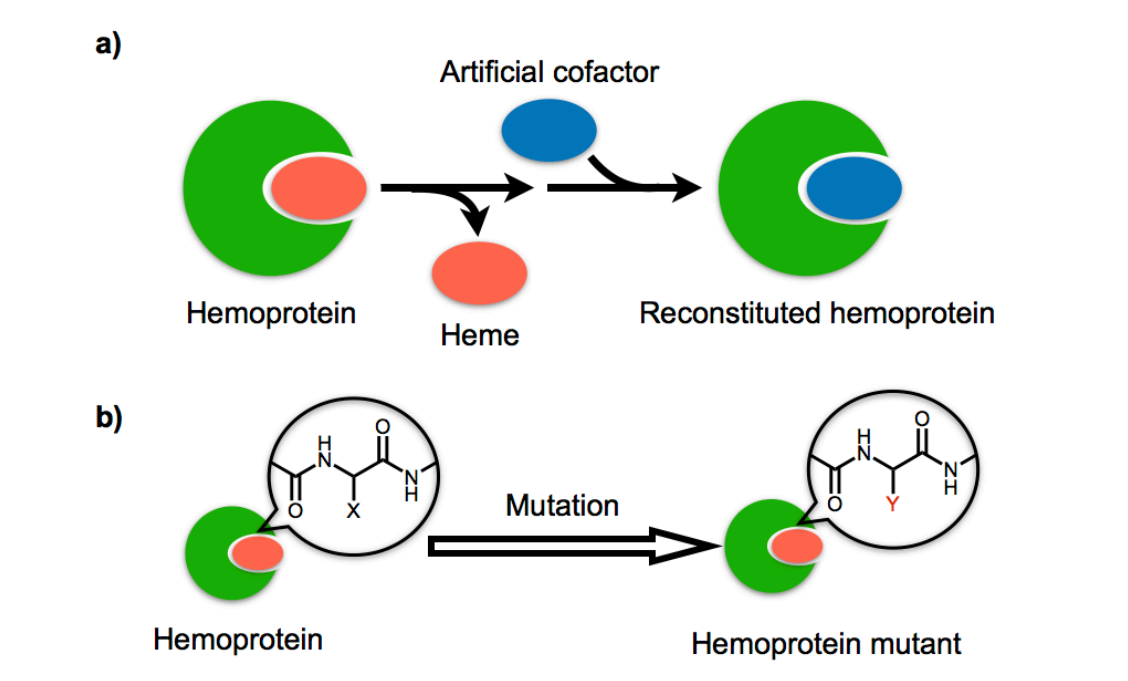

Figure 2. Schematic representation of (a) the reconstitution method and (b) the mutagenesis method to modify the hemoprotein.

Over the last few decades, the reconstitution method has been mostly utilized for modifying hemoproteins. In addition, it is known that the combination of two methods leads to more efficient variants for catalysis. The representative example was a report of Hayashi and Hisaeda *et al.* who demonstrated that Mb reconstituted with iron porphycene, a constitutional isomer of porphyrin, showed 1400-fold enhancement of O_2 binding affinity compared with that of native Mb (Figure 3a).[10] In addition, Mb reconstituted with iron corrole showed 180-fold higher peroxidase reactivity toward the oxidation of 2-methoxyphenol than that of native Mb (Figure 3b).[11] Hayashi *et al.* focused on the reconstitution of the heme of Mb with manganese porphycene that exhibited unexpected catalytic performance for the H_2O_2-dependent hydroxylation of ethylbenzene to 1-phenylethanol with a turnover number of 13 at 25 °C in pH 8.5 (Figure 3c), in stark contrast to the observed no catalytic activity of native Mb and other modified Mb for C−H bond hydroxylation of

alkanes.[12] This pioneering work prompted by Zhang *et al.* to conduct replacement of the iron atom by the manganese atom at the native heme cofactor, protoporphyrin IX; however, such the simple reconstituted manganese myoglobin had no catalytic reactivity for the epoxidation of styrene using H_2O_2 as an oxidant, and they finally found that the L29H/F43H mutant showed the catalytic reactivity for epoxidation of styrene using Oxone® (triple salts of $2KHSO_5/KHSO_4/K_2SO_4$) as an oxidant (Figure 3d).[13]

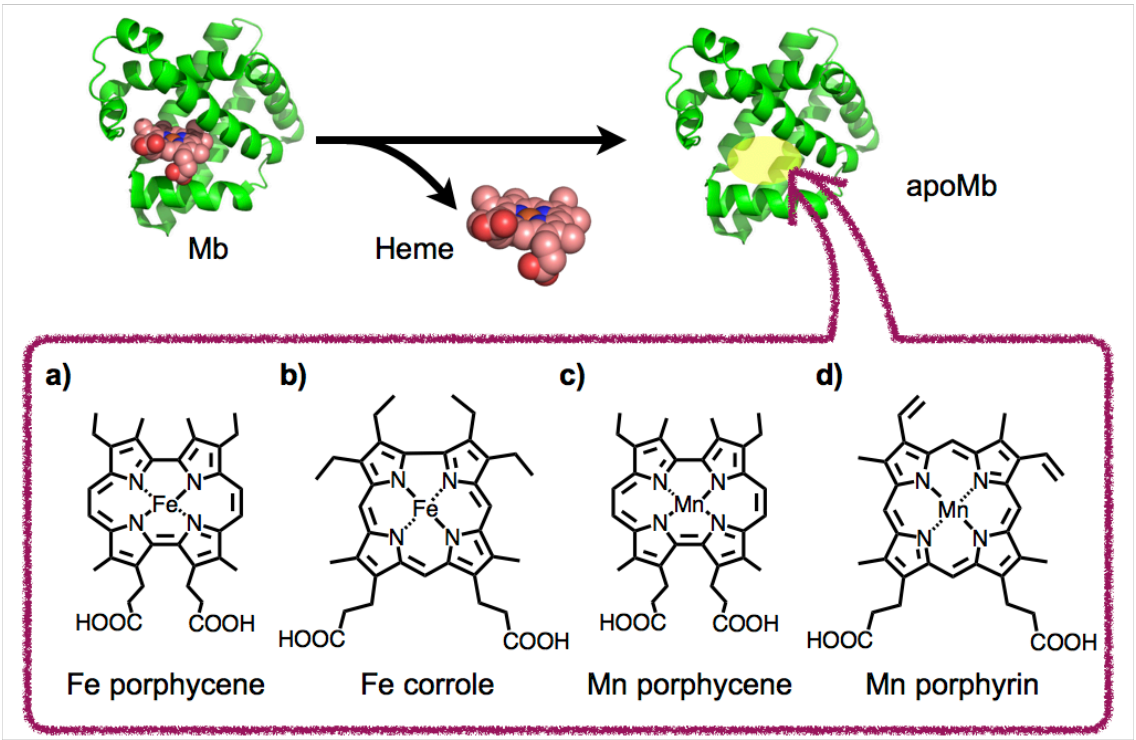

Figure 3. Representative examples for reconstitution of Mb with (a) Fe porphycene, (b) Fe corrole, (c) Mn porphycene and (d) Mn porphyrin.

Several groups have been particularly interested in carbene-mediated cyclopropanation using the artificial metalloenzymes based on the reconstituted hemoprotein. Hartwig *et al.* replaced the iron atom of the cytochrome P450 enzyme CYP119 by the iridium atom to form a reconstituted cytochrome P450 with iridium porphyrin that exhibited a high catalytic activity for the insertion of carbene into C–H bond with up to 98% enantiomeric excess, 35000 turnovers, and 2550 $hours^{-1}$ turnover frequency (Figure 4a).[14] Fasan *et al.* independently conducted the modification of

myoglobin by replacing the original heme with Fe-chlorin e6 which uniquely mediated the carbene-mediated cyclopropanation of aryl-substituted olefins under aerobic conditions to give the corresponding aryl-substituted cyclopropane derivatives in high turnover frequency (up to 6970) and an excellent diastereo- and enantioselectivity (up to 99%) (Figure 4b).[15]

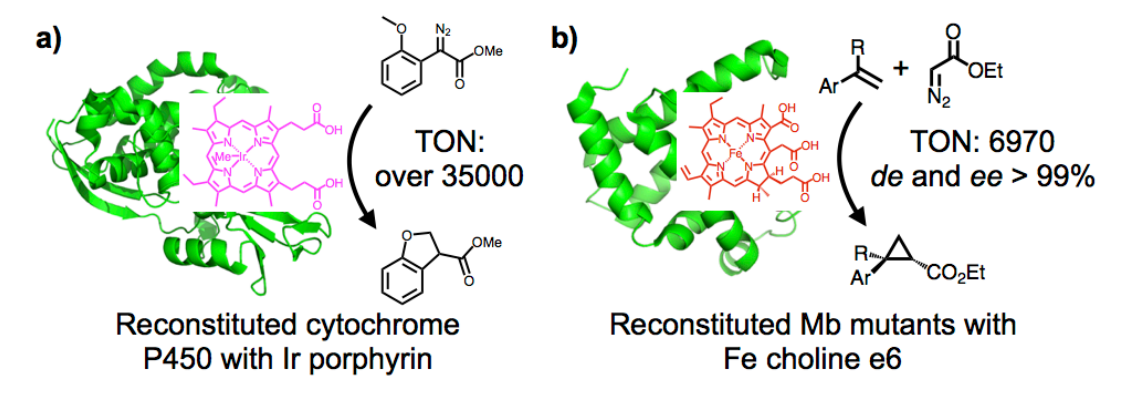

Figure 4. (a) Carbene insertion reaction catalyzed by reconstituted cytochrome P450 with Ir porphyrin. (b) Cyclopropanation reaction catalyzed by reconstituted Mb mutant with Fe choline e6.

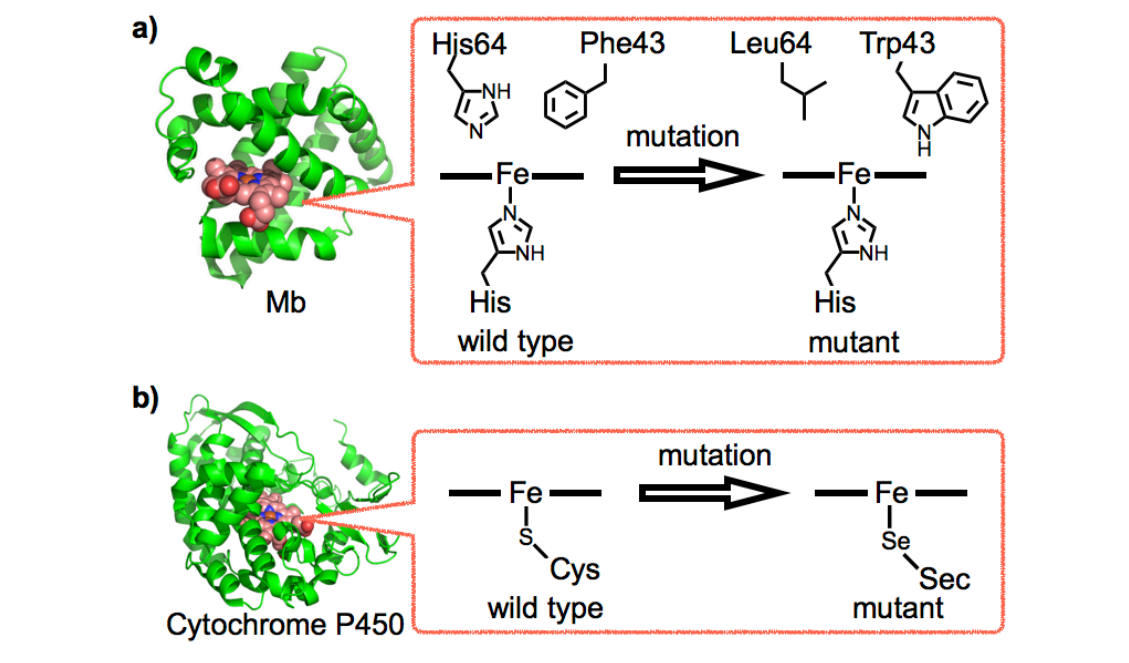

Figure 5. Representative examples for site directed mutations of (a) Mb and (b) cytochrome P450.

The mutagenesis method also provided unique variants of native metalloenzymes. Watanabe *et al.* reported that the F43W/H64L Mb mutant assisted the selective hydroxylation of Trp43 residue

close to the heme (Figure 5a).[16] Green *et al.* applied the mutgenesis method to cytochrome P450 by replacing the axial cysteine residue with a seleno-cysteine residue to prepare the selenolate-ligated cytochrome P450, in which the axial seleno-substitution dramatically enhanced the reactivity toward C-H bond activation reactions (Figure 5b).[17]

Modification of hemoproteins by supramolecular assembling

Supramolecular assembling has been tunably controlled by the same two methods, the reconstitution method and the mutagenesis one. Hayashi *et al*. found a unique assembling of heme-modified Mb, in which the heme cofactor was covalently attached to the Mb surface, and the heme of the modified protein was accordingly inserted to the other heme-binding site to form the

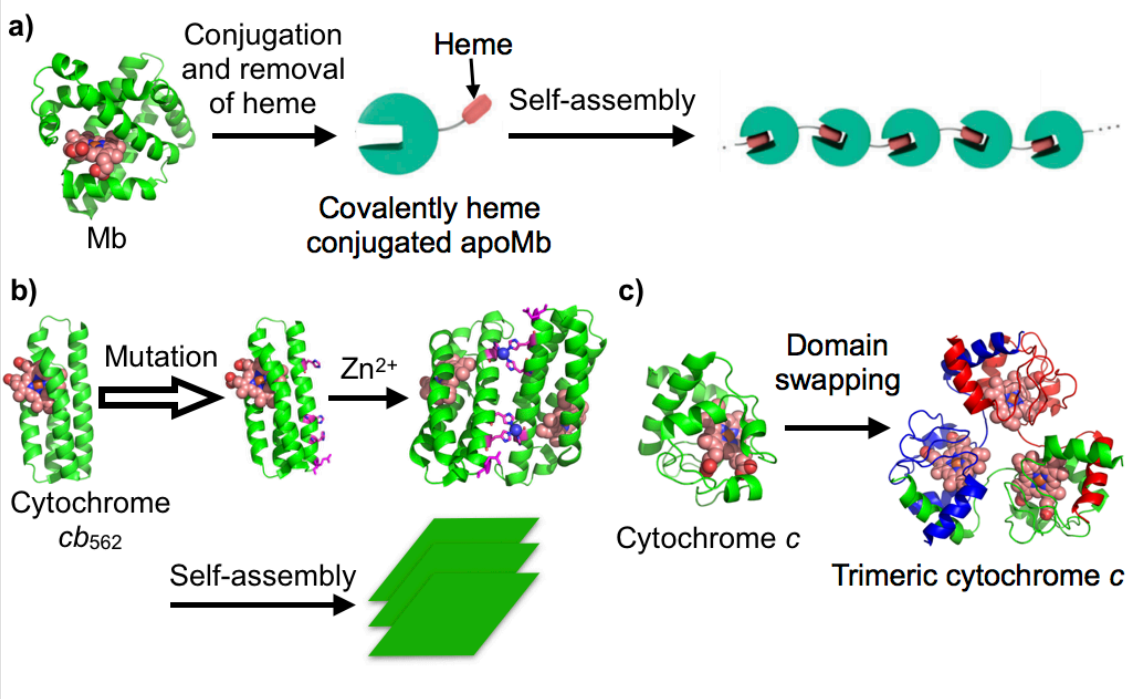

Figure 6. Examples of artificial hemoprotein assemblies. (a) Self-assembly of covalently heme-modified Mb with the interaction between heme-binding site and externally attached heme. (b) Self-assembly of cytochrome cb_{562} mutants by the metal coordinations with introduced histidine residues and Zn ions. (c) Formation of cytochrome *c* trimer by the domain swapping.

supramolecular assembling of the heme-modified Mb (Figure 6a).[18] Tezcan *et al*. prepared surface histidine-modified cytochrome cb_{562} where various histidine residues were introduced on the surface

of cytochrome cb_{562}(Figure 6b). Histidine moieties of each cytochrome cb_{562} coordinated to zinc ions in an intermolecular manner to form one-dimensional nanotubes as well as two- or three-dimensional crystalline arrays.[19] Hirota *et al.* prepared and characterized the trimer of cytochrome *c* with the domain swapping method, in which alcohol-dependent denatured cytochrome *c* proteins were trimerized spontaneously (Figure 7c).[20]

Hexameric tyrosine-coordinated hemoprotein (HTHP)

The author focuses on a circular hexameric heme protein, hexameric tyrosine- coordinated heme protein (HTHP, Figure 7), which is first reported by Dobbek *et al.* in 2007.[21] Marine bacteria, *silicibacter pomeroyi*, contains HTHP, which is a relatively small protein and whose molecular weight is approximately 9 kDa as a monomer and approximately 53 kDa as a hexamer. The six heme molecules are oriented in the protein matrix at intervals of 1.8 nm between the iron atoms of heme and fixed in a same orientation. The hexameric structure of HTHP is constructed by supramolecular interaction such as hydrogen bonding and hydrophobic interaction between neighboring monomers. The narrowest portion of the center pore of HTHP is several Å and covered by glutamines. HTHP is thermally stable even above 90 ˚C and whose surface charges are highly distributed due to the presence of charged amino acid residues on the surface of HTHP. Notably, a positive charge was located around the heme-binding site, while the furthest side from the heme-binding site was surrounded by a negative charge. Additional feature was an axial ligation of tyrosine, which coordinates to the iron center of the heme and whose oxygen atom forms a hydrogen-bonding network with the neighboring arginine (Arg42). Another arginine (Arg25) on the distal side of the heme molecule interacts with the heme via π–cation interaction, making the heme accessible to solvent and substrates. Consequently, HTHP shows both of catalase activity and peroxidase activity; however, these activities are relatively low compared with those of other natural hemoenzymes. Furthermore, details of HTHP's function in nature have not been well elucidated.

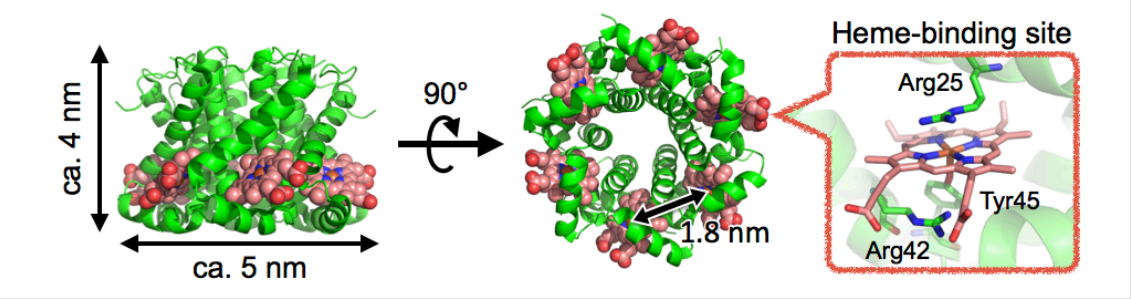

Figure 7. The crystal structure of wild type HTHP (PDB ID: 2OYY).

Outline of this thesis

The author has focused attention on the unique features of HTHP and modified HTHP with two approaches: construction of photosensitizer assembly within the HTHP matrix by supramolecular and covalent linkage (Chapters 1 and 2, Figure 9a) and substitution of axial ligand of the heme in HTHP from tyrosine to histidine for enhancing peroxidase activity (Chapter 3, Figure 9b).

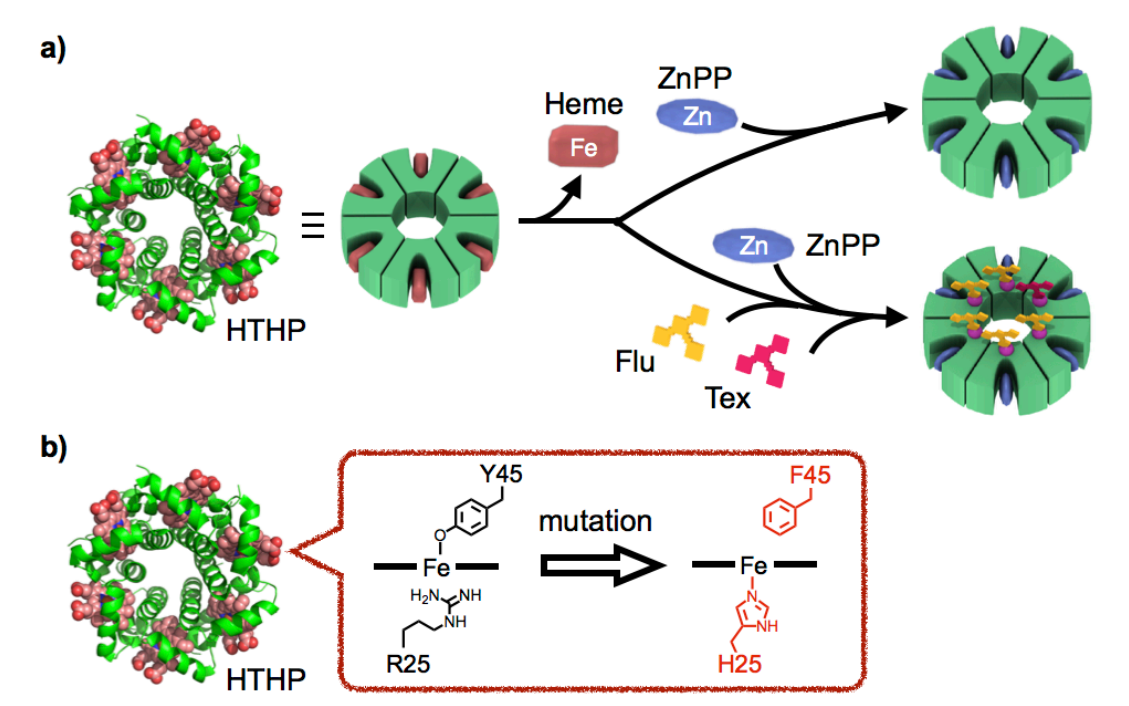

Figure 9. Schematic representation of (a) assemblies of photosensitizers within the HTHP matrix and (b) the substitution of axial ligand of HTHP.

Chapter 1: Assembly of photosensitizer within the HTHP matrix toward artificial light harvesting system

HTHP was employed as a suitable scaffold to construct an array of porphyrinoid photosensitizers by replacing the native heme of HTHP with Zn protoporphyrin IX (ZnPP) and Zn chlorin e6 (ZnCe6), leading to the synthesis of two-types of the hexameric proteins reconstituted with photosensitizers. Flash photolysis along with a fluorescence quencher titration provided an

insight into the successive and rapid energy migration process, which mainly occurred within the Zn-cofactor-substituted HTHP, suggesting that these assembled photosensitizers have a light harvesting ability.

Chapter 2: Assembly of multiple photosensitizers within the HTHP matrix and evaluation of energy transfer mechanism

The HTHP served as a scaffold of a light harvesting model for understanding the successive energy transfer within photosensitizer assemblies in natural systems. Six ZnPP molecules were arrayed at the heme-binding site of HTHP through supramolecular assembling, and five fluorescein (Flu) molecules and one Texas Red (Tex) molecule were further introduced to the HTHP reconstituted with six ZnPP molexules as the donor and acceptor photosensitizers respectively to enhance the light harvesting ability. Fluorescence spectroscopy and fluorescence lifetime measurement revealed that the excited energy originating at five Flu and six ZnPP molecules was collected at one Tex molecule as a funnel-like bottom for light harvesting.

Chapter 3: Substitution of axial ligand from to enhance the peroxidase activity of HTHP

An originally tyrosine-coordinated heme was modified to histidine-coordinated heme in HTHP, where Tyr45, a residue coordinating to the heme cofactor, and Arg25, a residue located at the distal site, were replaced with Phe45 and His25, respectively. Comparison of UV-vis absorption spectra of the ferric-, ferrous-, CO- and CN-forms of $HTHP^{R25H/Y45F}$ with those of several well-known His-ligated hemoproteins suggested that the heme was coordinated by the His25 residue. The Michaelis–Menten kinetics showed that peroxidase activities of $HTHP^{R25H/Y45F}$ for H_2O_2-dependent oxidation of ABTS and guaiacol were 10- and 100-fold higher, respectively, compared with those of wild type HTHP.

Reference

1. (a) G. N. Phillips, Jr., *Handbook of Metalloproteins***,** ed A. Messerschmidt, R. Huber, T. Poulos and K. Wieghardt, John Wiley & Sons, Chichester, U.K., 2001, vol. 1; (b) M. Paoli, J. Marles-Wright and A. Smith, *DNA Cell Biol.*, 2002, **4**, 271–280; (c) S. K. Chapman, S. Daff and A. W. Munro, *Struct. Bond.*, 1997, **88**, 39–70.
2. A. B. Springer, S. G. Sligar, J. S. Olson and G. N. Phillips Jr., *Chem. Rev.*, 1994, **94**, 699–714.
3. (a) M. Zamocky and F. Koller, *Progr. Biophys. Mol. Biol.*, 1999, **72**, 19–66; (b) I. Fita and M. G. Rossmann, *J. Mol. Biol.*, 1985, **185**, 21–37.
4. (a) G. W. Pettigrew and G. R. Moore, Cytochrome c—Biological Aspects, Springer-Verlag, Berlin, 1987; (b) X. Jiang and X. Wang, *Annu. Rev. Biochem.*, 2004. **73**, 87–106.
5. W. K. Aldrrton, C. E. C ooper and R. G. Knowles, *Biochem. J.*, 2001, **357**, 593–615.
6. P. R. Oritz de Montellano, *Chem. Rev.*, 2010, **110**, 932–948.
7. C. J. Reedy and B. R. Gibney, *Chem. Rev.*, 2004, **104**, 617–649.
8. (a) K. Sakamotoa, M. Kamiyab, M Imaid, K. Shinzawa-Itohe, T. Uchida, K. Kawano, S. Yoshikawa and K. Ishimori, *Proc. Natl. Acad. Sci.*, 2011, **108**, 12271–12276; (b) W. Sato, S. Hitaoka, K. Inoue, M. Imai , T. Saio, T. Uchida, K. Shinzawa-Itoh, S. Yoshikawa, K. Yoshizawa and K. Ishimori, *J. Biol. Chem.*, 2016, **291**, 15320–15331.
9. (a) F. M. Perutz, *Nature*, 1970, **228**, 726–734; (b) B. Shaanan, *J. Mol. Biol.*, 1983, **171**, 31–59.
10. T. Hayashi, H. Dejima, T. Matsuo, H. Sato, D. Murata and Y. Hisaeda, *J. Am. Chem. Soc.*, 2002, **124**, 11226–11227.
11. T. Matsuo, A. Hayashi, M. Abe, T. Matsuda, Y. Hisaeda and T. Hayashi, *J. Am. Chem. Soc.*, 2009, **131**, 15124–15125.
12. K. Oohora, Y. Kihira, E. Mizohata, T. Inoue and T. Hayashi, *J. Am. Chem. Soc.*, 2013, **135**, 17282−17285.
13. Y.-B. Cai, S.-Y. Yao, M. Hu, X. Liu and J.-L. Zhang, *Inorg. Chem. Front.*, 2016, **3**, 1236–1244.
14. P. Dydio, H. M. Key, A. Nazarenko, J. Y.-E. Rha, V. Seyedkazemi, D. S. Clark and J. F. Hartwig, *Science*, 2016, **354**, 102–106.
15. G. Sreenilayam, E. J. Moore, V. Steck and R. Fasan, *ACS Catal.*, 2017, **7**, 7629–7633.
16. (a) I. Hara, T. Ueno, S. Ozaki, S. Itoh, K. Lee, N. Ueyama, Y. Watanabe, *J. Biol. Chem.,* 2001, **276**, 36067−36070; (b) T. D. Pfister, T. Ohki, T. Ueno, I. Hara, S. Adachi, Y. Makino, N. Ueyama, Y. Lu, Y. Watanabe, *J. Biol. Chem.*, 2005, **280**, 12858−12866.
17. E. L. Onderko, A. Silakov, T. H. Yosca and M. T. Green, *Nat. Chem.*, 2017, **9**, 623–628.

18. K. Oohora, A. Onoda, H. Kitagishi, H. Yamaguchi, A. Harada and T. Hayashi, *Chem. Sci.,* 2011*,* **2***,* 1033–1038.
19. J. D. Brodin, X. I. Ambroggio, C. Tang, K. N. Parent, T. S. Baker and F. A. Tezcan, *Nat. Chem.*, 2012, **4**, 375–382.
20. S. Hirota, Y. Hattori, S. Nagao, M. Taketa, H. Komori, H. Kamikubo, Z. Wang, I. Takahashi, S. Negi, Y. Sugiura, M. Kataoka and Y. Higuchi, *Proc. Natl. Acad. Sci.*, 2010, **107**, 12854–12859.
21. J. Jeoung, D. A. Pippig, B. M. Martins, N. Wagener and H. Dobbek, *J. Mol. Biol.,* 2007, **368**, 1122–1131.

Chapter 1
Assembly of photosensitizer within the HTHP matrix toward artificial light harvesting system

1-1. Introduction

An array of natural pigments achieves efficient capture of sunlight in natural photosynthetic systems.[1] For example, LH2, a simple light harvesting complex from purple bacterium containing a precise array of eighteen Mg-bacteriochlorin molecules, demonstrates energy migration via successive and rapid energy transfer within protein matrices (Figure 1-1).[2] To mimic such a structure and function, a number of efforts to reproduce an array of photosensitizers (especially porphyrin derivatives) have been undertaken using synthetic,[3] supramolecular,[4] and coordination-bonding[5] approaches. Several proteins have also been found to provide appropriate scaffolds for accumulating photosensitizers by supramolecular interactions[6] or covalent modifications.[7] In this chapter, the author focuses on the use of the native oligomer of hexameric tyrosine-coordinated heme protein (HTHP)[8] as a scaffold for construction of a new array of photosensitizers. Reconstitution of the hemoprotein with zinc porphyrinoid complexes[9] provides an array of photosensitizers with well-defined orientations in the HTHP matrices (Figure 1-2). The modified HTHP is found to provide a model of the light harvesting complex which demonstrates energy migration within an array of chromophores. The present system will serve as the versatile strategy to create a light harvesting complex based on a series of porphyrinoid photosensitizers.

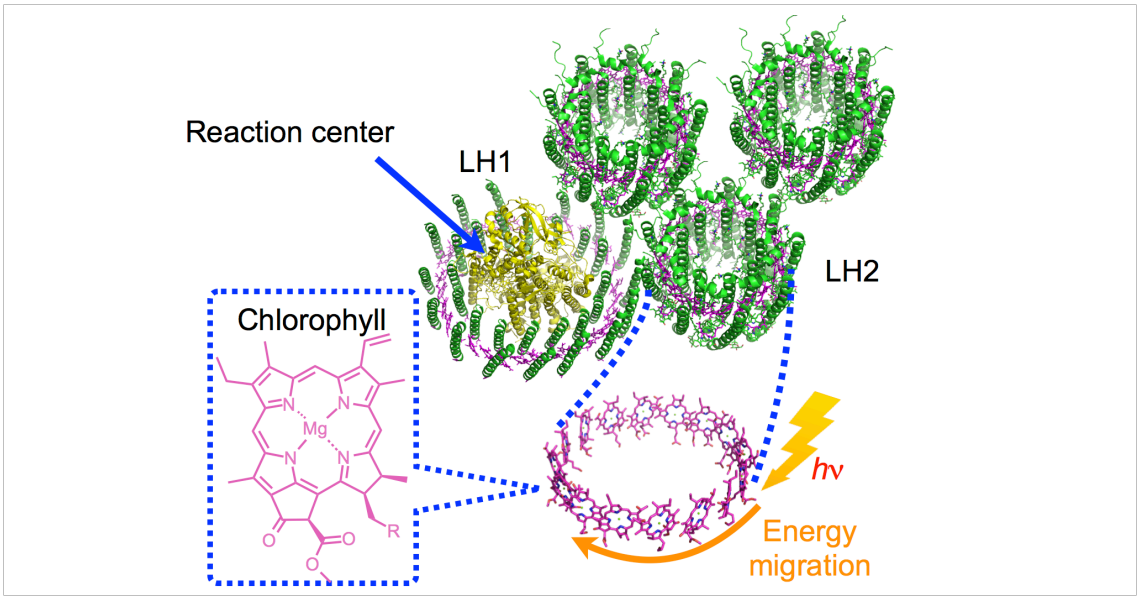

Figure 1-1. Light harvesting complex of *Rhodopseudomonas virdisxs* (LH1 and LH2).

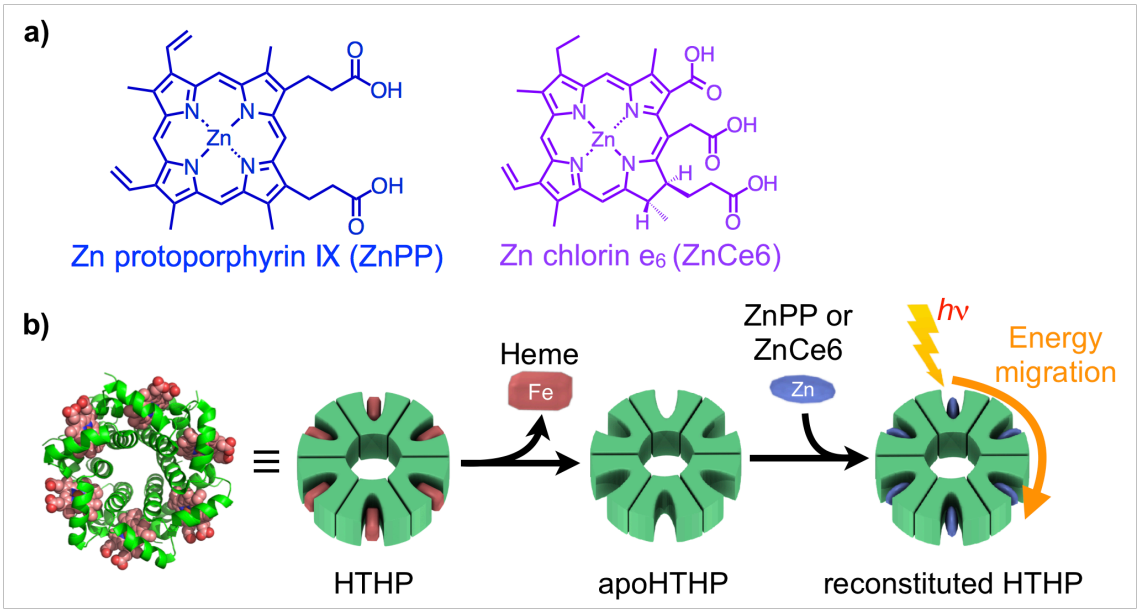

Figure 1-2. (a) Molecular structures of Zn porphyrinoids, ZnPP and ZnCe6. (b) Schematic representation of the preparation of reconstituted HTHP.

1-2. Results and discussion

Preparation and characterization of reconstituted HTHP with ZnPP

HTHP is expressed in a recombinant *E. coli* system and purified by anion exchange and size exclusion chromatography (SEC). The obtained HTHP was characterized by the UV-vis spectroscopy (Figure 1-3) and ESI-TOF MS, which showed the desired mass numbers of the multiply ionized holo-hexameric species (Figure 1-4): found m/z = 3318.2 and 3539.4; calcd m/z = 3318.5 (z = 16+) and 3539.7 (z = 15+). Analytical SEC (Figure 1-5) and DLS (dynamic light scattering, Table 1-1) reveal a monodisperse species with a hydrodynamic diameter of 5.4 nm, which is consistent with the value expected from the hexameric structure observed in X-ray crystallography,[8] and the apo-form of HTHP (apoHTHP) was prepared by a conventional method using acid and 2-butanone,[10] and the resulting protein has no absorption in the visible region (Figure 1-3). The hexameric structure in the apo-form was confirmed by analytical SEC and DLS measurements. In addition, the CD spectrum of apoHTHP in the far-UV region is consistent with that of HTHP, showing that the α-helices are maintained in the absence of the heme cofactors (Figure 1-6). Addition of excess amounts of Zn protoporphyrin IX (ZnPP) into an apoHTHP solution under pH-neutral conditions yields reconstituted HTHP ($rHTHP^{ZnPP(6/6)}$), where 6/6 represents the complete incorporation of the zinc complex into the six heme pockets in apoHTHP.

The titration curve supports the 1 : 1 binding of a ZnPP molecule into a heme pocket (Figure 1-7). The affinity of ZnPP to apoHTHP are approximately $K_a > 10^6$ M^{-1}, because the characteristic UV-vis absorption spectrum of ZnPP bound in the HTHP matrices completely remains under highly diluted conditions (<1 mM). The UV-vis absorption spectrum of rHTHP$^{ZnPP(6/6)}$ has maxima at 421, 548, and 584 nm (Figure 1-3). This pattern is similar to that of tyrosine-coordinated ZnPP in human serum albumin.[11] Analytical SEC measurements for rHTHP$^{ZnPP(6/6)}$ indicate that the protein has the same elution volume as HTHP (Figure 1-5). DLS measurements indicate a hydrodynamic diameter of 5.6 nm and confirm that the thermodynamically stable hexameric structure is maintained (Table 1-1).

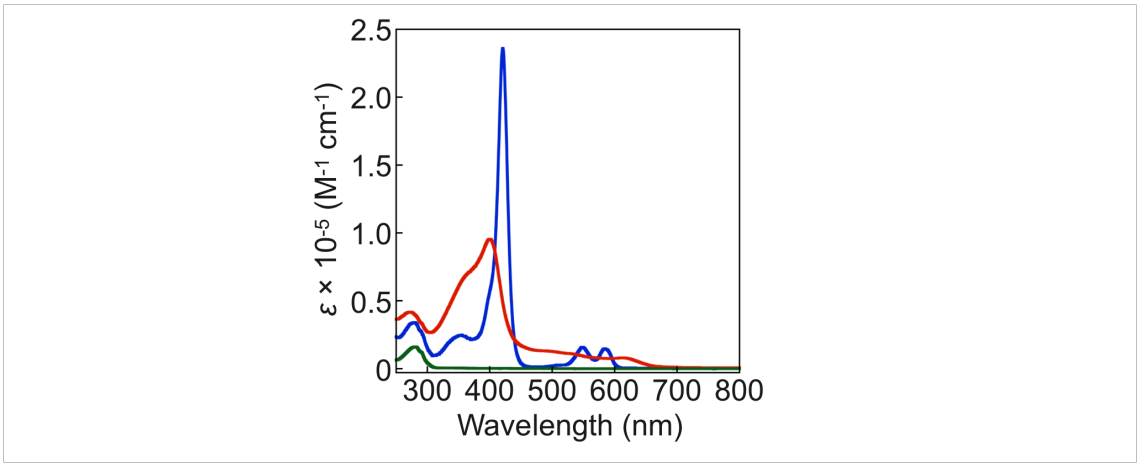

Figure 1-3. UV-vis spectra of HTHP (red), apoHTHP (green) and rHTHP$^{ZnPP(6/6)}$ (blue).

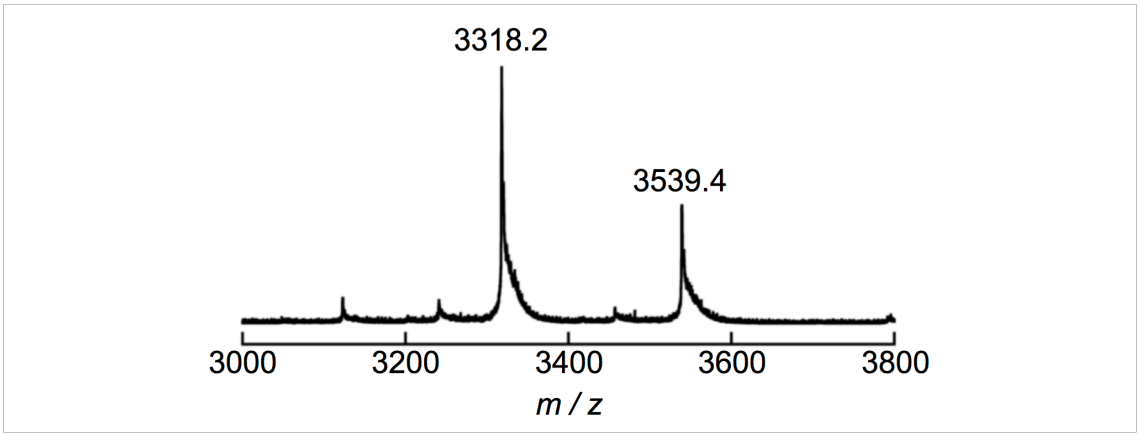

Figure 1-4. ESI-TOF mass spectrum of the holo-hexameric form of HTHP. The sample was dissolved in 10 mM NH4OAc aqueous solution at pH 6.9. Multiply ionized species were observed: found m/z = 3318.2 and 3539.4; calcd m/z = 3318.5 (z = 16+) and 3539.7 (z = 15+).

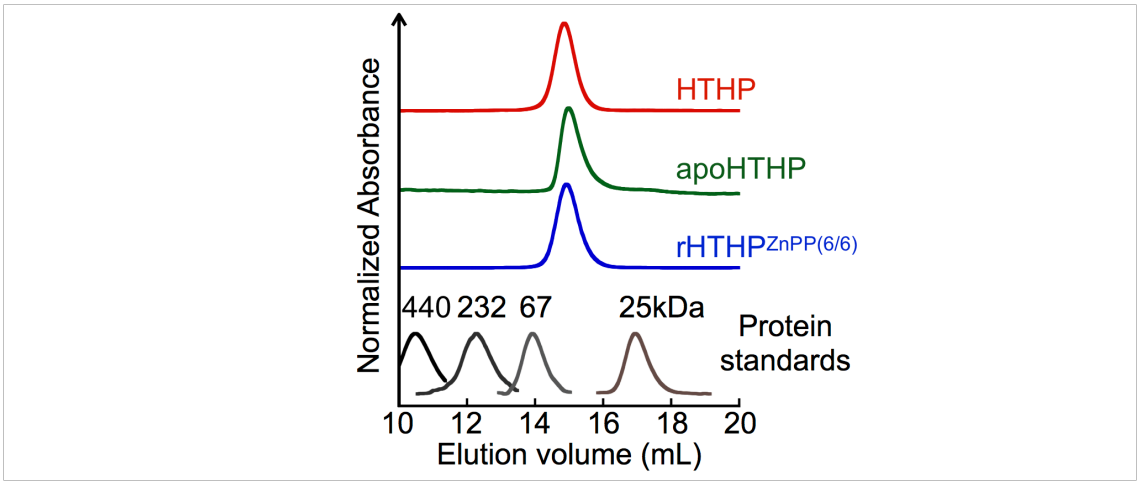

Figure 1-5. Analytical SEC traces of HTHP (red), apoHTHP (green) and rHTHP$^{ZnPP(6/6)}$ (blue). Black traces show protein standards. Red, green, blue, and black traces were detected by absorptions at 402, 280, 421, 418 and 280 nm, respectively.

Table 1-1. Hydrodynamic diameters estimated from dynamic light scattering measurements [a]

	HTHP	apoHTHP	rHTHP$^{ZnPP(6/6)}$
Hydrodynamic diameter (nm)	5.4	6.2	5.6

[a] Protein samples were dissolved in 100 mM potassium phosphate buffer, pH 7.0, at 25 ˚C.

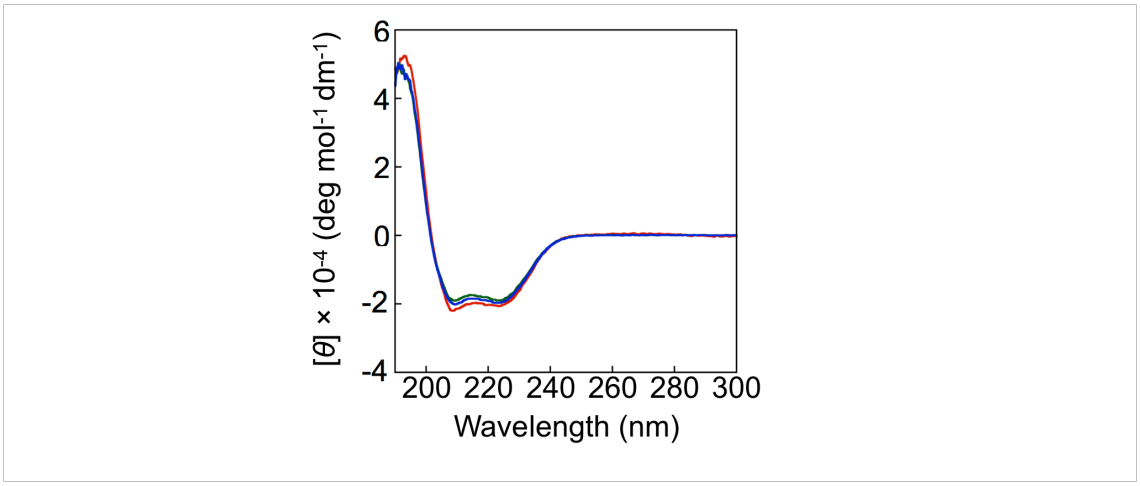

Figure 1-6. CD spectra in far-UV region of HTHP (red), apo-HTHP (green) and rHTHP$^{ZnPP(6/6)}$ (blue) in 100 mM potassium phosphate buffer, pH 7.0, at 25 ˚C.

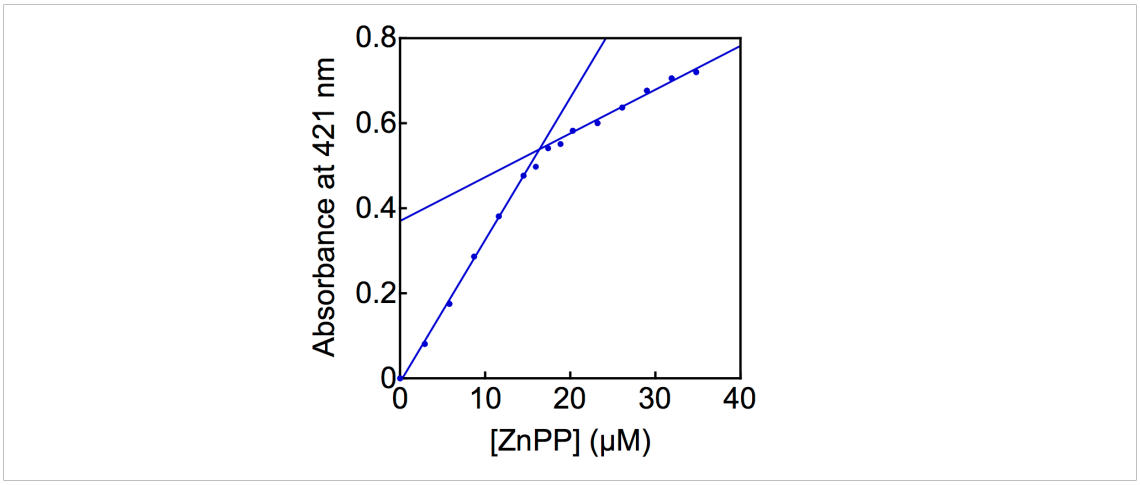

Figure 1-7. ZnPP titration experiments of apoHTHP (17 μM as monomer concentrations, respectively) in 100 mM potassium phosphate buffer, pH 7.0, at 25 ˚C.

Evaluation of photosensitizer assembly within the HTHP matrix

To evaluate the effect of photosensitizer assembly, incompletely-reconstituted HTHP were prepared. Addition of apoHTHP into a rHTHP$^{ZnPP(6/6)}$ aqueous solution increases the intensity of fluorescence derived from ZnPP moieties (Figure 1-9), indicating re-equilibration toward reconstituted HTHP with less than six ZnPP molecules, rHTHP$^{ZnPP(n/6)}$, where *n* represents the apparent number of the photosensitizer molecules in the six heme pockets. Here, the apparent number of n is determined by the amount of apoHTHP added into a solution of rHTHP$^{ZnPP(6/6)}$. The fluorescence lifetime (τ) of rHTHP$^{ZnPP(6/6)}$ was determined to be 1.43 ns, which is slightly shorter than that of rHTHP$^{ZnPP(1/6)}$ (τ = 1.56 ns). Taken together with lower fluorescence intensity in rHTHP$^{ZnPP(6/6)}$, it appears that singlet–singlet annihilation occurs in the protein hexamer.[3a–c,4c] The visible absorption spectrum of rHTHP$^{ZnPP(n/6)}$ is similar to that of rHTHP$^{ZnPP(6/6)}$, indicating that the coordination environments of the two proteins are similar (Figure 1-10). In the CD spectroscopy, rHTHP$^{ZnPP(1/6)}$ shows only a positive Cotton effect in the region from 360 nm to 480 nm and is generally consistent with that of rHTHP$^{ZnPP(0.7/6)}$, indicating a lack of cooperative binding of the cofactor molecules for adjacent monomers. This re-equilibration is also confirmed by a differential CD spectrum obtained by subtracting the spectrum of rHTHP$^{ZnPP(1/6)}$ from that of rHTHP$^{ZnPP(6/6)}$. The observed split type Cotton effect (Figure 1-11) induced by ZnPP–ZnPP exciton coupling strongly suggests the formation of conformationally-defined Zn porphyrin arrays.[12,13] These findings also indicate that the ZnPP molecules can be incorporated into each subunit of apoHTHP while maintaining the intrinsic hexameric structure, whereas re-equilibration

upon addition of apoHTHP provides a mixture of incompletely-reconstituted photosensitizer-containing proteins.

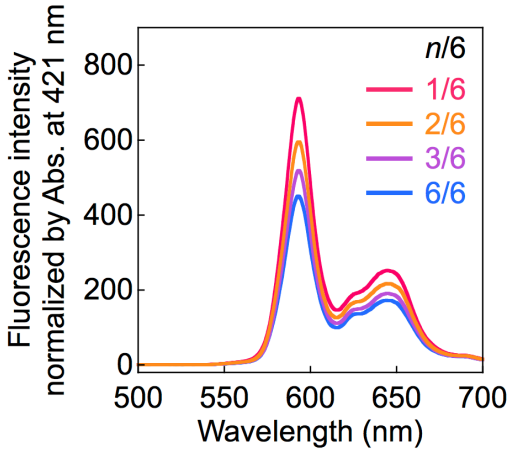

Figure 1-9. Fluorescence spectra of rHTHP$^{ZnPP(n/6)}$ in 100 mM potassium phosphate buffer, pH 7.0, at 25 ˚C. The intensities were normalized by absorbance at 421 nm.

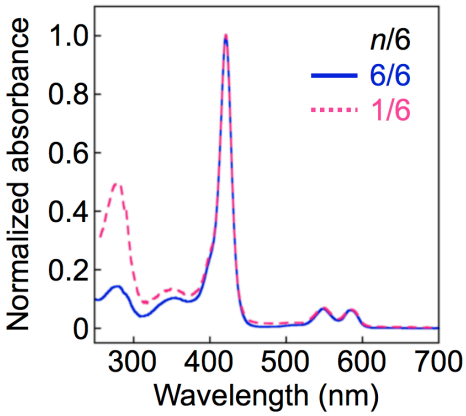

Figure 1-10. UV-vis absorption spectra of rHTHP$^{ZnPP(6/6)}$ (solid blue line) and rHTHP$^{ZnPP(1/6)}$ (pink broken line) in 100 mM potassium phosphate buffer, pH 7.0, at 25 ˚C.

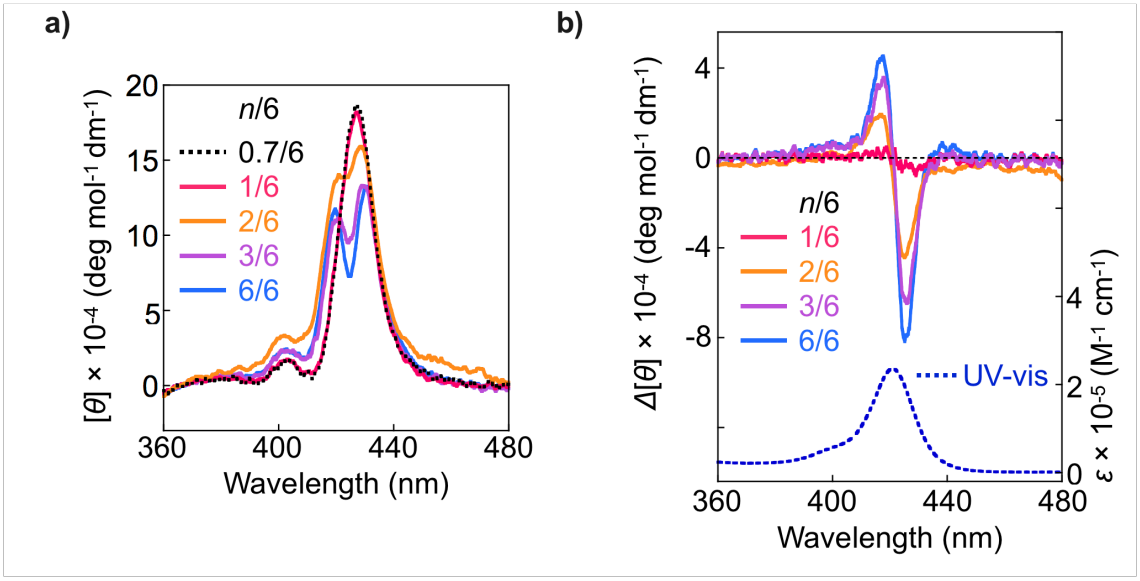

Figure 1-11. CD spectra of (a) rHTHP$^{ZnPP(n/6)}$ and (b) differential CD spectra generated by subtraction of rHTHP$^{ZnPP(0.7/6)}$ from rHTHP$^{ZnPP(n/6)}$ and UV-vis spectrum of rHTHP$^{ZnPP(6/6)}$. The samples were dissolved in 100 mM potassium phosphate buffer, pH 7.0, at 25 ˚C.

Singlet-singlet annihilation

The transient absorption spectral changes which occur 3 ns after excitation by a femtosecond pulse laser at 420 nm were recorded (Figure 1-12) and the time courses of absorption at 500 nm are shown in Figure 1-12. Table 1-2 summarizes the lifetimes of the absorption decay at 500 nm, which are derived from triple- or double-exponential fitting. Interestingly, rapid singlet–singlet annihilation was observed for rHTHP$^{ZnPP(6/6)}$ with a lifetime of 4 ps, whereas such rapid absorption decay was not observed in rHTHP$^{ZnPP(1/6)}$. The level of the rapid decay species clearly depends on the excitation laser power per pulse (Table 1-3). This indicates that the annihilation event occurs through energy migration. The lifetime of the rapid annihilation event is comparable with those reported for other synthetic or supramolecular photosensitizer arrays (0.5 – 20 ps).[3a-c,4c] The lifetime τ_2 is also accelerated in the case of rHTHP$^{ZnPP(6/6)}$, possibly as a result of the annihilation. It is a challenging effort to assign the decays with lifetimes around 100 ps. However, the decays may be caused by water-induced vibrational relaxation[14] or electron transfer between the photosensitizer molecule and the ligated Tyr residue in the heme binding site[15] because free Zn-porphyrin in organic solvent generally decays on the order of nanoseconds, which is dominantly caused by intersystem crossing to the triplet excited state.

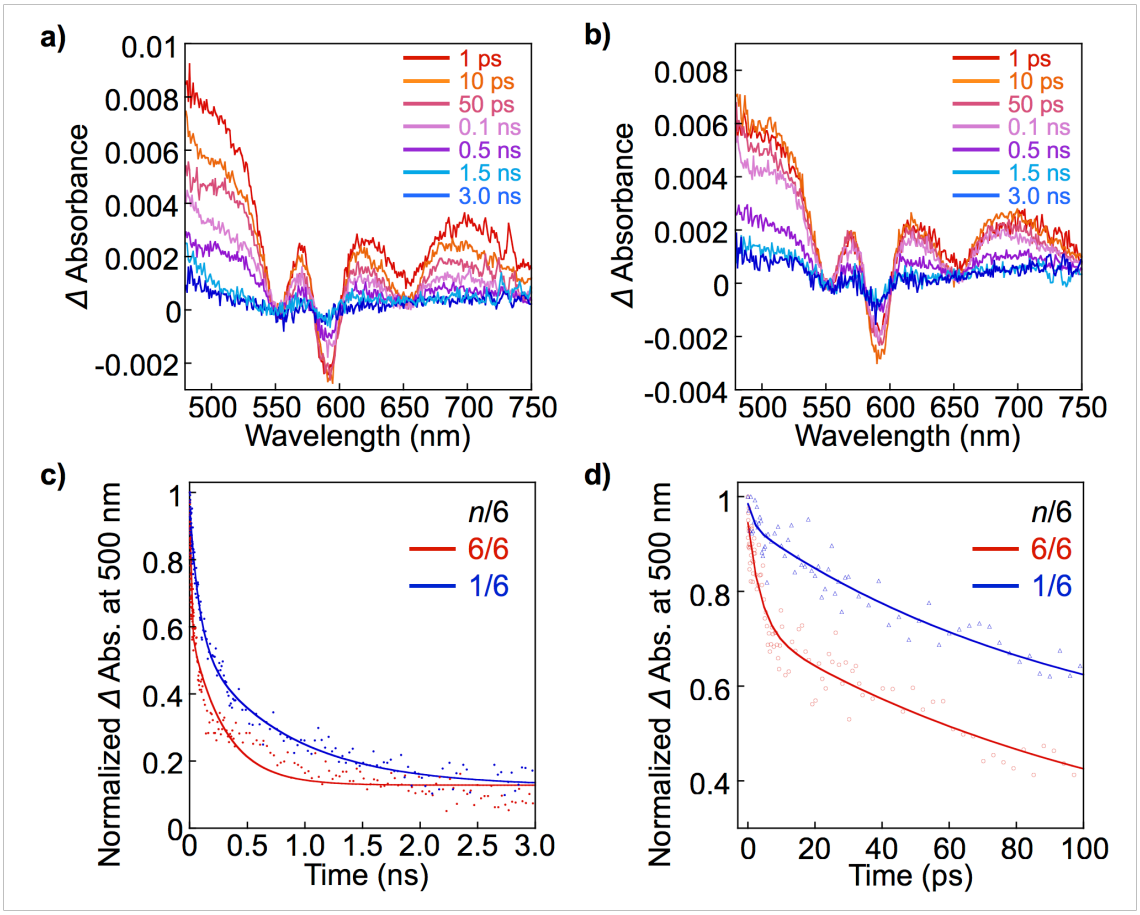

Figure 1-12. Transient absorption spectra of (a) rHTHP$^{ZnPP(6/6)}$, (b) rHTHP$^{ZnPP(1/6)}$ and time courses of the absorption at 500 nm after excitation for (c) rHTHP$^{ZnPP(6/6)}$, (d) rHTHP$^{ZnPP(1/6)}$. Solid lines are triple- or double-exponentially fitted curves: $\Delta Abs(\tau) = y_0 + A_1\exp(-t/\tau_1) + A_2\exp(-t/\tau_2) + A_3\exp(-t/\tau_3)$ for rHTHP$^{ZnPP(6/6)}$ and $\Delta Abs(\tau) = y_0 + A_2\exp(-t/\tau_2) + A_3\exp(-t/\tau_3)$ for rHTHP$^{ZnPP(1/6)}$, where A and t are population and lifetime of the decay, respectively. For τ_3, each fluorescence lifetime was applied. Conditions: [ZnPP] = 10 μM in 100 mM potassium phosphate buffer, pH 7.0, at 22 ˚C under N_2 atmosphere, fwhm = 130 fs, laser power = 24 μJ pulse^{-1}.

Table 1-2. Transient absorption decay parameters for evaluation of annihilation. [ab]

Protein	τ_1 (ps)	τ_2 (ps)	τ_3 (ns) [c]
rHTHP$^{ZnPP(6/6)}$ [d]	4 [23%]	79 [46 %]	1.4 [31%]
rHTHP$^{ZnPP(1/6)}$ [d]	n. d.	117 [58 %]	1.6 [42 %]

[a] Parameters are derived from the fitting curves in Figure 1-13. Populations are shown as the percentage in square brackets. [b] Excitation laser power = 24 μJ pulse^{-1}. [c] Fluorescence lifetime. [d] The residual population is assigned as the slow decay over the experimental range.

Table 1-3. Population of ultra fast decay in transient absorption decay of $rHTHP^{ZnPP(6/6)}$ excited by various laser power. [a]

	24 μJ	18 μJ	12 μJ
Population (τ_1 < 10 ps)	23 ± 2 %	18 ± 2 %	< 5 %

[a] Conditions: [ZnPP] = 10 μM in 100 mM potassium phosphate buffer, pH 7.0, at 22 ˚C under N_2 atmosphere.

Fluorescence quenching measurements

To reveal the energy transfer efficiency within assembled ZnPP molecules, fluorescence quenching measurement were preformed with methyl viologen dichloride (MV^{2+}) as a quencher. Stern–Volmer plots of steady-state and time-resolved emission against the concentration of MV^{2+} are shown in Figure 1-13 and Figure 1-14, respectively. Quenching of steady state fluorescence by MV^{2+} (Figure 1-13) was observed at relatively high concentrations ([MV^{2+}] >1 mM), whereas no changes in lifetimes upon the addition of MV^{2+} were observed (Figure 1-14).[16] This indicates static quenching of fluorescence of $rHTHP^{ZnPP(n/6)}$ by MV^{2+}. The slopes of the Stern–Volmer plots for steady state fluorescence of $rHTHP^{ZnPP(n/6)}$ were determined to be 21 M^{-1} (n = 6) and 9.2 M^{-1} (n = 1) as apparent binding constants. The actual binding constant of MV^{2+} for $rHTHP^{ZnPP(6/6)}$ evaluated by UV-vis spectral changes to form the charge-transfer complex (Figure 1-15) is consistent with that of $rHTHP^{ZnPP(1/6)}$ (ca. 9 M^{-1}). Taken together, these results indicate that the higher apparent value of the protein hexamer fully occupied by photosensitizers is a result of efficient quenching which occurs due to the energy migration within the ZnPP molecule array.[20]

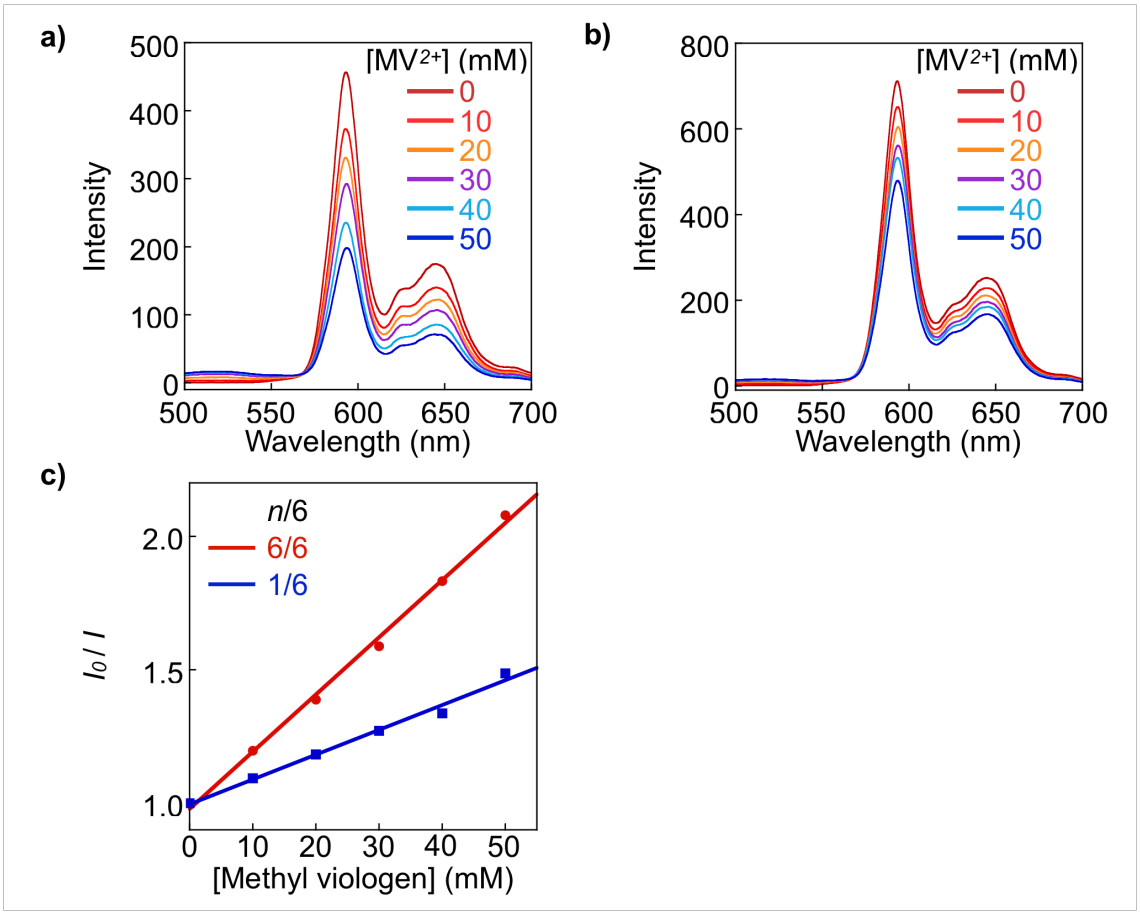

Figure 1-13. Fluorescence spectra of (a) rHTHP$^{ZnPP(6/6)}$ and (b) rHTHP$^{ZnPP(1/6)}$ with various concentrations of methyl viologen. (c) Stern-Volmer plots of steady-state fluorescence against the concentration of methyl viologen as a quencher molecule for rHTHP$^{ZnPP(n/6)}$. Solid lines show corresponding least square fitting. Conditions: [ZnPP] = 4.0 μM in 100 mM potassium phosphate buffer, pH 7.0, at 25 ˚C under N_2 atmosphere, λ_{ex} = 421 nm , λ_{em} = 592 nm.

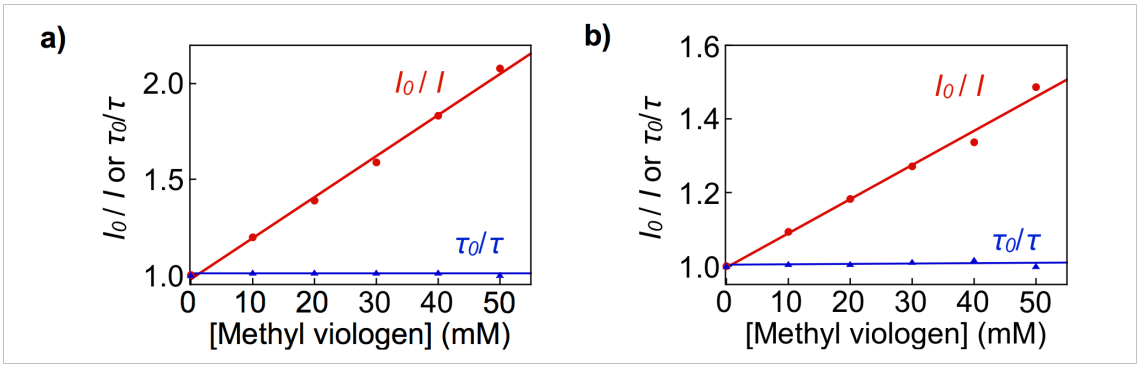

Figure 1-14. Stern-Volmer plots of steady-state (closed circle) and time-resolved (closed triangle) fluorescence emissions of (a) rHTHP$^{ZnPP(6/6)}$ and (b) rHTHP$^{ZnPP(1/6)}$ by titration of methyl viologen. Conditions (steady-state experiments): [ZnPP] = 4.0 μM in 100 mM potassium phosphate buffer, pH 7.0, at 25 ˚C under N_2 atmosphere, λ_{ex} = 421 nm, λ_{em} = 592 nm. Conditions (time-resolved experiments): [ZnPP] = 3.1 μM in 100 mM potassium phosphate buffer, pH 7.0, at 25 ˚C under N_2 atmosphere, λ_{ex} = 390 nm and λ_{em} = 592 nm.

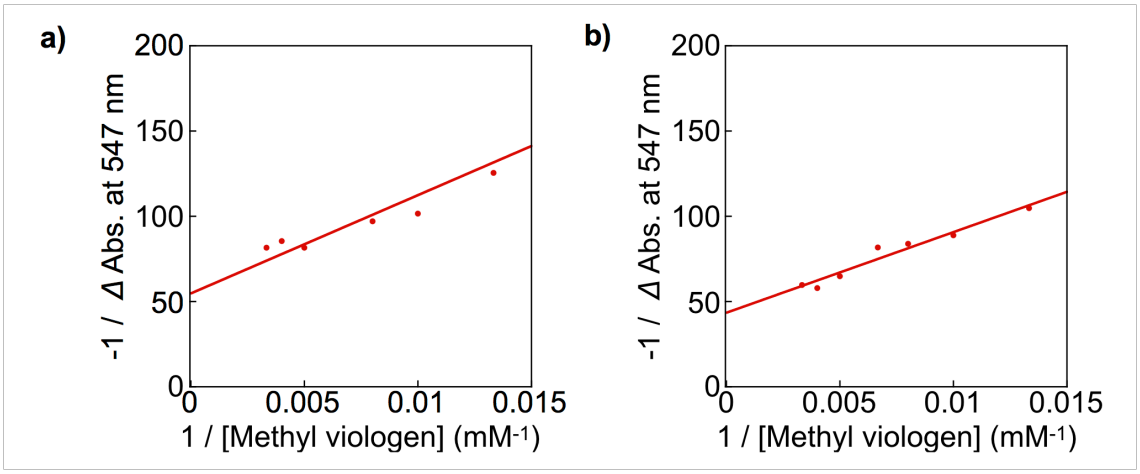

Figure 1-15. The Benesi-Hildebrand plots of (a) rHTHP$^{ZnPP(6/6)}$, (b) rHTHP$^{ZnPP(1/6)}$ at 547 nm absorption against various concentrations of methyl viologen. The plots were analyzed by the following equation: $(\Delta Abs)^{-1} = (K_a(\Delta\varepsilon)[ZnPP]_0[MV^{2+}])^{-1} + ((\Delta\varepsilon)[ZnPP]_0)^{-1}$, where K_a and $\Delta\varepsilon$ is the binding constant and differential extinction coefficient by subtraction of that of the MV^{2+}-free photosensitizer from that of the MV^{2+}- bound photosensitizer, respectively. Conditions: $[ZnPP]_0$ = 4.0 μM in 100 mM potassium phosphate buffer, pH 7.0, at 25 ˚C.

Assembly of ZnCe6 within HTHP matrix

Similar results were obtained using Zn chlorin e (ZnCe6) instead of ZnPP (Figure 1-2). The reconstituted protein, rHTHP$^{ZnCe6(6/6)}$, was also characterized by analytical SEC, DLS, UV-vis and CD spectroscopic measurements (Figure 1-16 and Table 1-4). The fluorescence intensity of rHTHP$^{ZnCe6(n/6)}$ is found to depend on the *n* value, the ratio of the bound photosensitizer for apoHTHP (Figure 1-17). Furthermore, a lifetime of 9 ps for the rapid singlet–singlet annihilation (24 μJ pulse^{-1}: 36 ± 2%) was determined for rHTHP$^{ZnCe6(6/6)}$ (Figure 1-18, Table 1-5). The apparent binding constants of MV^{2+} derived from the Stern–Volmer plots for steady state

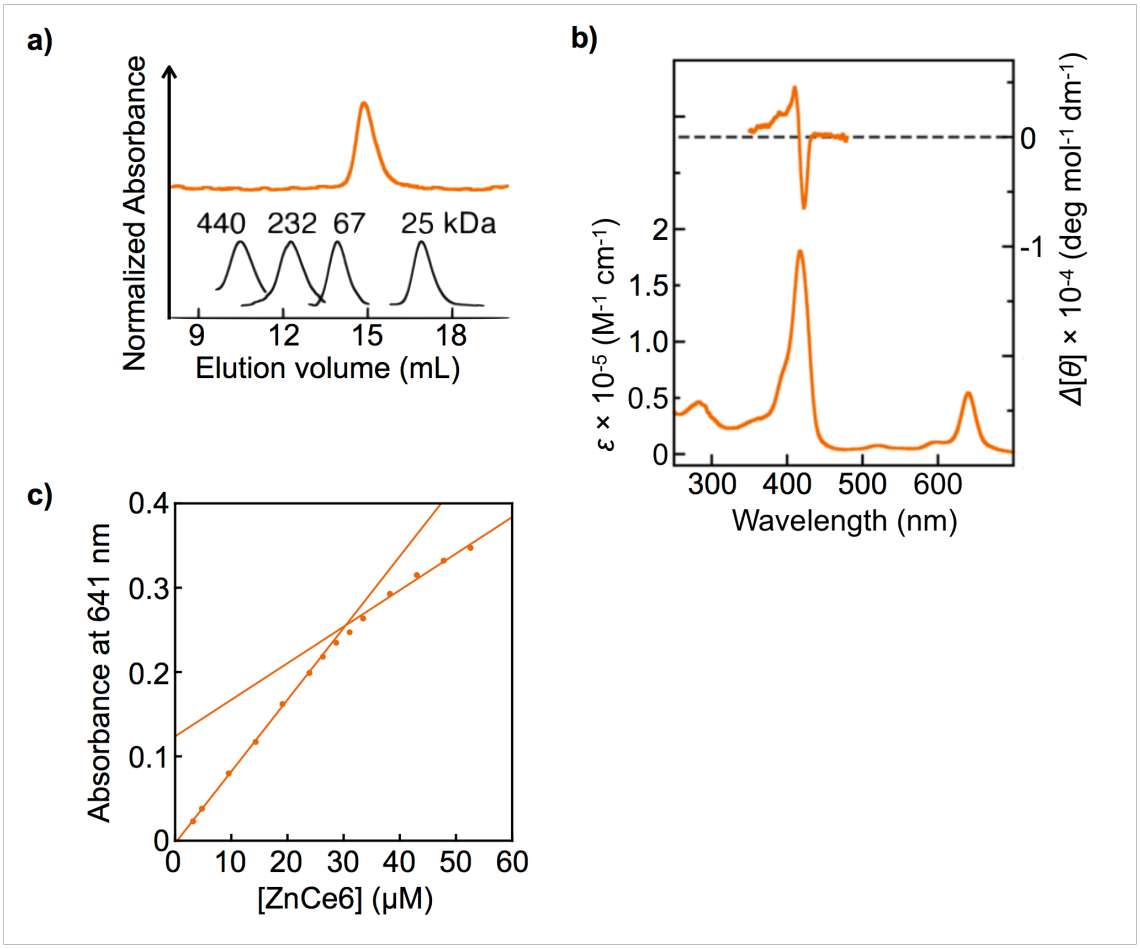

Figure 1-16. (a) Analytical SEC trace and (b) UV-vis absorption and spectra of rHTHP$^{ZnCe6(6/6)}$ (orange). In (a), the black traces show various protein standards and orange and black traces were detected by absorptions at 418 and 280 nm, respectively. In (b), the upper orange line is a differential CD spectrum generated by subtraction of the CD spectrum of rHTHP$^{ZnCe6(1/6)}$ from that of rHTHP$^{ZnCe6(6/6)}$. (c) ZnCe6 titration experiments of apoHTHP (29 μM as monomer concentrations, respectively) in 100 mM potassium phosphate buffer, pH 7.0, at 25 ˚C.

fluorescence of rHTHP$^{ZnCe6(6/6)}$ and rHTHP$^{ZnCe6(1/6)}$ are 1.2×10^3 M^{-1} and 4.7×10^2 M^{-1}, respectively (Figure 1-19, 1-20). In contrast, the actual binding constants of MV^{2+} for rHTHP$^{ZnCe6(n/6)}$ determined by UV-vis spectral changes (Figure 1-21) are 5×10^2 M^{-1} (n = 6) and 4×10^2 M^{-1} (n = 1).[17] Therefore, the 2.6-fold greater apparent binding constant of rHTHP$^{ZnCe6(6/6)}$ relative to rHTHP$^{ZnCe6(1/6)}$ suggests that the energy migration occurs within the ZnCe6 array as well as rHTHP$^{ZnPP(6/6)}$.[20]

Table 1-4. Hydrodynamic diameter of rHTHP $^{ZnCe6(6/6)}$ estimated from dynamic light scattering measurements [a]

	rHTHP$^{ZnCe6(6/6)}$
Hydrodynamic diameter (nm)	5.6

[a] Protein samples were dissolved in 100 mM potassium phosphate buffer, pH 7.0, at 25 ˚C.

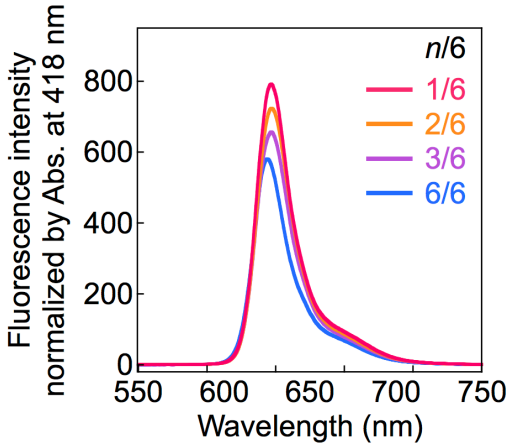

Figure 1-17. Fluorescence spectra of rHTHP$^{ZnCe6(n/6)}$ in 100 mM potassium phosphate buffer, pH 7.0, at 25 ˚C. The intensities were normalized by absorbance at 418 nm.

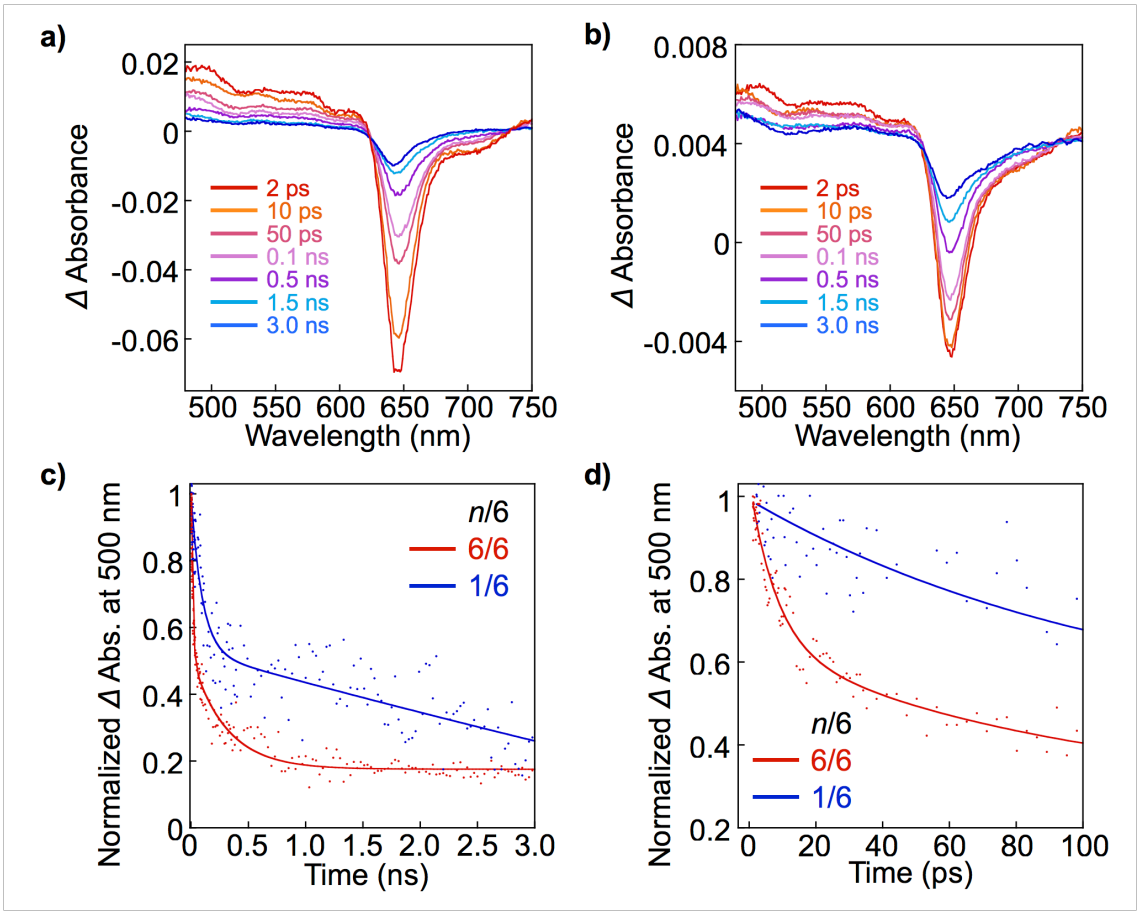

Figure 1-18. Transient absorption spectra of (a) rHTHP$^{ZnCe6(6/6)}$, (b) rHTHP$^{ZnCe6(1/6)}$ and time courses of the absorption at 500 nm after excitation for (c) rHTHP$^{ZnCe6(6/6)}$, (d) rHTHP$^{ZnCe6(1/6)}$. Solid lines are triple- or double-exponentially fitted curves: $\Delta Abs(\tau) = y_0 + A_1\exp(-t/\tau_1) + A_2\exp(-t/\tau_2) + A_3\exp(-t/\tau_3)$ for rHTHP$^{ZnCe6(6/6)}$, and $\Delta Abs(\tau) = y_0 + A_2\exp(-t/\tau_2) + A_3\exp(-t/\tau_3)$ for rHTHP$^{ZnCe6(1/6)}$, where A and t are population and lifetime of the decay, respectively. For τ_3, each fluorescence lifetime was applied. Conditions: [ZnCe6] = 14 μM, 100 mM potassium phosphate buffer, pH 7.0, at 22 ˚C under N_2 atmosphere, fwhm = 130 fs, laser power = 24 μJ pulse^{-1}.

Table 1-5. Transient absorption decay parameters for evaluation of annihilation. [ab]

Protein	τ_1 (ps)	τ_2 (ps)	τ_3 (ns) [c]
rHTHP$^{ZnCe6(6/6)}$ [d]	9 [36 %]	106 [33 %]	1.9 [17 %]
rHTHP$^{ZnCe6(1/6)}$ [d]	n. d.	122 [35 %]	1.9 [27 %]

[a] Parameters are derived from the fitting curves in Figure 1-18. Populations are shown as the percentage in square brackets. [b] Excitation laser power = 24 μJ pulse^{-1}. [c] Fluorescence lifetime.

[d] The residual population is assigned as the slow decay over the experimental range.

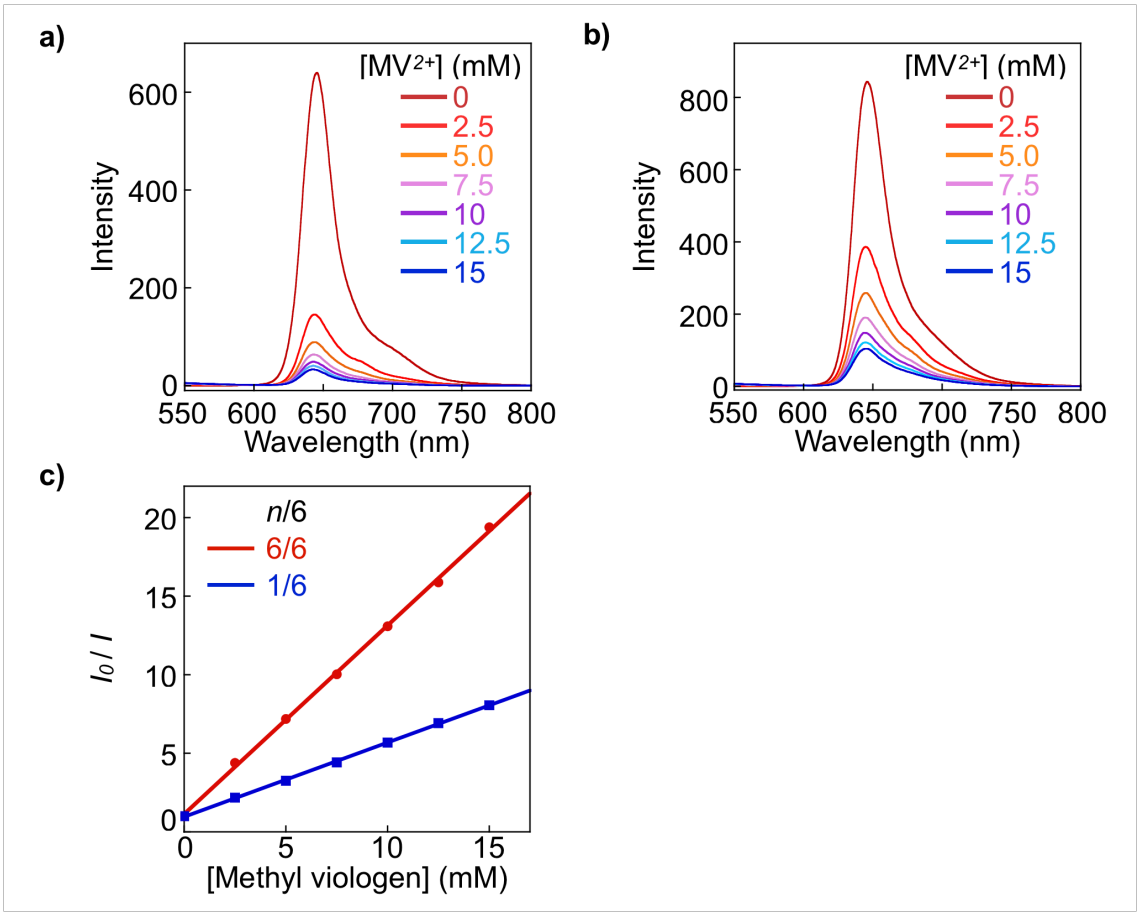

Figure 1-19. Fluorescence spectra of (a) rHTHP$^{ZnCe6(6/6)}$ and (b) rHTHP$^{ZnCe6\ (1/6)}$ with various concentrations of methyl viologen. (c) Stern-Volmer plots of steady-state fluorescence against the concentration of methyl viologen as a quencher molecule for rHTHP$^{ZnCe6(n/6)}$. Solid lines show corresponding least square fitting. Conditions: [ZnCe6] = 2.0 μM in 100 mM potassium phosphate buffer, pH 7.0, at 25 ˚C under N_2 atmosphere, λ_{ex} = 418 nm , λ_{em} = 645 nm.

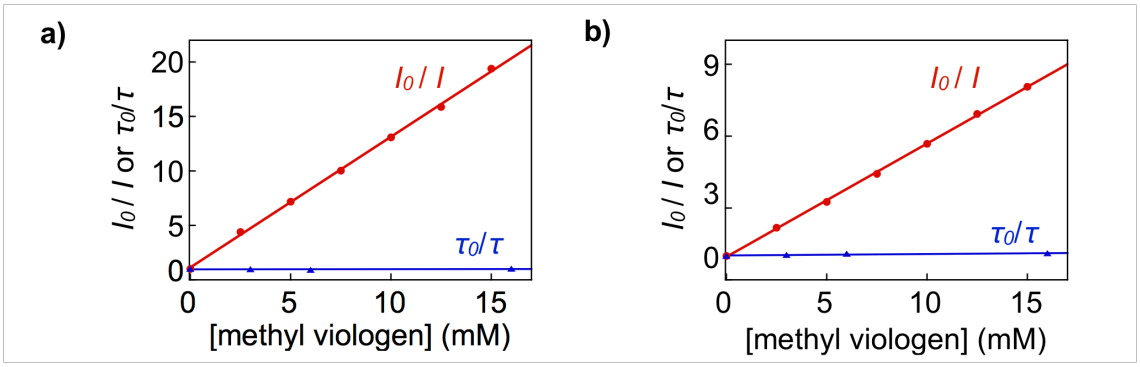

Figure 1-20. Stern-Volmer plots of steady-state (closed circle) and time-resolved (closed triangle) fluorescence emissions of (a) rHTHP$^{ZnCe6(6/6)}$ and (b) rHTHP$^{ZnCe6(1/6)}$ by titration of methyl viologen. Conditions (steady-state experiments): [ZnCe6] = 2.0 μM in 100 mM potassium phosphate buffer, pH 7.0, at 25 ˚C under N_2 atmosphere, λ_{ex} = 418 nm, λ_{em} = 645 nm. Conditions (time-resolved experiments): [ZnCe6] = 1.6 μM in 100 mM potassium phosphate buffer, pH 7.0, at 25 ˚C under N_2 atmosphere, λ_{ex} = 390 nm and λ_{em} = 645 nm.

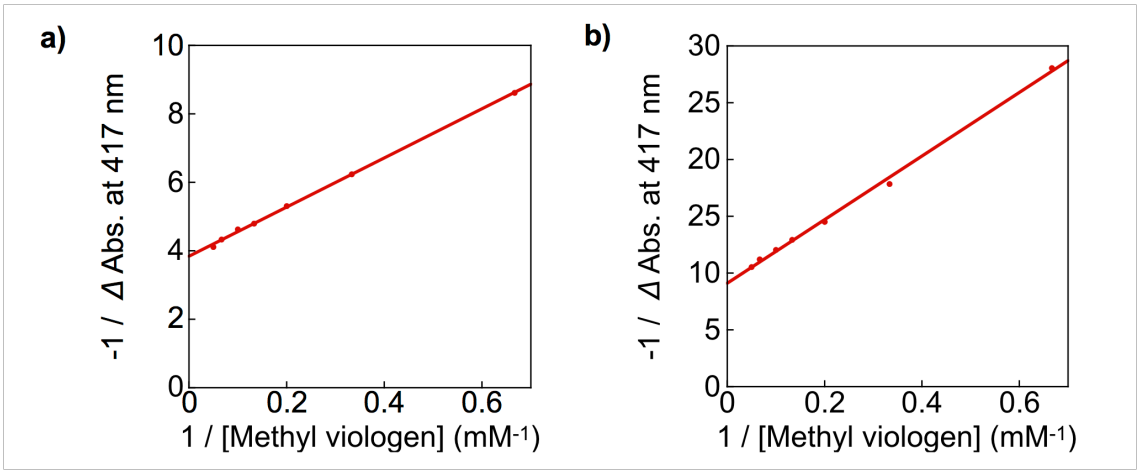

Figure 1-21. The Benesi-Hildebrand plots of (a) rHTHP$^{ZnCe6(6/6)}$, (b) rHTHP$^{ZnCe6(1/6)}$ at 417 nm absorption against various concentrations of methyl viologen. The plots were analyzed by the following equation: $(\Delta Abs)^{-1} = (K_a(\Delta\varepsilon)[ZnPP]_0[MV^{2+}])^{-1} + ((\Delta\varepsilon)[ZnPP]_0)^{-1}$, where K_a and $\Delta\varepsilon$ is the binding constant and differential extinction coefficient by subtraction of that of the MV^{2+}-free photosensitizer from that of the MV^{2+}- bound photosensitizer, respectively. Conditions: $[ZnCe6]_0$ = 2.7 and 2.8 μM for rHTHP$^{ZnCe6(6/6)}$ and rHTHP$^{ZnCe6(1/6)}$, respectively, in 100 mM potassium phosphate buffer, pH 7.0, at 25 ˚C.

1-3 Summary

Photosensitizers, Zn protoporphyrin IX and Zn chlorin e6, are completely inserted into each heme pocket of a hexameric apohemoprotein. The singlet–singlet annihilation within the assembled ZnPP and ZnCe6 molecules was confirmed by transient absorption spectroscopy with femtosecond pulse laser. The fluorescence quenching efficiencies upon addition of methyl viologen are 2.3 and 2.6 fold-higher than those of the partially photosensitizer-inserted proteins, respectively, indicating that the energy migration occurs within the proteins.

1-4. Experimental section

Instruments

UV-vis spectral measurements were carried out with a Shimadzu UV-3150 or UV-2550 double-beam spectrophotometer, or a Shimadzu BioSpec-nano spectrometer. Fluorescence spectra were recorded with a JASCO FP-8600 fluorescence spectrometer. Circular dichroism (CD) spectra were recorded at 25 °C on a JASCO spectropolarimeter (Model J-820). ESI-TOF MS analyses were performed with a Bruker Daltonics micrOTOF-II mass spectrometer. ICP-OES (inductively coupled plasma optical emission spectroscopy) was performed on a Shimadzu ICPS-7510 emission spectrometer. The pH measurements were made with an F-52 Horiba pH meter. Size exclusion column chromatography was performed using an ÄKTApurifier system equipped with Superdex 200 10/300 GL (GE Healthcare) at 4 ˚C. Air-sensitive manipulations were performed in a UNILab glove box (MBraun, Germany). Fluorescence lifetime measurements were recorded by a HORIBA Fluoromax-4 fluorescence spectrophotometer by excitation at 390 nm. Dynamic light scattering was measured by a Malvern Zetasizer μV light scattering analyzer with 830 nm laser at 25 ˚C. The equipment used for flash photolysis experiments is described below.

Materials

Syntheses of Zn protoporphyrin IX, ZnPP,[18] and Zn chlorin e6, ZnCe6,[19] were reported in previous papers. The pUC19 plasmid containing optimized hexameric tyrosine-coordinated heme protein (HTHP) gene was purchased from FASMAC. Distilled water was demineralized using a Millipore Integral 3 apparatus. Other all reagents were of the highest guaranteed grade commercially available and were used as received unless otherwise indicated. A standard zinc solution for ICP-OES was purchased from Wako Pure Chemical Industries.

Amino acid sequence of HTHP (monomer)

SETWLPTLVTATPQEGFDLAVKLSRIAVKKTQPDAQVRDTLRAVYEKDANALIAVSH FAVVATQTIAAANDYWKD (75 residues)

Experimental procedures

Expression and purification of HTHP. The pUC19 plasmid containing the optimized HTHP gene was used as a template for PCR with oligonucleotide primers:

(i) 5'-GGGGACAAGTTTGTACAAAAAAGCAGGCTTCGAAG-3' and

(ii) 5'-GGGGACCACTTTGTACAAGAAAGCTGGGTC-3'.

The PCR product was inserted into a pDONR vector and then a pDEST14 expression vector according to standard protocols for Gateway technology (InvitrogenTM). DNA sequencing was performed to verify the correct insertion of the gene sequence into the expression vector. The resulting expression plasmid was transformed into *E. coli* BL21(DE3). 1 L volumes of a LB medium containing ampicillin (100 mg) were inoculated with 10 mL of the culture (OD = 0.5) of the relevant transformed cells. After the cells were grown aerobically with vigorous shaking at 37 ˚C until the OD600 reached ~0.5, isopropyl-β-D-1-thiogalactopyranoside (IPTG) was added to a final concentration of 1.0 mM to induce the protein expression. The incubation was continued at 37 ˚C for approximately 8 h. The cells were harvested by centrifugation at 4000 x g for 10 min. The harvested cells from 4 L of culture were re-suspended in ca. 50 mL of a 10 mM Tris-HCl buffer (pH 8.0) containing 1mM EDTA and lysed by freeze–thaw cycles with subsequent sonication for 30 sec x 10 times at 4 ˚C. The lysate was then centrifuged and the supernatant was collected. The solution was loaded onto a DEAE Fast Flow (GE healthcare) anion-exchange column which was pre-equilibrated in a 10 mM potassium phosphate buffer (pH 6.0). The fraction of the target protein was collected by a 10 mM potassium phosphate buffer (pH 6.0) containing 0.3 M NaCl, and concentrated using an Amicon stirred ultrafiltration cell with a 30-kDa molecular weight cut-off membrane (Millipore). The concentrated solution was passed through a Sephadex G-150 size exclusion column equilibrated with 100 mM potassium phosphate buffer, pH 7.0. The fractions with Rz > 2.8 (Rz is the ratio of absorbance values at 402 nm and 280 nm) were collected and concentrated. The obtained HTHP was characterized by SDS-PAGE and ESI-TOF MS (Figure 1-4), and stored at –80 ˚C.

Analytical SEC measurements

For SEC analysis, 100 mM potassium phosphate buffer at pH 7.0 was used as an eluent. The

analysis was performed at 4 ˚C at a flow rate of 0.5 mL min^{-1} with monitoring of the absorbance at 280, 402, 418 or 421 nm for detection. The Superdex 200 column was calibrated using the following reagents: Blue Dextran (2000 kDa, used to determine the void volume of the column), ferritin (400 kDa), catalase (232 kDa), albumin (67 kDa), and chymotrypsinogen (25 kDa).

Preparation of apoHTHP

Removal of heme was performed using Teale's method as follows. A solution of HTHP (50 μM as a monomer) in 100 mM of L-histidine solution at 4 ˚C was acidified to pH 1.7 by addition of 1 M HClaq. Unbound heme was extracted with 2-butanone (5 times) and the colorless aqueous solution was neutralized by dialysis with 100 mM potassium phosphate buffer, pH 7.0, (3 times) at 4 ˚C. The resulting solution was readily used for experiments.

Reconstitution of HTHP with ZnPP or ZnCe6

$rHTHP^{ZnPP(6/6)}$: A DMSO solution of ZnPP (2 mM, 180 μL) was added to a solution of apoHTHP (30 μM equivalent as a monomer, 10 mL) in 100 mM potassium phosphate buffer, pH 7.0. After standing overnight under an N_2 atmosphere at 4 ˚C, the solution was loaded onto a DEAE FF column equilibrated with 100 mM potassium phosphate buffer and the reconstituted protein was eluted with the same buffer containing 500 mM NaCl. The buffer was exchanged to 100 mM potassium phosphate buffer, pH 7.0 using a HiTrap Desalting column. The purified protein was characterized by UV-vis, CD, DLS and SEC measurements. The molar extinction coefficient was determined by ICP-MS analysis: $\varepsilon_{421} = 2.4 \times 10^5\ M^{-1}cm^{-1}$.

$rHTHP^{ZnCe6(6/6)}$: An aqueous solution of ZnCe6 (0.23 mM, 0.65 mL) in glycine-NaOH buffer at pH 10 was added to the apoHTHP solution (15 μM equivalent as a monomer, 10 mL) in 100 mM potassium phosphate buffer, pH 7.0, in the dark. The obtained mixture was dialyzed with 100 mM potassium phosphate buffer, pH 7.0, (3 times) at 4 ˚C. The purified protein was characterized by UV-vis, CD, DLS and SEC measurements. The molar extinction coefficient was determined by ICP-MS analysis: $\varepsilon_{418} = 1.8 \times 10^5\ M^{-1}cm^{-1}$.

Titration experiments of photosensitizer molecules to apoHTHP

To a cuvette containing a solution of apoHTHP (17 or 29 μM as a monomer for titration of ZnPP or ZnCe6, respectively) in 100 mM potassium phosphate buffer, pH 7.0, at 4 ˚C, various equivalents of ZnPP or ZnCe6 solutions in 0.1 M NaOHaq were added. After 12 h under an N_2 atmosphere in the dark, UV-vis spectra were measured (Figure 1-7, 1-16c).

Preparation of rHTHP$^{ZnPP(1/6)}$ or rHTHP$^{ZnCe6(1/6)}$

In the dark, an apoHTHP solution (30 μM equivalent as a monomer, 1.67 mL) in 100 mM potassium phosphate buffer, pH 7.0, was added to rHTHP$^{ZnPP(6/6)}$ or rHTHP$^{ZnCe6(6/6)}$ solution (10 mM equivalent as a monomer, 1 mL) in the same buffer at 25 ˚C. After standing for 24 h, equilibration was confirmed by fluorescence measurements.

Flash photolysis measurements

Transient absorption spectroscopy measurements after photoexcitation by femtosecond pulse laser were conducted using an ultrafast source: Integra-C (Quantronix Corp.), an optical parametric amplifier: TOPAS (Light Conversion Ltd.) and a commercially available optical detection system: Helios provided by Ultrafast Systems LLC. The source for the pump and probe pulses were derived from the fundamental output of Integra-C (λ = 786 nm, 2 μJ per pulse and fwhm = 130 fs) at a repetition rate of 1 kHz. 75% of the fundamental output of the laser was introduced into TOPAS for excitation light generation at λ = 420 nm, while the rest of the output was used for white light generation. The laser pulse was focused on a sapphire plate of 3 mm thickness and then a white light continuum covering the visible region from λ = 410 nm to 800 nm was generated *via* self-phase modulation. A variable neutral density filter, an optical aperture, and a pair of polarizers were inserted in the path in order to generate a stable white light continuum. Prior to generating the probe continuum, the laser pulse was fed to a delay line that provides an experimental time window of 3.2 ns with a maximum step resolution of 7 fs. In the experiments, a wavelength at λ = 420 nm of SHG output was irradiated at the sample cell with a spot size of 1 mm diameter where it was merged with the white probe pulse in a close angle (< 10°). The power of the pump pulse ranging from 12 μJ to 24 μJ was regulated by a variable neutral density filter. The probe beam after passing through the 2 mm sample cell was focused on a fiber optic cable that was connected to a CMOS spectrograph for recording the time-resolved spectra (λ = 450 - 800 nm). Typically, 3000 excitation pulses were averaged for 3 seconds to obtain the transient spectrum at a set delay time. Kinetic traces at appropriate wavelengths were assembled from the timeresolved spectral data. All measurements were conducted at room temperature, 22 ˚C.

1-5. References and notes

1. (a) G. D. Scholes, G. R. Fleming, A. Olaya-Castro and R. van Grondelle, *Nat. Chem.*, 2011, **3**, 763–774.
2. G. McDermott, S. M. Prince, A. A. Freer, A. M. Hawthornthwaite-Lawless, M. Z. Papiz, R. J. Cogdell and N. W. Isaacs, *Nature*, 1995, **374**, 517–521.
3. (a) F. Hajjaj, Z. S. Yoon, M.-C. Yoon, J. Park, A. Satake, D. Kim and Y. Kobuke, *J. Am. Chem. Soc.*, 2006, **128**, 4612–4623; (b) N. Aratani, D. Kim and A. Osuka, *Acc. Chem. Res.*, 2009, **42**, 1922–1934; (c) J. Yang, M.-C. Yoon, H. Yoo, P. Kim and D. Kim, *Chem. Soc. Rev.*, 2012, **41**, 4808–4826; (d) S. Fukuzumi and K. Ohkubo, *J. Mater. Chem.*, 2012, **22**, 4575–4587; (e) S. Cho, W.-S. Li, M.-C. Yoon, T. K. Ahn, D.-L. Jiang, J. Kim, T. Aida and D. Kim, *Chem. – Eur. J.*, 2006, **12**, 7576–7584; (f) S. Fukuzumi, K. Ohkubo and T. Suenobu, *Acc. Chem. Res.*, 2014, **47**, 1455–1464.
4. (a) T. Miyatake and H. Tamiaki, *Coord. Chem. Rev.*, 2010, **254**, 2593–2602; (b) S.Sengupta and F. Würthner, *Acc.Chem.Res.*, 2013, **46**, 2498–2512; (c) M. R. Wasielewski, *Acc. Chem. Res.*, 2009, **42**, 1910–1921; (d) T. S. Balaban, *Acc. Chem. Res.*, 2005, **38**, 612–623.
5. H.-J. Son, S. Jin, S. Patwardhan, S. J. Wezenberg, N. C. Jeong, M. So, C. E. Wilmer, A. A. Sarjeant, G. C. Schatz, R. Q. Snurr, O. K. Farha, G. P. Wiederrecht and J. T. Hupp, *J. Am. Chem. Soc.*, 2013, **135**, 862–869.
6. (a) A. Onoda, Y. Kakikura, T. Uematsu, S. Kuwabata and T. Hayashi, *Angew. Chem., Int. Ed.*, 2012, **51**, 2628–2631; (b) K. Oohora, A. Onoda and T. Hayashi, *Chem. Commun.*, 2012, **48**, 11714–11726; (c) I. Cohen-Ofri, M. van Gastel, J. Grzyb, A. Brandis, I. Pinkas, W. Lubitz and D. Noy, *J. Am. Chem. Soc.*, 2011, **133**, 9526–9535; (d) J. L. R. Anderson, C. T. Armstrong, G. Kodali, B. R. Lichtenstein, D. W. Watkins, J. A. Mancini, A. L. Boyle, T. A. Farid, M. P. Crump, C. C. Moser and P. L. Dutton, *Chem. Sci.*, 2014, **5**, 507–514; (e) F. A. Tezcan, B. R. Crane, J. R. Winkler and H. B. Gray, *Proc. Natl. Acad. Sci. U. S. A.*, 2001, **98**, 5002–5006; (f) T. Koshiyama, M. Shirai, T. Hikage, H. Tabe, K. Tanaka, S. Kitagawa and T. Ueno, *Angew. Chem., Int. Ed.*, 2011, **50**, 4849–4852; (g) H. Zemel and B. Hoffman, *J. Am. Chem. Soc.*, 1981, **103**, 1192–1201; (h) A. Kuki and S. G. Boxer, *Biochemistry*, 1983, **22**, 2923–2933; (i) J. W. Springer, P. S. Parkes-Loach, K. R. Reddy, M. Krayer, J. Jiao, G. M. Lee, D. M. Niedzwiedzki, M. A. Harris, C. Kirmaier, D. F. Bocian, J. S. Lindsey, D. Holten and P. A. Loach, *J. Am. Chem. Soc.*, 2012, **134**, 4589–4599.
7. (a) R. A. Miller, N. Stephanopoulos, J. M. McFarland, A. S. Rosko, P. L. Geissler and M. B. Francis, *J. Am. Chem. Soc.*, 2010, **132**, 6068–6074; (b) L. S. Witus and M. B. Francis, *Acc.*

Chem. Res., 2011, **44**, 774–783; (c) Y. S. Nam, T. Shin, H. Park, A. P. Magyar, K. Choi, G. Fantner, K. A. Nelson and A. M. Belcher, *J. Am. Chem. Soc.*, 2010, **132**, 1462–1463; (d) M. Endo, M. Fujitsuka and T. Majima, *Chem. – Eur. J.*, 2007, **13**, 8660–8666.

8. J.-H. Jeoung, D. A. Pippig, B. M. Martins, N. Wagener and H. Dobbek, *J. Mol. Biol.*, 2007, **368**, 1122–1131.
9. (a) T. Hayashi, in *Handbook of Porphyrin Science*, ed. K. M. Kadish, K. Smith and R. Guilard, World Scientific, Singapore, 2010, vol. 5, pp. 1–69; (b) T. Hayashi, in *Coordination Chemistry in Protein Cages: Principles, Design, and Applications*, ed. T. Ueno, Y. Watanabe, John Wiley & Sons, Hoboken, NJ, 2013, pp. 87–110.
10. F. W. J. Teale, *Biochim. Biophys. Acta*, 1959, **35**, 543.
11. T. Komatsu, R.-M. Wang, P. A. Zunszain, S. Curry and E. Tsuchida, J. Am. Chem. Soc., 2006, 128, 16297–16301.
12. (a) X. Huang, K. Nakanishi and N. Berova, *Chirality*, 2000, **12**, 237–255; (b) N. Berova, L. D. Bari and G. Pescitelli, *Chem. Soc. Rev.*, **2007**, 36, 914–931.
13. Examples of a long-range exciton coupling: (a) S. Matile, N. Berova, K. Nakanishi, J. Fleischhauer and R. W. Woody, *J. Am. Chem. Soc.*, 1996, **118**, 5198–5206; (b) K. Tsubaki, K. Takaishi, H. Tanaka, M. Miura and T. Kawabata, *Org. Lett.*, 2006, **8**, 2587–2590.
14. L. Luo, C.-H. Chang, Y.-C. Chen, T.-K. Wu and E. W.-G. Diau, *J. Phys. Chem. B,* 2007, **111**, 7656–7664.
15. (a) F. D'Souza, M. E. Zandler, P. Tagliatesta, Z. Ou, J. Shao, E. V. Caemelbecke and K. M. Kadish, *Inorg. Chem.*, 1998, **37**, 4567– 4572. (b) J. Li, D. Kuang, Y. Feng, F. Zhang, Z. Xu, M. Liu and D. Wang, *Microchim. Acta*, 2013, **180**, 49–58. (c) A. S. Razavian, S. M. Ghoreishi, A. S. Esmaeily, M. Behpour, L. M. A. Monzon and J. M. D. Coey, *Microchim. Acta*, 2014, **181**, 1947–1955.
16. The decay components with lifetimes derived from electron transfer in the excited charge transfer complexes were not observed due to the instrument response (fwhm = ca. 1 ns).
17. The difference between the binding constants of MV^{2+} for $rHTHP^{ZnCe6(n/6)}$ and $rHTHP^{ZnPP(n/6)}$ may be derived from the number of carboxylate groups of the cofactors.
18. T. Hayashi, T. Ando, T. Matsuda, H. Yonemura, S. Yamada, Y. Hisaeda, *J. Inorg. Biochem.,* 2000, **82**, 133–139.
19. A. Mennenga, W. Gärtner, W. Lubitz, H. Görner, *Phys. Chem. Chem. Phys.*, 2006, 8, 5444–5453.

Chapter 2
Assembly of multiple photosensitizers within the HTHP matrix and evaluation of energy transfer mechanism

2-1. Introduction

A light-harvesting system which is composed of chlorophyll and carotenoid pigments in purple bacterium absorbs sunlight and transfers the excited energy to a reaction center for photosynthesis.[1] In the array, two different types of chlorophyll molecules, B800 and B850, and carotenoid pigments collectively absorb a wide spectrum of visible light and energy migration subsequently occurs. Several pathways from excited photosensitizers to a reaction center have been reported.[2] Efficient energy transfer from multiple photosensitizers to the reaction center enables the light harvesting function to utilize solar energy. While much remains to be done in terms of understanding the energy transfer mechanism, a number of efforts to replicate the sophisticated photosensitizer arrays have been reported and have provided artificial light harvesting systems. To demonstrate continuous energy transfer between multiple donor and acceptor photosensitizers, covalently linked photosensitizer arrays,[3] clay scaffolds,[4] membrane scaffolds,[5] metal-organic frameworks,[6] self-assembled supramolecules[7], and DNA scaffolds[8] have been reported. In this decade, several proteins have been found to provide appropriate scaffolds for accumulating photosensitizers by supramolecular interactions[9] or covalent modifications.[10] A protein-based system would have the advantage of utilizing the protein's intrinsically large and sophisticated structure to achieve a well-defined photosensitizer assembly. However, examples of controlling the ratio of the donor and acceptor photosensitizers in protein matrices have had limited success.

In chapter 1, the author has developed an artificial light harvesting system with a hexameric tyrosine-coordinated heme protein (HTHP)[11] as a scaffold. An array of photosensitizers within the HTHP matrix can be assembled. A supramolecular interaction was observed in the HTHP matrix. The HTHP system allows expansion of covalent conjugation with donor and/or acceptor photosensitizers. This paper describes the construction of a multiple photosensitizer assembly based on a hexameric hemoprotein scaffold using supramolecular and covalent interactions and a mechanistic evaluation of successive energy transfer as a sophisticated light harvesting model. Figure 2-1 schematically illustrates the strategy of this study using fluorescein (Flu) and Texas Red (Tex) as donor and acceptor photosensitizers for ZnPP, respectively. The combination of the three photosensitizers enables use of the entire spectrum of visible-light. In the present work, the author constructed three systems using the HTHP scaffold: (i) a Flu-attached ZnPP array, (ii) a

Tex-attached ZnPP array, and (iii) a Flu- and Tex-attached ZnPP array. Control of the ratio of donor and acceptor photosensitizers for the latter was established.

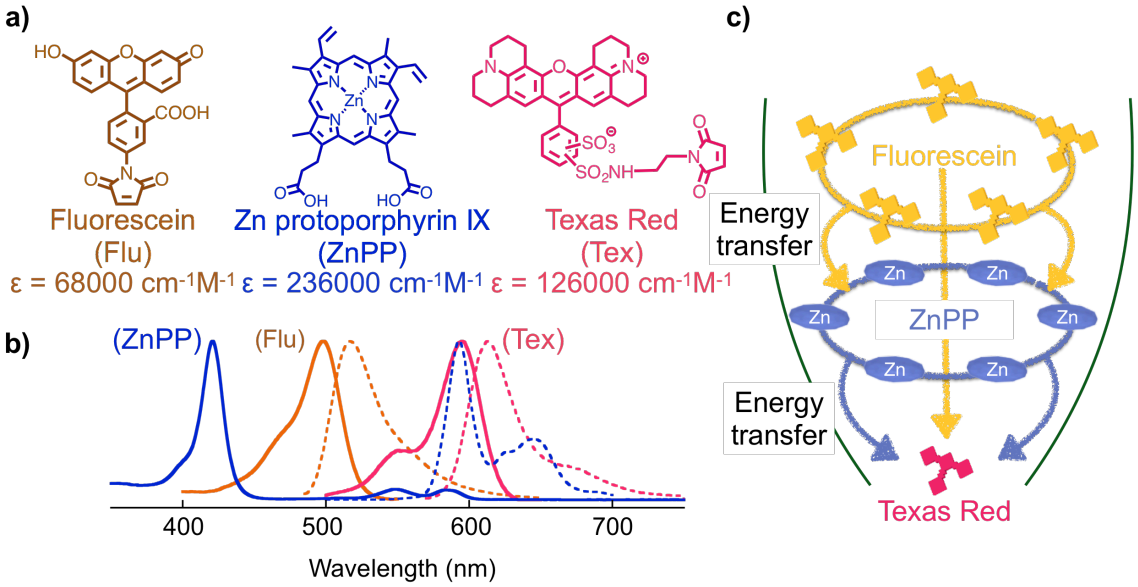

Figure 2-1. (a) Molecular structures of photosensitizers (fluorescein, Zn protoporphyrin IX, and Texas Red) used in this study. (b) Normalized absorption (solid line) and emission (dotted line) spectra; orange: Flu, blue: ZnPP, and pink: Tex. (c) Schematic diagram of energy transfer in the assembled photosensitizers, Flu, ZnPP, and Tex, within the HTHP matrix.

2-2. Results and discussion

Preparation and characterization of cysteine-introduced HTHP mutants

To introduce the photosensitizers onto the surfaces of the HTHP^{Cys} mutants, a thiol-maleimide coupling reaction was employed for site-selective modification because there are no cysteine residues in the sequence of the native protein. Two helices of each monomer unit in the crystal structure of HTHP are exposed to solvent molecules. Three residues within one of the helices, T12, D18, and K29, were selected as mutation sites (Figure. 2-2). Each mutant has six cysteine residues because HTHP is a homohexamer. The mutants were prepared by an *E.coli* recombinant expression system and purified by anion exchange and size exclusion chromatography (SEC) in the presence of DTT, a reductant for cleavage of disulfide bonds. The three mutants, HTHP^{T12C}, HTHP^{D18C}, and HTHP^{K29C}, were characterized by MALDI-TOF MS, UV-vis spectroscopy, and analytical SEC (Table 2-1 and Figure 2-3, 2-4).

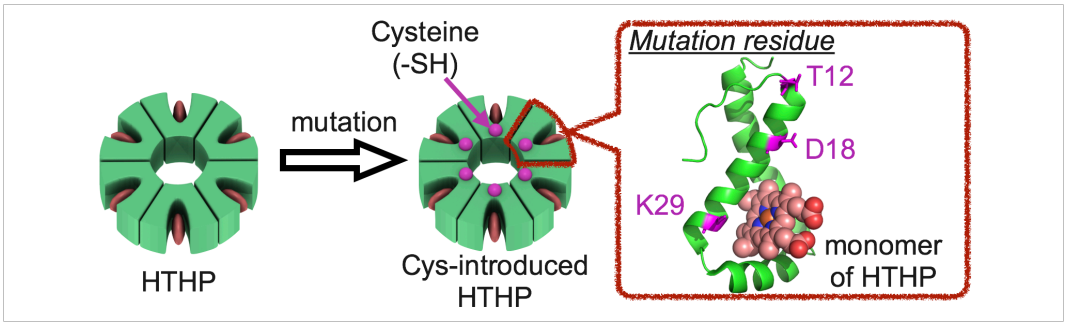

Figure 2-2. The schematic representation of site directed mutation and he three mutated residues are shown as purple in the crystal structure of each monomer of HTHP.

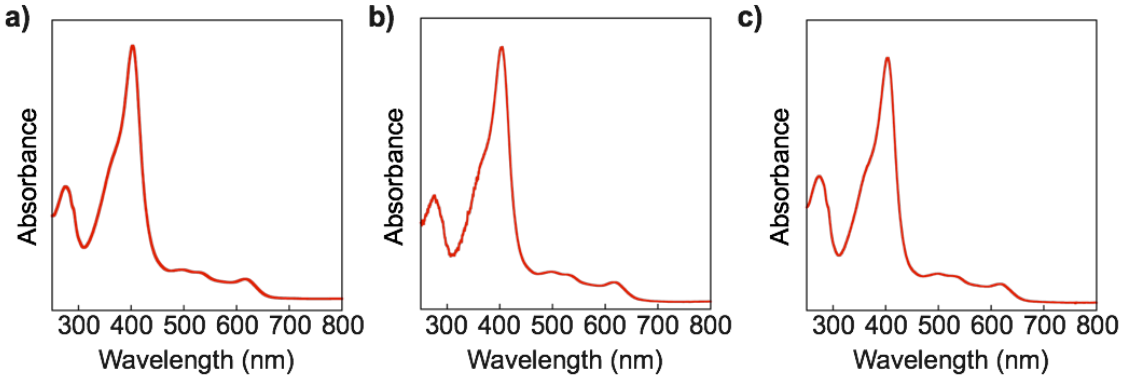

Figure 2-3. UV-vis absorption spectra of (a) HTHP^{T12C}, (b) HTHP^{D18C}, and (c) HTHP^{K29C} in 100 mM potassium phosphate buffer at pH 7.0 and 25 ˚C.

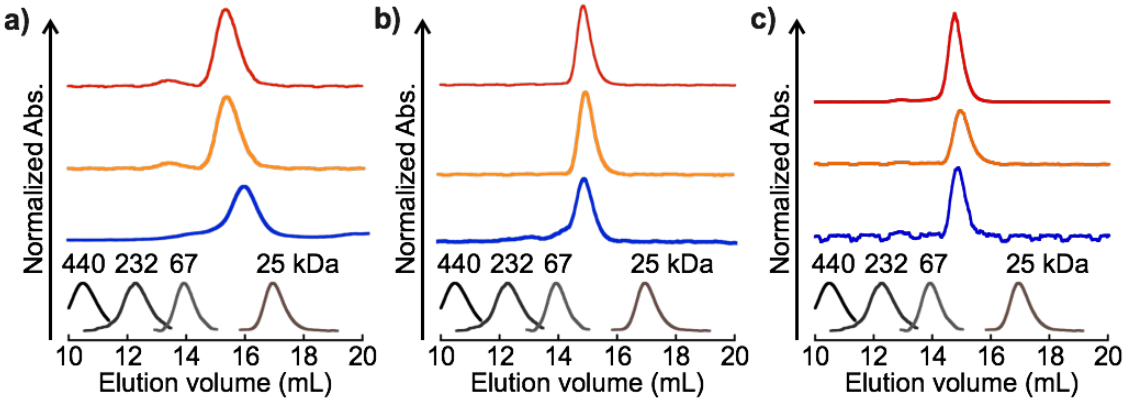

Figure 2-4. Analytical SEC traces of (a) HTHP^{T12C} (red), Flu-HTHP^{T12C} (orange) and Flu-apoHTHP^{T12C} (blue); (b) HTHP^{D18C} (red), Flu-HTHP^{D18C} (orange) and Flu-apoHTHP^{D18C} (blue); and (c) HTHP^{K29C} (red), Flu-HTHP^{K29C} (orange) and Flu-apoHTHP^{K29C} (blue). The black profiles were obtained by various protein standards. Red, orange, blue, and black profiles were detected by absorptions at 402, 495, 495, and 280 nm, respectively. Eluent is 100 mM potassium phosphate buffer at pH 7.0 and 4 ˚C at a flow rate of 0.5 mL min^{-1}.

Table 2-1 MALDI-TOF MS results of HTHP^{Cys} mutants and Flu-HTHP^{Cys} mutants

Protein	Found m/z	Calcd m/z[a]
HTHP^{T12C}	8231.7	8232.3
Flu-HTHP^{T12C}	8658.8	8659.6
HTHP^{D18C}	8221.2	8218.3
Flu-HTHP^{D18C}	8665.3	8668.6[b]
HTHP^{K29C}	8204.7	8205.2
Flu-HTHP^{K29C}	8633.0	8632.5

[a] z = 1. Heme was removed from the heme binding site of HTHP mutants under the ionization condition. [b]The value was calculated as a sodium adduct.

Preparation and characterization of fluorescein-attached HTHP

The scheme for the preparation of the series of Flu-attached proteins is shown in Figure 2-5. To conjugate Flu onto the HTHP surface, HTHP^{Cys} mutants were reacted with 2 eq of fluorescein-5-maleimide, and the obtained Flu-HTHP^{Cys} mutants were purified by SEC (Figure 2-4). The apo-forms of the HTHP^{Cys} mutants (Flu-apoHTHP^{Cys} mutants) were prepared by the conventional 2-butanone method.[12] A solution of ZnPP in DMSO was added to each solution of Flu-apoHTHP^{Cys} mutant at pH 7.0 to yield Flu-HTHP^{Cys} mutants reconstituted with ZnPP (Flu-rHTHP^{Cys} mutants). The 1:1 binding of ZnPP within each heme pocket was confirmed by the titration experiment (Figure 2-6). The analytical SEC traces of the HTHP^{Cys} mutants after reduction with DTT, Flu-HTHP^{Cys} mutants, and Flu-apoHTHP^{Cys} mutants show the single peak at the same elution volume as the wild type protein, indicating maintenance of the hexameric structure in this series of modified proteins (Figure 2-4). Representative UV-vis spectra of these proteins are shown in Figure 2-7 and 2-8. HTHP^{Cys} mutants have a heme Soret band at 402 nm and Flu-HTHP^{Cys} mutants have another peak at 498 nm arising from the Flu moiety attached to the protein surface. Completion of conjugation was confirmed by comparing UV-vis spectra of the Flu-HTHP^{Cys} mutants to simulated spectra using the extinction coefficients of HTHP and Flu (Figure 2-7). In the spectra of the Flu-apoHTHP^{Cys} mutants, the absence of the peak at 402 nm indicates removal of the heme. After reconstitution of Flu-HTHP^{Cys} mutants with ZnPP, the characteristic Soret band of ZnPP at 421 nm was observed. The MALDI-TOF mass spectra of Flu-HTHP^{Cys} mutants only have a peak indicating the presence of the apo-form of the Flu-attached monomer, as a result of the ionization conditions (Table 2-1). Thus, a series of Flu-HTHP^{Cys} mutants were successfully prepared

and characterized.

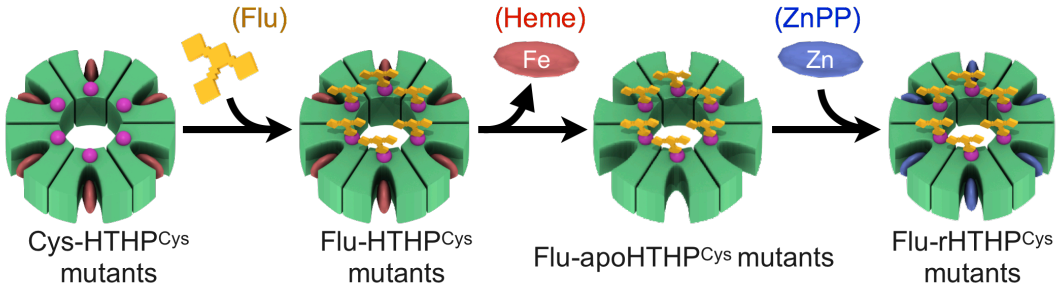

Figure 2-5. Schematic representation of the preparation of Flu-rHTHP^{Cys} mutants.

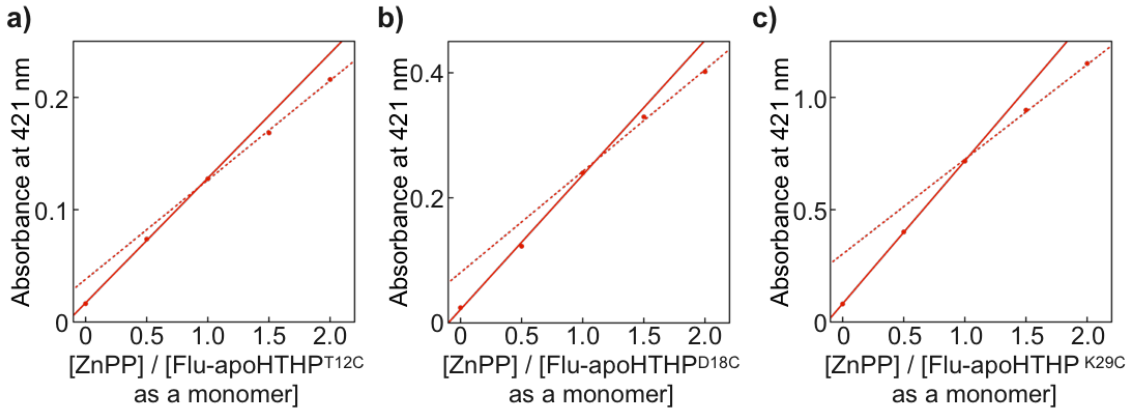

Figure 2-6. ZnPP titration experiments of (a) Flu-apoHTHP^{T12C}, (b) Flu-apoHTHP^{D18C}, and (c) Flu-apoHTHP^{K29C}. The protein concentrations are 1.3 μM, 1.0 μM, and 2.8 μM as a monomer, respectively, in 100 mM potassium phosphate buffer at pH 7.0 and 25 ˚C.

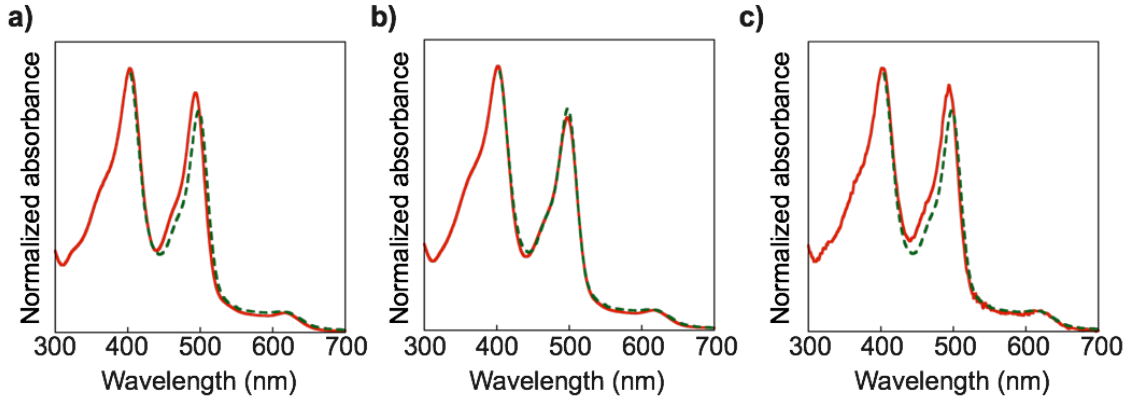

Figure 2-7. UV-vis spectra of (a) Flu-HTHP^{T12C}, (b) Flu-HTHP^{D18C}, and (c) Flu-HTHP^{K29C} in 100 mM potassium phosphate buffer at pH 7.0 and 25 ˚C. Solid lines were obtained by experimental spectra and dotted lines are simulated spectra by the sum of HTHP and photosensitizer spectra with the extinction coefficients. (Heme: 95000 $M^{-1}cm^{-1}$ at 402 nm and fluorescein: 68000 $M^{-1}cm^{-1}$ at 497 nm).

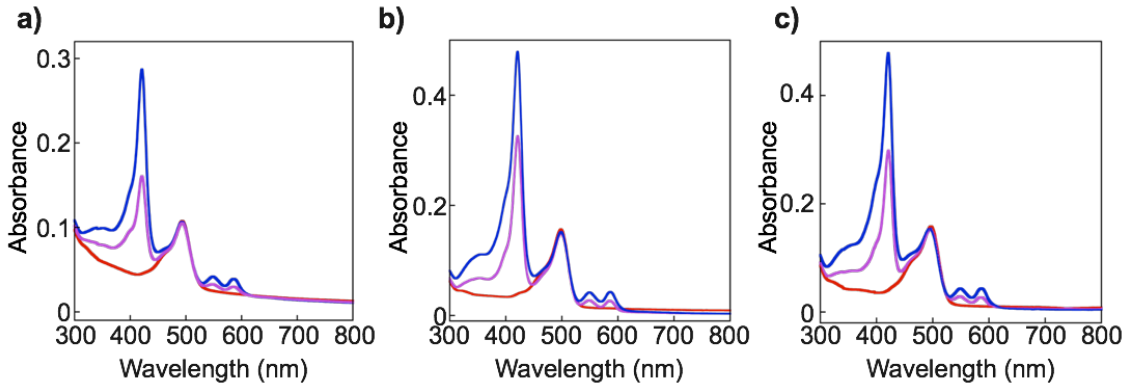

Figure 2-8. UV-vis spectral changes of (a) Flu-apoHTHP^{T12C}, (b) Flu-apoHTHP^{D18C} and (c) Flu-apoHTHP^{K29C} (The protein concentrations are 1.0 μM, 2.0 μM, and 2.0 μM as a monomer, respectively) occurring upon adding ZnPP at 0 (red), 0.5 (purple), and 1.0 equivalent (blue) in 100 mM potassium phosphate buffer at pH 7.0 and 25 ˚C under a nitrogen atmosphere.

Energy transfer from fluorescein to ZnPP within fluorescein-attached HTHP reconstituted with ZnPP

Fluorescence spectra and fluorescence excitation spectra of Flu-apoHTHP^{Cys} mutants and Flu-rHTHP^{Cys} mutants measured under a nitrogen atmosphere are shown in Figure. 2-9 and 2-10, respectively.[13] The Flu molecule attached to the surface of HTHP has an absorption peak at 498 nm, while there is no absorption derived from ZnPP in the heme binding site of HTHP in the range between 460 and 520 nm. Thus, the Flu moieties within the Flu-rHTHP^{Cys} mutants were selectively excited at 460 nm to measure the Flu emission of the reconstituted protein. Grater fluorescence intensity of Flu-apoHTHP^{Cys} mutants was observed relative to that of Flu-rHTHP^{Cys} mutants. The fluorescence quenching efficiency, E_q, is evaluated by the fluorescence intensity changes of Flu according to the following equation (1):[14]

$$E_q = 1 - \frac{I_{\text{Flu•ZnPP}}}{I_{\text{Flu}}} \quad (1)$$

where I_{Flu} is fluorescence intensity (λ_{ex} = 460 nm) of Flu-apoHTHP^{Cys} at 520 nm and $I_{\text{Flu•ZnPP}}$ is fluorescence intensity (λ_{ex} = 460 nm) of Flu-rHTHP^{Cys} at 520 nm.[15] The E_q values are 62% for Flu-rHTHP^{T12C}, 69% for Flu-rHTHP^{D18C} and 56% for Flu-rHTHP^{K29C} (Table 2-3). However, no correlation of the E values against the expected distances between the donor and the acceptor was observed (*vide infra*).

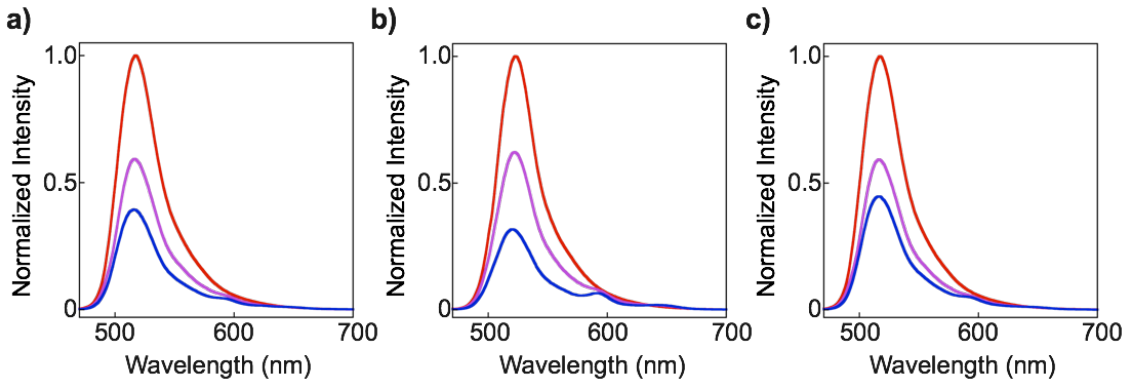

Figure 2-9. Fluorescence spectral changes of (a) Flu-apoHTHP^{T12C}, (b) Flu-apoHTHP^{D18C}, and (c) Flu-apoHTHP^{K29C} upon addition of ZnPP ([ZnPP] / [Flu-apoHTHP^{Cys} mutants as monomers] = 0 (red), 0.5 (purple), 1.0 (blue)). The intensities were normalized at the fluorescence maximum of the Flu-apoHTHP^{Cys} mutants. Conditions: [Flu-apoHTHP^{Cys} mutants as monomers] = ca. 1 μM in 100 mM potassium phosphate buffer at pH 7.0 and 25 ˚C under a nitrogen atmosphere. λ_{ex} = 460 nm.

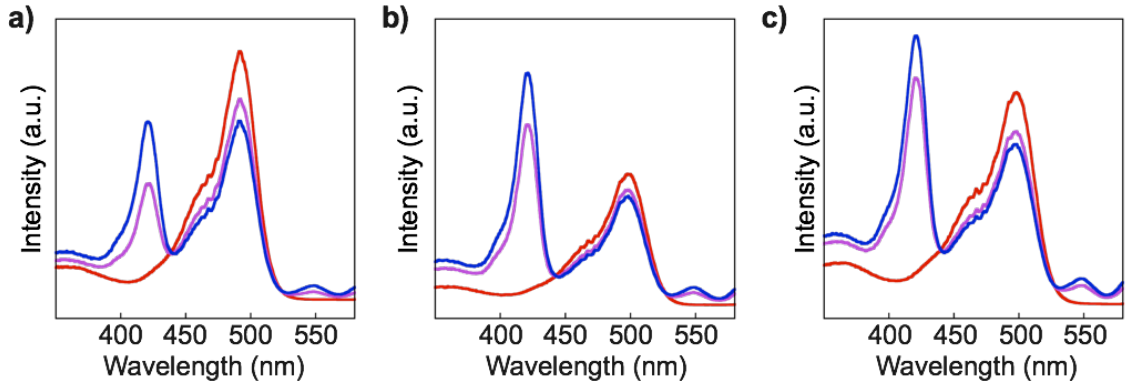

Figure 2-10. Fluorescence excitation spectra of (a) Flu-apoHTHP^{T12C}, (b) Flu-apoHTHP^{D18C}, and (c) Flu-apoHTHP^{K29C} upon addition of ZnPP ([ZnPP] / [Flu-apoHTHP^{Cys} mutants as monomers] = 0 (red), 0.5 (purple), 1.0 (blue)). Conditions: [Flu-apoHTHP^{Cys} mutants as monomers] = ca. 1 μM in 100 mM potassium phosphate buffer at pH 7.0 and 25 ˚C under a nitrogen atmosphere. λ_{em} = 590 nm.

In addition to steady state fluorescence spectroscopy, time-resolved fluorescence spectra of Flu-apoHTHP^{Cys} mutants and Flu-rHTHP^{Cys} mutants were measured to determine the fluorescence lifetime values (Figure 2-11). Table 2-2 summarizes the fluorescence lifetime values of the Flu moieties in the series of the HTHP mutants. The reconstitution of Flu-apoHTHP^{Cys} mutants with

ZnPP accelerates the Flu decay to shorten the fluorescence lifetime of Flu. Each fluorescence decay was analyzed by double or triple exponentially fitting curves to determine the lifetime. There appears to be one or more metastable conformations in each protein and the shorter lifetime (< 1 ns) is attributed to quenching amino acids such as tryptophan,[16] whereas the lifetime of Flu is typically > 2 ns.[17] Since the fluorescence decays were found to be multiexponential, average lifetime constants, $<\tau_{Flu}>$ and $<\tau_{Flu\cdot ZnPP}>$, determined by the sum of the $\alpha_i\tau_i$ products, are utilized for the investigation. Flu-apoHTHP^{T12C} and Flu-apoHTHP^{K29C} both have two components in fluorescence decays and average lifetimes of 2.11 and 1.55 ns were determined, respectively. In contrast, three components were found in the fluorescence decay curve of Flu-apoHTHP^{D18C} and the average lifetime is 1.01 ns. This finding suggests that the D18 residue should be unsuitable for conjugation of donor-photosensitizer in the mutants because the short average lifetime is a disadvantage for efficient energy transfer. Changes of the average lifetime upon addition of ZnPP provide the efficiency (E) of the FRET from Flu to ZnPP. The E value is calculated according to the following equation (2):[14]

$$E = 1 - \frac{\langle \tau_{Flu\cdot ZnPP} \rangle}{\langle \tau_{Flu} \rangle} \quad (2)$$

where $<\tau_{Flu}>$ and $<\tau_{Flu\cdot ZnPP}>$ represent the averages of the fluorescence lifetimes for Flu-apoHTHP^{Cys} mutants, and Flu-rHTHP^{Cys} mutants, respectively. The quenching efficiency value (E_q) evaluated from steady state and the energy transfer efficiency value (E) evaluated from time-resolved fluorescence experiments, and distances between the Zn center and the a carbon of mutated residue are summarized in Table 2-3. The E values of Flu-apoHTHP^{T12C} and Flu-apoHTHP^{K29C} derived from the fluorescence lifetime are generally consistent with the corresponding E_q values. However, in the case of Flu-apoHTHP^{D18C}, the E_q value is different from the E value. Here, the fluorescence quantum yields of Flu-apoHTHP^{Cys} mutants are strongly dependent on the position modified with the Flu molecule (Table 2). The mutant with the higher quantum yield shows the longer averaged lifetime, which is typical in the fluorescence molecules.[14] These results indicate that the conformation and the surrounding residues of the attached Flu molecule significantly influence the fluorescence property. It means that the E value should be more plausible. Hence the difference between E_q and E within Flu-rHTHP^{D18C} is derived from the occurrence of the new quenching pathway. Next, the fluorescence intensities of ZnPP within Flu-rHTHP^{D18C} and Flu-rHTHP^{K29C} upon excitation of the Flu-moiety were smaller than the intensity expected by E_q and Φ_f (< 3%) of

ZnPP in rHTHP . In addition, the distances between donor and acceptor were estimated with values of *E* (Table 2-4) using Förster theory. In the case of Flu-rHTHP^{D18C} and Flu-rHTHP^{K29C}, the estimated distances are much deviated from the structurally plausible donor–acceptor distances. It is speculated that the large deviation are caused by quenching with the electron transfer and non-negligible conformational changes of the Flu molecules by insertion of ZnPP into the protein matrix, which affects the quantum yield of the Flu molecules. In contrast, the distance estimated for Flu-rHTHP^{T12C} is mostly corresponding with the structurally plausible donor–acceptor distance. This result suggests that the condition of the residues around Flu moiety within Flu-rHTHP^{T12C} is maintained upon the insertion of ZnPP into the protein matrix. Hence, the quenching within Flu-rHTHP^{T12C} is due to the FRET system. These findings indicate that HTHP^{T12C} is a better scaffold than HTHP^{D18C} and HTHP^{K29C} for a model of the light harvesting system. Thus, HTHP^{T12C} was used in the following experiments.

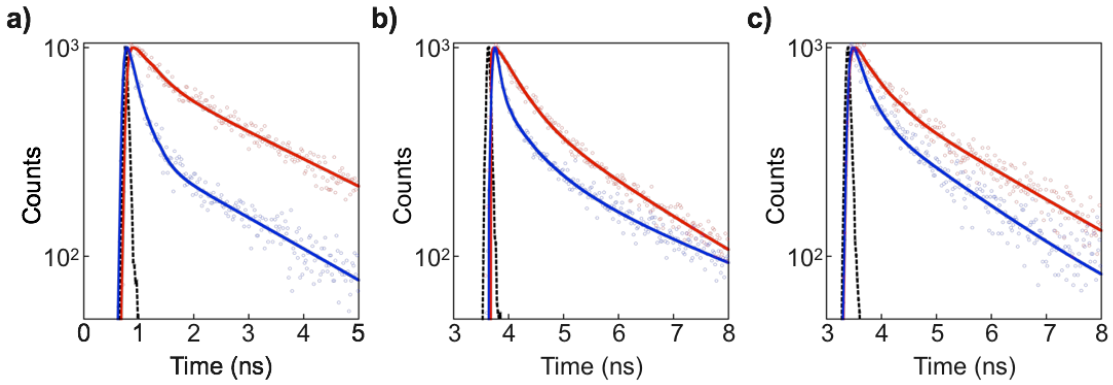

Figure 2-11. Time-resolved fluorescence decay profiles of (a) Flu-apoHTHP^{T12C} (red) and Flu-rHTHP^{T12C} (blue); (b) Flu-apoHTHP^{D18C} (red) and Flu-rHTHP^{D18C} (blue); and (c) Flu-apoHTHP^{K29C} (red) and Flu-rHTHP^{K29C} (blue). The instrument responses are shown by the black broken lines. Decay plots were analyzed by double- or triple-exponentially fitted curves (solid lines): $y = y_0 + A_1\exp(-t/\tau_1) + A_2\exp(-t/\tau_2)$, or $y = y_0 + A_1\exp(-t/\tau_1) + A_2\exp(-t/\tau_2) + A_3\exp(-t/\tau_3)$, where A and t are population and lifetime of the decay, respectively (Table 2-2). Conditions: The samples are dissolved in 100 mM potassium phosphate buffer at pH 7.0 and 25 ˚C under a nitrogen atmosphere. λ_{ex} = 464 nm and λ_{em} = 550 nm.

Table 2-2 Decay parameters of Flu-apoHTHP^{Cys} mutants and Flu-rHTHP^{Cys} mutants in the time-resolved fluorescence measurements[a] and fluorescence quantum yields (Φ_f) of Flu-apoHTHP^{Cys} mutants

Protein	$<\tau_{Flu}>$ or $<\tau_{Flu\bullet ZnPP}>$ (ns)[b]	τ_1 (ns)	α_1[c]	τ_2 (ns)	α_2[c]	τ_3 (ns)	α_3[c]	X^2	Φ_f[d]
Flu-apoHTHP^{T12C}	2.11	0.380	0.42	3.369	0.58			1.076	34 %
Flu-rHTHP^{T12C}	0.76	0.219	0.81	3.013	0.19			0.971	
Flu-apoHTHP^{D18C}	1.01	0.105	0.34	0.621	0.39	2.725	0.27	1.162	13%
Flu-rHTHP^{D18C}	0.75	0.092	0.58	0.520	0.24	3.151	0.18	1.024	
Flu-apoHTHP^{K29C}	1.55	0.382	0.52	2.823	0.48			1.197	18%
Flu-rHTHP^{K29C}	0.71	0.243	0.76	2.201	0.24			0.988	

[a] Conditions: [protein as a monomer] = ca. 1 μM in 100 mM potassium phosphate buffer, pH = 7.0 and 25 ˚C under a nitrogen atmosphere, λ_{ex} = 464 nm. [b] Average fluorescence lifetime determined by the sum of the $\alpha_i t_i$ products . [c] α is population for each component. [d] λ_{ex} = 460 nm.

Tabale 2-3 FRET efficiency and donor–acceptor distance of Flu-rHTHP^{Cys} mutants

Protein	E_q [a]	E [b]	Distance (nm) [c]
Flu-rHTHP^{T12C}	62%	64%	2.3
Flu-rHTHP^{D18C}	69%	26%	1.3
Flu-rHTHP^{K29C}	56%	54%	0.9

[a] E_q values were determined with steady state fluorescence results (Figure 2-9). [b] E values were determined with time resolved fluorescence results(Table 2-2). [c]Distances between the Fe center and the a carbon of the mutated residue in the crystal structure of wild type HTHP.

Table 2-4 Expected distances between Fluorescein and ZnPP

Protein	Expected distance (nm)	Maximum possible distance (nm)[a]	R_0 (nm)
Flu-rHTHP^{T12C}	3.3	3.0	3.6
Flu-rHTHP^{D18C}	3.7	2.1	3.1
Flu-rHTHP ^{K29C}	3.1	1.7	3.2

[a] The maximum possible distance was estimated as the sum of distances from the Fe center to the α carbon of the mutated residue in the crystal structure of wild type HTHP and distances from the α carbon to fluorescein. The distance between the α carbon to fluorescein was estimated with ChemBio3D® Ultra.

Preparation and characterization of Texas Red-attached HTHP^{T12C}

Tex was utilized as an acceptor photosensitizer for ZnPP. According to the results obtained Flu as a donor photosensitizer, HTHP^{T12C} was employed as a scaffold protein. Tex-attached HTHP^{T12C} (Tex-HTHP^{T12C}) was successfully obtained by coupling Texas Red C_2 maleimide with HTHP^{T12C} in the same manner used in preparations and purification of Flu-HTHP^{T12C} (Figure 2-12). The UV-vis spectrum of Tex-HTHP^{T12C} includes the characteristic two absorption peaks at 402 nm and 593 nm, which are derived from heme and Tex moieties, respectively (Figure 2-13a). Completion of conjugation was confirmed by comparing the UV-vis spectrum of Tex-HTHP^{T12C} with its simulated spectrum using the extinction coefficients of HTHP and Tex. In MALDI-TOF MS

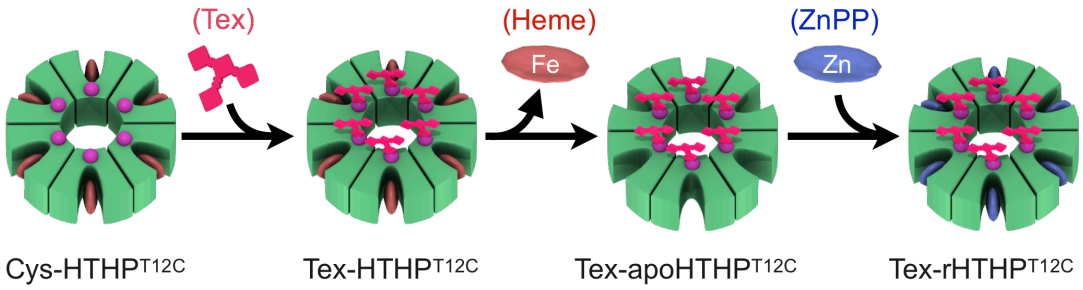

Figure 2-12. Schematic representation of the preparation of Tex-rHTHP^{T12C}.

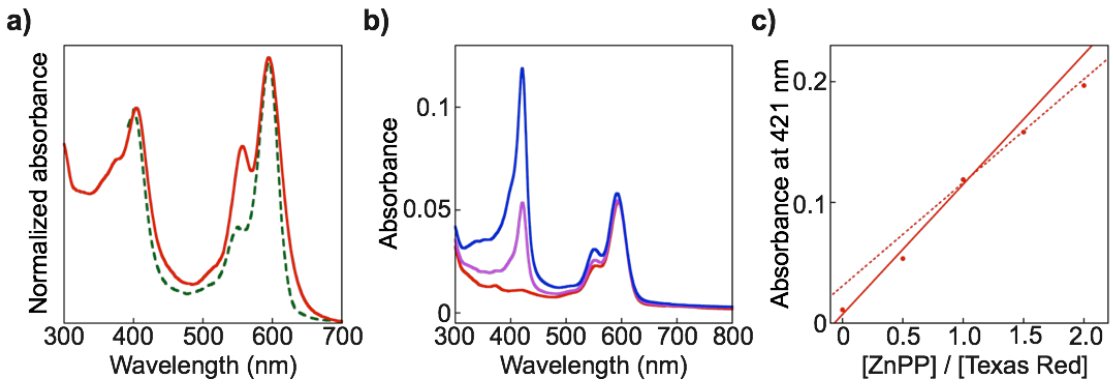

Figure 2-13. (a) UV-vis spectra of Tex-HTHP^{T12C} in 100 mM potassium phosphate buffer at pH 7.0 and 25 ˚C. Solid lines were obtained by experimental spectra and dotted lines are simulated spectra by the sum of HTHP and photosensitizer spectra with the extinction coefficients. (Heme: 95000 $M^{-1}cm^{-1}$ at 402 nm and Texas Red: 112000 $M^{-1}cm^{-1}$ at 593 nm). (b) UV-vis spectral changes of Tex-apoHTHP^{T12C} ([Protein as a monomer] = ca. 0.5 μM) occurring upon adding ZnPP at 0 (red), 0.5 (purple), and 1.0 equivalent (blue) in 100 mM potassium phosphate buffer at pH 7.0 and 25 ˚C under a nitrogen atmosphere. (c) ZnPP titration experiments of Tex-apoHTHP^{T12C}. The protein concentration is 1.0 μM in 100 mM potassium phosphate buffer at pH 7.0 and 25 ˚C.

of the obtained protein, the desired mass number was observed as a monomer without heme (found: m/z = 8964.9, calcd: m/z = 8961.1). The apo-form of Tex-HTHP^{T12C} (Tex-apoHTHP^{T12C}) and Tex-HTHP reconstituted with ZnPP (Tex-rHTHP^{T12C}) were prepared by the same method described above and the UV-vis spectra are shown in Figure 2-13b. The 1:1 binding of ZnPP for a monomer unit of Tex-apoHTHP was confirmed by the titration experiment (Figure 2-13c).

Energy transfer from ZnPP to Texas Red within Texas Red-attached HTHP^{T12C} reconstituted with ZnPP

The fluorescence intensity of Tex in Tex-rHTHP^{T12C} excited at 421 nm, which corresponds to the Soret band of ZnPP, was dramatically enhanced upon addition of ZnPP (Figure 2-14) due to energy transfer from ZnPP to Tex within the protein. The energy transfer efficiency, $E_{\mathrm{ZnPP\bullet Tex}}$, was calculated according to the following equation (3):[18]

$$E_{\mathrm{ZnPP\bullet Tex}} = \frac{I^{\mathrm{FRET}}{}_{421}}{I^{\mathrm{A}}{}_{593}} \frac{\varepsilon^{\mathrm{A}}{}_{593}}{\varepsilon^{\mathrm{D}}{}_{421}} \quad (3)$$

where $I^{\mathrm{FRET}}{}_{421}$ is the fluorescence intensity of Tex measured at 680 nm with excitation at the peak of the Soret band of ZnPP (421 nm), $I^{\mathrm{A}}{}_{593}$ is the fluorescence intensity at 680 nm with excitation at the absorbance peak of Tex (593 nm), $\varepsilon^{\mathrm{A}}{}_{593}$ and $\varepsilon^{\mathrm{D}}{}_{421}$ represent the extinction coefficient of Tex at 593 nm (126000 M^{-1} cm^{-1}) and ZnPP at the peak of the Soret band at 421nm (236000 M^{-1} cm^{-1}), respectively.[11] This equation ignores the contribution of Tex absorption due to its insufficient excitation coefficient at 421 nm (Figure 2-13b). The $E_{\mathrm{ZnPP\bullet Tex}}$ value was determined to be 35 %, indicating moderately efficient energy transfer. The energy transfer efficiency from ZnPP to Tex within Tex-rHTHP^{T12C} was also determined by fluorescence excitation spectra of Tex-rHTHP^{T12C} (Figure 2-15). The comparison of the absorbance and excitation intensity at 421 nm, a peak in the absorption spectrum of the donor moiety, provides 36% efficiency using the normalized spectra. This value is mostly consistent with the above efficiency, supporting the fact that the obtained value is correct. Additionally, the Φ_f (19%) of Tex-apoHTHP^{T12C} was measured and the distance between ZnPP and Tex was estimated by Förster theory. The distance in Tex-rHTHP^{T12C} is mostly consistent with the structurally possible distance (Table 2-5). Here, two excited states of ZnPP, S_1 and S_2 (S_2 is the higher order excited state than S_1), should be considered. The excited states S_1 and S_2 are generated by excitation at the Q and Soret bands, respectively. In the process of energy transfer from

ZnPP to Tex, excited energy at the S_2 state could be transferred to Tex after relaxation from S_2 to S_1, because the relaxation occurs rapidly (< 10 ps). Thus, this estimated energy transfer efficiency includes relaxation efficiency from S_2 to S_1 within the arrayed ZnPPs. Although the non-negligible overlap of the absorption region of the Q band and Tex prevent direct evaluation of the energy transfer from the excited ZnPP at the S_1 state to Tex, the efficiency appears to be higher than the

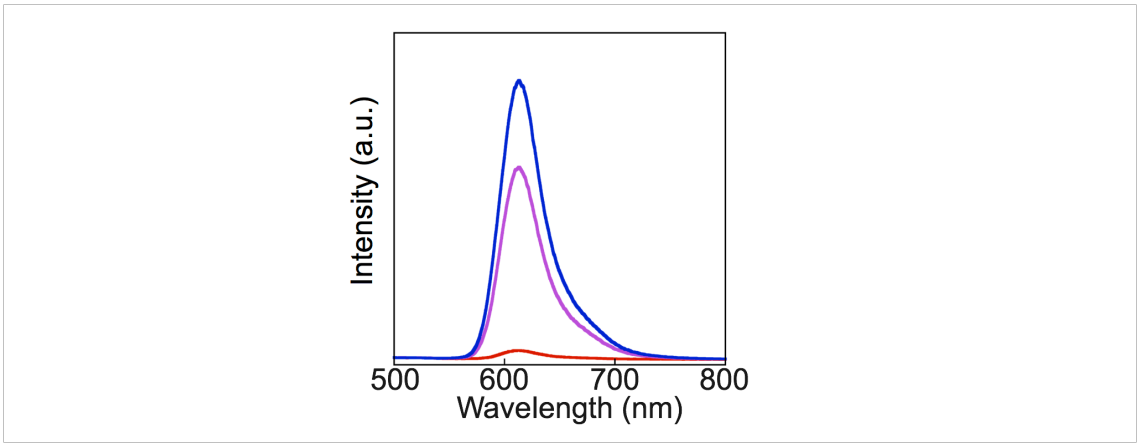

Figure 2-14. Fluorescence spectral changes of Tex-apoHTHP^{T12C} occurring addition of ZnPP ([ZnPP] / [Tex-apoHTHP^{T12C} as monomer] = 0 (red), 0.5 (purple), 1 (blue)). Conditions: [Tex-apoHTHP^{T12C} as a monomer] = ca. 1 μM in 100 mM potassium phosphate buffer at pH 7.0 and 25 ˚C under a nitrogen atmosphere. λ_{ex} = 421 nm.

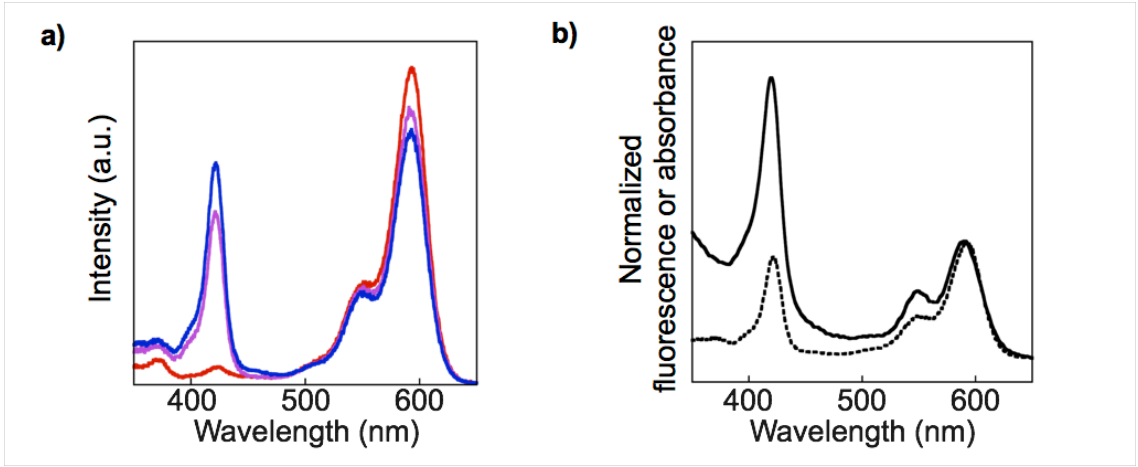

Figure 2-15. (a) Fluorescence excitation spectral changes of Tex-HTHP^{T12C} occurring addition of ZnPP ([ZnPP] / [Tex-apoHTHP^{T12C} as a monomer] = 0 (red), 0.5 (purple), 1 (blue)). (b) UV-vis spectra (solid line) and fluorescence excitation spectra (dotted line) of Tex-rHTHP^{T12C} were normalized at the acceptor excitation at 593 nm. Conditions: [Tex-apoHTHP^{T12C} as a monomer] = ca. 0.5 μM in 100 mM potassium phosphate buffer at pH 7.0 and 25 ℃ under a nitrogen atmosphere, λ_{em} = 680 nm.

calculated energy transfer value at 421 nm excitation. In addition, reverse energy transfer from Tex to ZnPP was also confirmed by observation of a decrease in the fluorescence intensity of Tex moieties excited at the absorbance peak of Tex (595 nm) upon addition of ZnPP (Figure 2-16). These results indicate that Tex works as an acceptor and a weak donor photosensitizer for ZnPP. Its energy transfer efficiency appears to be due to relaxation from S_2 to S_1 and the reverse energy transfer.

Table 2-5 Expected distances between ZnPP and Texas red

Protein	Expected distance (nm)	Maximum possible distance (nm)[a]	R_0 (nm)
Tex-rHTHP^{T12C}	4.0	3.5	3.7

[a] The maximum possible distance was estimated as the sum of distances from the Fe center to the α carbon of the mutated residue in the crystal structure of wild type HTHP and distances from the α carbon to Texas red. The distance between the α carbon to Texas red was estimated with ChemBio3D® Ultra.

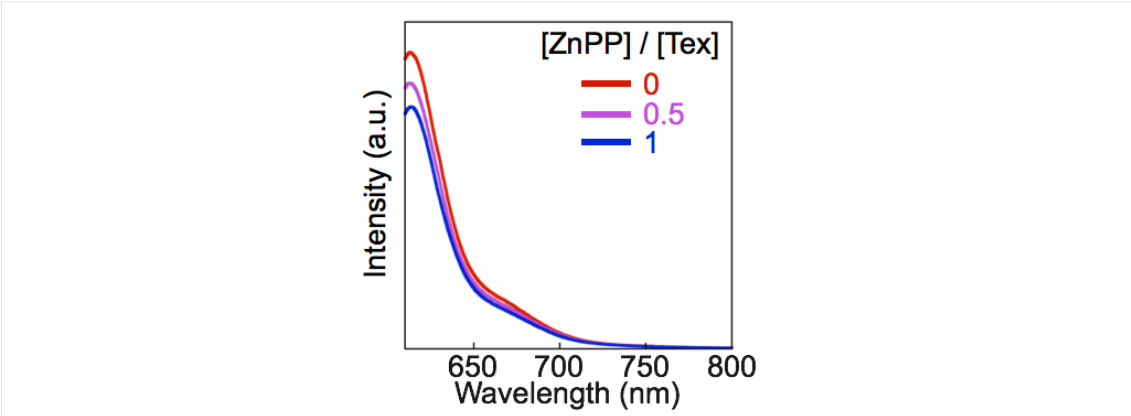

Figure 2-16. Fluorescence spectral changes of Tex-apoHTHP^{T12C} occurring upon addition of ZnPP ([ZnPP] / [Tex-apoHTHP^{T12C} as a monomer] = 0 (red), 0.5 (purple), 1 (blue)). Conditions: [Tex-apoHTHP^{T12C} as a monomer] = 0.5 μM in 100 mM potassium phosphate buffer at pH 7.0 and 25 ˚C under a nitrogen atmosphere. λ_{ex} = 593 nm.

Preparation and characterization of fluorescein- and Texas Red-attached HTHP^{T12C}

To construct a model of a light harvesting system collecting excited energy from multiple donor molecules at a single acceptor photosensitizer, five Flu and one Tex molecules were conjugated to the HTHP^{T12C} surface according to the procedure shown in Figure 2-17. First, a disulfide dimer of HTHP^{T12C} was prepared by oxidation of HTHP^{T12C} upon addition of potassium ferricyanide. After purification of the disulfide dimer with SEC, fluorescein-5-maleimide was reacted with the HTHP^{T12C} dimer. Reductive cleavage of the disulfide bond in the obtained dimer using DTT yielded HTHP^{T12C} with five attached Flu moieties and one free cysteine residue. The protein was then reacted with excess Texas Red C_2 maleimide. The product HTHP^{T12C} has five attached Flu moieties and one attached Tex moiety (Flu_5-Tex_1-HTHP^{T12C}). Flu_5-Tex_1-HTHP^{T12C} was purified by SEC and characterized by UV-vis spectroscopy (Figure 2-18a). In MALDI-TOF MS the desired mass numbers were observed, indicating the presence of monomers of Flu-HTHP^{T12C} and Tex-HTHP^{T12C} (found: m/z = 8656.9, calcd: m/z = 8654.4 and m/z = 8957.5, calcd: m/z = 8955.5, respectively). The apo-forms of Flu_5-Tex_1-HTHP^{T12C} (Flu_5-Tex_1-apoHTHP^{T12C}) and Flu_5-Tex_1-HTHP^{T12C} reconstituted with ZnPP (Flu_5-Tex_1-rHTHP^{T12C}) were also prepared and the UV-vis spectra are shown in Figure 2-18b. The 1:1 binding of ZnPP for the monomer unit of Flu_5-Tex_1-apoHTHP was confirmed by the titration experiment (Figure 2-18c).

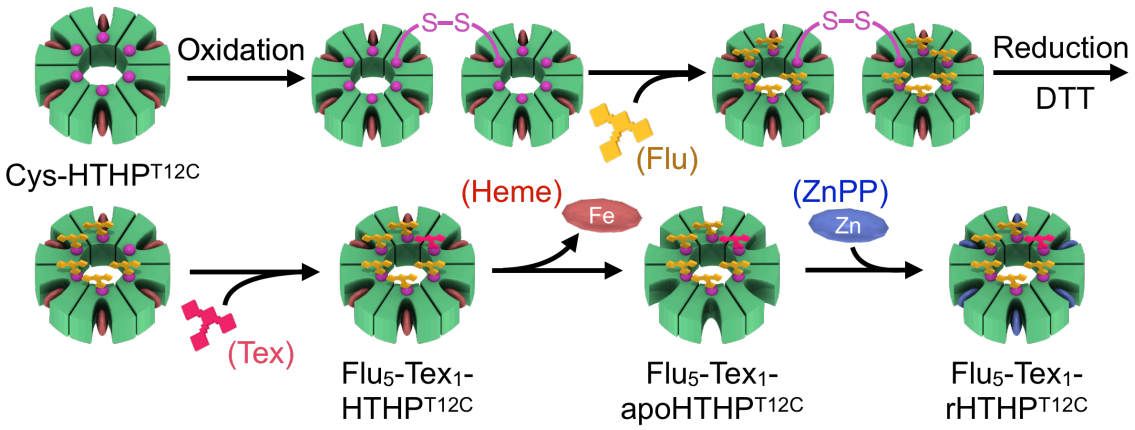

Figure 2-17. Schematic representation of the preparation of Flu_5-Tex_1-HTHP^{T12C}.

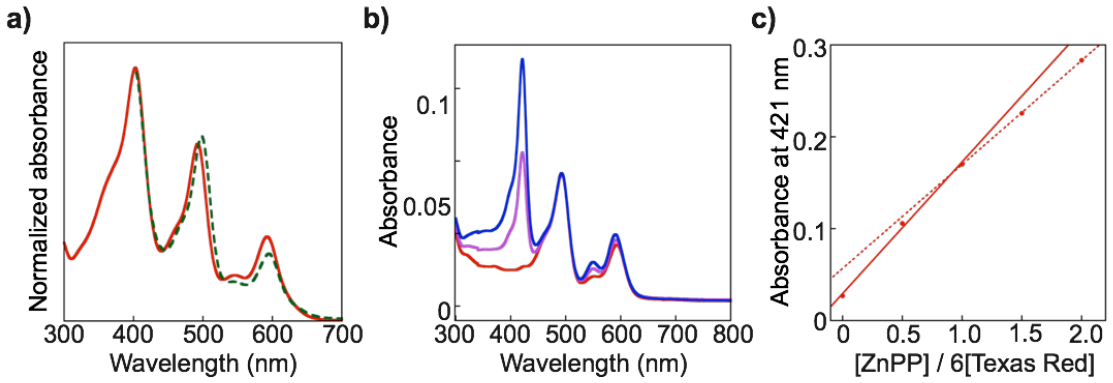

Figure 2-18. (a) UV-vis spectra of Flu_5-Tex_1-$HTHP^{T12C}$ in 100 mM potassium phosphate buffer at pH 7.0 and 25 ˚C. Solid lines were obtained by experimental spectra and dotted lines are simulated spectra by the sum of HTHP and photosensitizer spectra with the extinction coefficients. (Heme: 95000 $M^{-1}cm^{-1}$ at 402 nm, fluorescein: 68000 $M^{-1}cm^{-1}$ at 497 nm, and Texas Red: 112000 $M^{-1}cm^{-1}$ at 593 nm). (b) UV-vis spectral changes of Flu_5-Tex_1-$apoHTHP^{T12C}$ ([Protein as a monomer] = ca. 0.7 μM) occurring upon adding ZnPP at 0 (red), 0.5 (purple), and 1.0 equivalent (blue) in 100 mM potassium phosphate buffer at pH 7.0 and 25 ˚C under a nitrogen atmosphere. (c) ZnPP titration experiments of Tex-$apoHTHP^{T12C}$. The protein concentration is 0.7 μM in 100 mM potassium phosphate buffer at pH 7.0 and 25 ˚C.

Energy transfer from fluorescein to Texas Red within fluorescein- and Texas Red-attached $HTHP^{T12C}$ reconstituted with ZnPP

Fluorescence excitation spectra of Flu_5-Tex_1-apoHTHP and Flu_5-Tex_1-rHTHP were measured. The emission wavelength at 615 nm represents a peak in the fluorescence spectrum of Tex (Figure 2-19). The peak absorptions for the Flu and Tex moieties were observed in the fluorescence excitation spectrum of Flu_5-Tex_1-apoHTHP. Figure 2-20a shows an overlay of fluorescence excitation and absorption spectra for Flu_5-Tex_1-$apoHTHP^{T12C}$, in which the emission intensity and absorbance are normalized at 593 nm, a peak in the absorption spectrum of the acceptor moiety. The energy transfer efficiency from Flu to Tex within Flu_5-Tex_1-$apoHTHP^{T12C}$ was determined to be 42% by comparison of the absorbance and excitation spectra at 497 nm, a peak in the absorption spectrum of the donor moiety (Figure 2-20a). Similarly, the apparent energy transfer efficiency from Flu to Tex within Flu_5-Tex_1-rHTHP was also determined to be 38% (Figure 2-20b).[19]

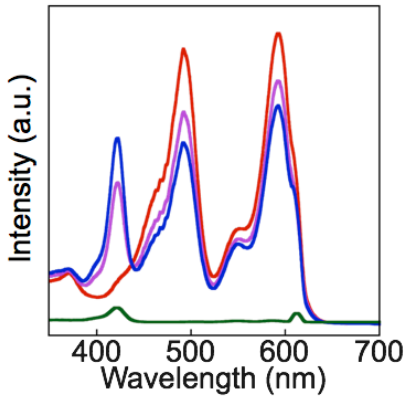

Figure 2-19. Fluorescence excitation spectral changes of Flu_5-Tex_1-$HTHP^{T12C}$ occurring addition of ZnPP ([ZnPP] / [Flu_5-Tex_1-apo$HTHP^{T12C}$ as a monomer] = 0 (red), 0.5 (purple), 1 (blue)). Conditions: [Flu_5-Tex_1-apo$HTHP^{T12C}$ as a monomer] = ca. 0.7 μM in 100 mM potassium phosphate buffer at pH 7.0 and 25 ˚C under a nitrogen atmosphere, λ_{em} = 615 nm. Green solid line is the reference spectrum of buffer solution without protein, indicating the negligible scattering of excitation light at 615 nm.

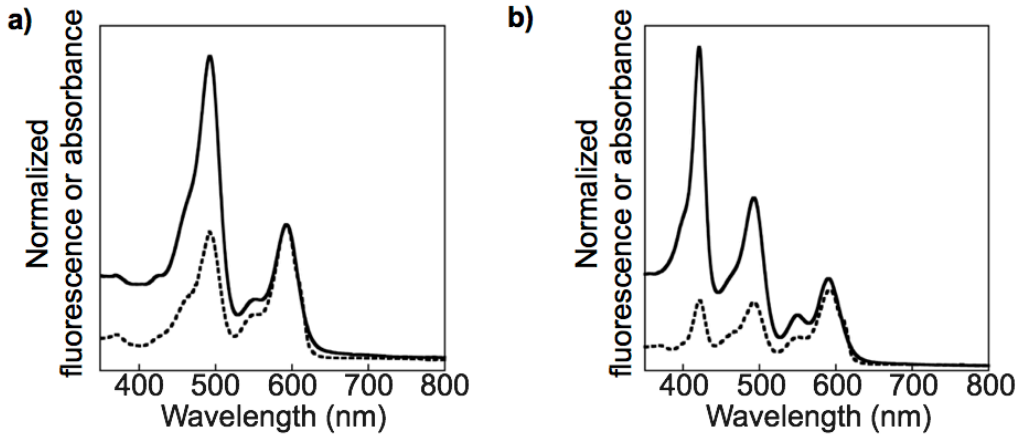

Figure 2-20. UV-vis spectra (solid line) and fluorescence excitation spectra (dotted line, λ_{em} = 615 nm) of (a) Flu_5-Tex_1-apo$HTHP^{T12C}$ and (b) Flu_5-Tex_1-r$HTHP^{T12C}$ were normalized at the acceptor excitation at 593 nm and 607 nm, respectively. Conditions: [protein as a monomer] = ca. 0.7 μM in 100 mM potassium phosphate buffer at pH 7.0 and 25 ˚C under a nitrogen atmosphere.

Energy transfer pathway from fluorescein to Texas Red within fluorescein- and Texas Red-attached HTHPT12C reconstituted with ZnPP

In energy transfer from Flu to Tex within Flu_5-Tex_1-r$HTHP^{T12C}$, two pathways were proposed: Path 1 is direct energy transfer from Flu to Tex and path 2 is a two-step pathway *via* ZnPP. The

energy transfer mechanism of Flu_5-Tex_1-rHTHP^{T12C} was kinetically evaluated using a series of results of steady state and time-resolved fluorescence measurements (Figure 2-21). The relaxation rate of the excited Flu moiety within Flu_5-Tex_1-rHTHP^{T12C} is expressed by three rate constants (k_1, k_2, and k_3). k_1 is the rate of the sum of the fluorescence transition and the non-radiative transition of Flu on the HTHP^{T12C} matrix. The value of k_1 was calculated to be 0.47 ns^{-1} with the following equation (4):

$$\langle \tau_{\mathrm{Flu}} \rangle = \frac{1}{k_1} \tag{4}$$

where $<\tau_{Flu}>$ is the average of fluorescence lifetime for Flu-apoHTHP^{T12C} (Table 2-2). k_2 is the rate of energy transfer from Flu to Tex. The value of k_2 was determined to be 0.34 ns^{-1} with the combination of following equations (5) and (6):

$$\langle \tau_{\mathrm{Flu\bullet Tex}} \rangle = \frac{1}{k_1 + k_2} \tag{5}$$

$$E_{\mathrm{Flu\bullet Tex}} = 1 - \frac{\langle \tau_{\mathrm{Flu\bullet Tex}} \rangle}{\langle \tau_{\mathrm{Flu}} \rangle} \tag{6}$$

where $<\tau_{Flu\bullet Tex}>$ is the average of the fluorescence lifetime of the Flu moiety within Flu_5-Tex_1-apoHTHP^{T12C}. In this case, the energy transfer efficiency from Flu to Tex within Flu_5-Tex_1-apoHTHP^{T12C} ($E_{Flu\bullet Tex}$) is determined to be 42% (*vide supra*). k_3 is the rate of energy transfer from Flu to ZnPP, and calculated to be 0.85 ns^{-1} with following equation (7):

$$\langle \tau_{\mathrm{Flu\bullet ZnPP}} \rangle = \frac{1}{k_1 + k_3} \tag{7}$$

where $<\tau_{Flu\bullet ZnPP}>$ is used as the average fluorescence decay for the Flu moiety within Flu-rHTHP^{T12C} (Table. 2-2).

The relaxation of Tex also consists of two processes. One is the sum of the fluorescence and the non-radiative transition of Tex on the HTHP matrix and the rate was defined as k_4. k_4 was determined to be 0.43 ns^{-1} with the following equation (8):

$$\langle \tau_{\mathrm{Tex}} \rangle = \frac{1}{k_4} \tag{8}$$

where $<\tau_{Tex}>$ is the average of the fluorescence lifetime for the Tex moiety within Tex-apoHTHP (Figure 2-22 and Table 2-6). Another constant is represented by the energy transfer from Tex to ZnPP. The apparent rate of the energy transfer, k_5, was determined to be 0.15 ns^{-1} with the following combination of equations (9) and (10):

$$\langle \tau_{\mathrm{Tex \bullet ZnPP}} \rangle = \frac{1}{k_4 + k_5} \tag{9}$$

$$E_{\mathrm{Tex \bullet ZnPP}} = 1 - \frac{\langle \tau_{\mathrm{Tex \bullet ZnPP}} \rangle}{\langle \tau_{\mathrm{Tex}} \rangle} \tag{10}$$

where $<\tau_{Tex•ZnPP}>$ is the average of the fluorescence lifetime of the Tex moiety within Flu_5-Tex_1-$rHTHP^{T12C}$. The energy transfer efficiency from Tex to ZnPP within Flu_5-Tex_1-$rHTHP^{T12C}$, $E_{Tex•ZnPP}$, was determined to be 26% (Figure 2-19).[20] $<\tau_{Tex}>$ is the average of fluorescence decay for the Tex moiety on the HTHP matrix.

The relaxation of the excited ZnPP moiety consists of two processes. One is the sum of the fluorescence and the non-radiative transition of the excited ZnPP in the HTHP matrix and the rate was defined as k_6. k_6 was determined to be 1.05 ns^{-1} with following equation (11):

$$\langle \tau_{\mathrm{ZnPP}} \rangle = \frac{1}{k_6} \tag{11}$$

where $<\tau_{ZnPP}>$ is the average of the fluorescence lifetime for HTHP reconstituted with ZnPP (Figure 2-23 and Table2-7). Another constant is represented by the energy transfer from ZnPP to Tex within the HTHP matrix and the rate was defined as k_7. k_7 is the rate of energy transfer from the excited ZnPP at the S_1 state to Tex. This value cannot be calculated by comparing the two spectra in Figure 2-20b due to the severe overlap of spectra of the photosensitizers. Thus, the value of k_7 was calculated to be 0.86 ns^{-1} with the value of energy transfer efficiency from Flu to Tex within Flu_5-Tex_1-$rHTHP^{T12C}$ and the combination of following equations (12), (13), and (14):

$$E_1 = \left(\frac{k_2}{k_1 + k_2 + k_3}\right)\left(\frac{k_4}{k_4 + k_5}\right) \quad (12)$$

$$E_2 = \left(\frac{k_3}{k_1 + k_2 + k_3}\right)\left(\frac{k_7}{k_6 + k_7}\right) \quad (13)$$

$$E = E_1 + E_2 \quad (14)$$

where E_1 and E_2 are represented by energy transfer efficiency from Flu to Tex via paths 1 and 2, respectively. E is the energy transfer efficiency from Flu to Tex within Flu_5-Tex_1-rHTHP^{T12C} (*vide supra*). These results provide an estimation of the ratio of two energy transfer pathways from Flu to Tex within Flu_5-Tex_1-apoHTHP^{T12C} to be path 1:path 2 = 39:61.

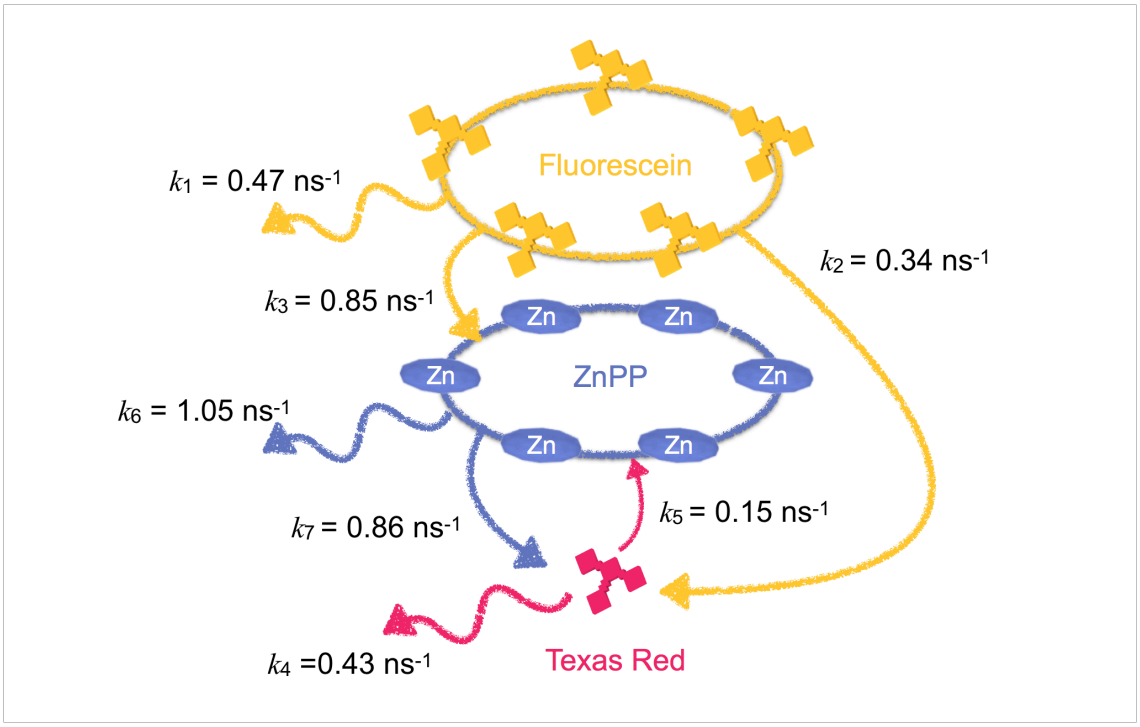

Figure 2-21. Energy transfer rate between photosensitizers within Flu_5-Tex_1-rHTHP^{T12C}.

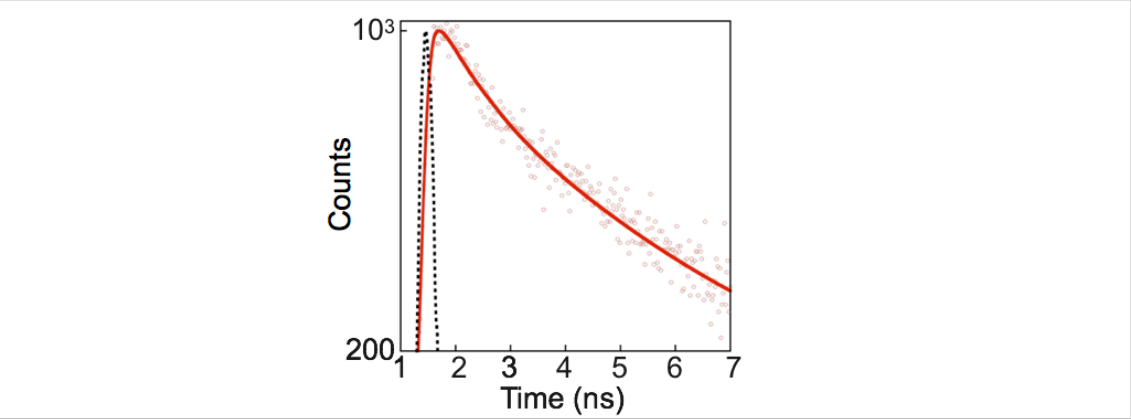

Figures 2-22. Time-resolved fluorescence decay profiles of Tex-apoHTHP^{T12C}. The instrument response is shown by the black broken line. Decay plots were analyzed by double-exponentially fitted curve (solid line): $y = y_0 + A_1\exp(-t/\tau_1) + A_2\exp(-t/\tau_2)$, where A and t are population and lifetime of the decay, respectively (Table 2-6). Conditions: [Tex-apoHTHP^{T12C} as a monomer] = 2 μM in 100 mM potassium phosphate buffer at pH 7.0 and 25 ˚C under a nitrogen atmosphere. λ_{ex} = 509 nm and λ_{em} = 613 nm.

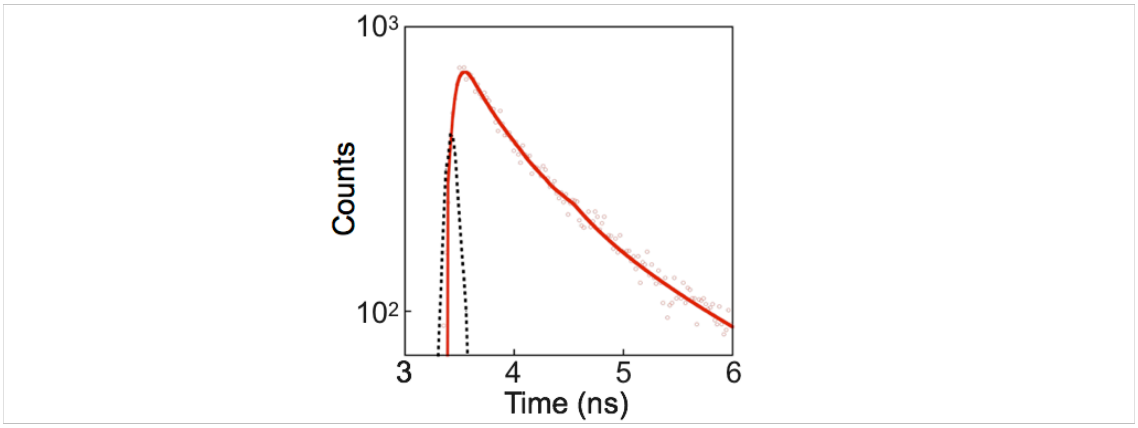

Figure 2-23. Time-resolved fluorescence decay profiles of wild type HTHP reconstituted with ZnPP (rHTHP). rHTHP is prepared by the same method as in chapter 1. The instrument response is shown by the black broken line. Decay plots were analyzed by a double-exponentially fitted curve (solid line): $y = y_0 + A_1\exp(-t/\tau_1) + A_2\exp(-t/\tau_2)$, where A and τ are population and lifetime of the decay, respectively (Table S1). Conditions: [rHTHP as a monomer] = 4 μM in 100 mM potassium phosphate buffer at pH 7.0 and 25 ˚C under a nitrogen atmosphere. λ_{ex} = 404 nm and λ_{em} = 592 nm.

Table 2-6. Decay parameters of Tex-apoHTHP^{T12C}

Protein	$<\tau>$ (ns) [a]	τ_1 (ns)	α_1 [b]	τ_2 (ns)	α_2 [b]	X^2
Tex-apoHTHP^{T12C}	2.33	0.628	0.378	3.36	0.622	1.004

[a] Average fluorescence lifetime determined by the sum of the $\alpha_i\tau_i$ products. [b] α is the population for each component. [c] λ_{ex} = 509 nm.

Table 2-7 Decay parameter of rHTHP

Protein	$<\tau>$ (ns)[a]	τ_1 (ns)	α_1 [b]	τ_2 (ns)	α_2 [b]	X^2
rHTHP	0.95	0.839	0.94	2.774	0.06	1.100

[a] Average fluorescence lifetime determined by the sum of the $\alpha_i\tau_i$ products. [b] α is the population for each component. [c] λ_{ex} = 404 nm.

2-3. Summary

The hexameric hemoprotein, HTHP, is employed as a scaffold for multiple photosensitizers attached to the protein via supramolecular and covalent conjugation. One of the advantages of this system is that it allows convenient attachment of two or three different photosensitizers into the proteins with a controlled ratio. Flu- and Tex-attached HTHPs reconstituted with ZnPP are found to exhibit energy transfer efficiency from Flu to ZnPP up to 65% and from ZnPP to Tex up to 34%, respectively. These findings indicate that Flu and Tex molecules work as a donor and acceptor moieties for ZnPP. Furthermore, in the Flu_5-Tex_1-rHTHP triad system, successive energy transfer from five Flu molecules to one Tex molecule via ZnPP was demonstrated, indicating collection of the photoenergy at the funnel-like bottom location of the Tex molecule (Figure 2-1c).

2-4 Experimental section

Instruments

UV-vis spectral measurements were carried out with a UV-2550 or UV-3150 double-beam spectrophotometer (Shimadzu), a V-670 UV-vis-NIR spectrophotometer (JASCO) or a BioSpec-nano spectrophotometer (Shimadzu). Fluorescence spectra were recorded with a JASCO FP-8600 fluorescence spectrophotometer. MALDI-TOF MS analysis was performed with a Bruker Daltonics Autoflex III mass spectrometer. The pH measurements were made with an F-52 Horiba pH

meter. Size exclusion column chromatography was performed using an ÄKTApurifier system equipped with a Superdex 200 Increase 10/300 GL column (GE Healthcare) at 4 ˚C. Air-sensitive manipulations were performed in a UNILab glove box (MBraun). Time-resolved fluorescence measurements were carried out using a picosecond fluorescence lifetime measurement system C11200 equipped with a picosecond light pulser PLP-10 as an excitation light source (Hamamatsu Photonics). Fluorescence quantum yield measurements were carried out with Quantaurus-QY C11347-01 (Hamamatsu Photonics).

Chemicals

ZnPP was prepared with same methods as in chapter 1. Ultrapure water (Milli-Q) was using a Millipore Integral 3 apparatus. Fluorescein-5-maleimide and Texas Red C_2 maleimide were purchased from TCI and Thermo Fischer Scientific, respectively. Other all reagents were of the highest guaranteed grade commercially available and were used as received unless otherwise indicated.

Protein sequences of HTHP mutants

$HTHP^{T12C}$;

SETWLPTLVTACPQEGFDLAVKLSRIAVKKTQPDAQVRDTLRAVYEKDANALIAVSAVVAT HFQTIAAANDYWKD

$HTHP^{D18C}$;

SETWLPTLVTATPQEGFCLAVKLSRIAVKKTQPDAQVRDTLRAVYEKDANALIAVSAVVAT HFQTIAAANDYWKD

$HTHP^{K29C}$;

SETWLPTLVTATPQEGFDLAVKLSRIAVCKTQPDAQVRDTLRAVYEKDANALIAVSAVVAT HFQTIAAANDYWKD

Expression and purification of HTHP mutants

The gene expression system for wild type HTHP was shown in chapter 1. Site-directed mutagenesis was performed by the polymerase chain reaction (PCR) using the LA PCR in vitro Mutagenesis Kit (Takara) according to the protocol of the manufacturer. The HTHP gene cloned into pDEST14 was used as a template to introduce T12C, D18C, or K29C single mutations into the HTHP matrix. The primer sequences used to generate each mutant were are:

T12C: (5'-GTTACCGACGTTGGTAACCGCATGCCCGCAGGAAGGCTTTGAT C-3') and the

complementary primer;

D18C: (5'-GCAACACCGCAGGAAGGCTTTTGCCTGGCCGTGAAACTGTCG CGC-3') and the complementary primer;

K29C: (5'-GAAACTGTCGCGCATTGCGGTCTGCAAAACCCAGCCAGATGC CC-3') and the complementary primer.

After PCR, the template DNA plasmids were digested with Dpn I (Thermo Fisher Scientific). *E. coli* DH5a competent cells were transformed with the PCR products. After the cultivation, the plasmids were purified with PureLink™ Quick Plasmid Miniprep Kit (Thermo Fisher Scientific). DNA sequencing was performed to verify each correct mutation in the gene sequence. The resulting expression plasmid was used to transform *E. coli* BL21 (DE3). LB medium (4 L) containing ampicillin (400 mg) was inoculated with 50 mL of the culture (OD = 0.5) of the transformed cells. After the cells were grown aerobically with vigorous shaking at 37 ˚C until the OD_{600} reached ~0.5, isopropyl-β-D-1-thiogalactopyranoside (IPTG, 1 mM as a final concentration) was added to the culture for induction of protein expression. The culture was continued at 37 ˚C overnight. The cells were harvested by centrifugation at 3200 x g for 10 min. The harvested cells from 4 L of culture were re-suspended in ca. 50 mL of a 10 mM Tris-HCl buffer, pH 8.0, and lysed by freeze-thaw cycles with subsequent sonication for 30 sec x 10 times at 4 ˚C. The lysate was then centrifuged and the supernatant was collected. The solution was incubated at 80 ˚C for 10 min and the precipitate was removed by centrifuge. The solution was loaded onto a DEAE Fast Flow (GE Healthcare) anion-exchange column pre-equilibrated with 10 mM potassium phosphate buffer at pH 6.0. The fraction of the target protein was collected by a 10 mM potassium phosphate buffer at pH 6.0 containing 0.3 M NaCl and 10 mM dithiothreitol (DTT). The obtained solution was concentrated using an Amicon stirred ultrafiltration cell with a 30-kDa molecular weight cut-off membrane (Millipore). The concentrated solution was passed through a Sephacryl S-200 column equilibrated with 100 mM potassium phosphate buffer at pH 7.0. The fractions with $R_z > 2$ (R_z is a ratio of absorbance values at 402 nm and 280 nm) were collected and concentrated. The obtained Cys-introduced HTHP mutants ($HTHP^{Cys}$ mutants) were characterized by SDS-PAGE and MALDI-TOF MS (Table 2-1), and stored at –80 ˚C.

Analytical SEC measurements

For SEC analysis, 100 mM potassium phosphate buffer at pH 7.0 was used as an eluent. The analysis was performed at 4 ˚C at a flow rate of 0.5 $mLmin^{-1}$ with monitoring of the absorbance at 280, 402, 495 or 593 nm for detection. The Superdex 200 Increase 10/300 GL column was calibrated

using the following reagents: Blue Dextran (2000 kDa, used to determine the void volume of the column), ferritin (400 kDa), catalase (232 kDa), albumin (67 kDa), and chymotrypsinogen (25 kDa).

Preparation of fluorescein-attached HTHP

The $HTHP^{Cys}$ mutants were reduced by 20 mM DTT and purified using the Superdex 200 Increase 10/300 GL column (eluent: 100 mM potassium phosphate buffer at pH 7.0 and 4 ˚C). A dimethylsulfoxide (DMSO) solution of fluorescein-5-maleimide (2.3 mM, 260 μL) was added to a solution of each mutant (100 μM as a monomer, 2 mL) and mildly mixed for 2h at 4 ˚C. The excess dye was removed using a HiTrap desalting column and purified using the Superdex 200 Increase 10/300 GL column (eluent: 100 mM potassium phosphate buffer at pH 7.0 and 4 ˚C). The obtained protein was characterized by analytical SEC measurements, UV-vis spectroscopy, and MALDI-TOF MS (Figure 2-4, 2-7 and Table 2-1).

Preparation of Texas Red-attached $HTHP^{T12C}$

$HTHP^{T12C}$ was reduced by 20 mM DTT and purified by Superdex 200 Increase 10/300 GL column (eluent: 100 mM potassium phosphate buffer at pH 7.0 and 4 ˚C). A DMSO solution of Texas Red C_2 maleimide (2.0 mM, 300 μL) was added to a solution of $HTHP^{T12C}$ (100 μM equivalent as a monomer, 2.0 mL) and mildly mixed for 2h at 4 ˚C. Excess dye was removed by HiTrap desalting column and purified by Superdex 200 Increase 10/300 GL column (eluent: 100 mM potassium phosphate buffer at pH 7.0 and 4 ˚C). The obtained protein was characterized by UV-vis spectroscopy (Figure 2-7, 2-13a, and 2-18a) and MALDI-TOF MS.

Preparation of fluorescein- and Texas Red-attached HTHP

$HTHP^{T12C}$ was reduced by 20 mM DTT and purified with the Superdex 200 Increase 10/300 GL column (eluent: 100 mM potassium phosphate buffer at pH 7.0 and 4 ˚C) to reduce all cysteine residues in the HTHP matrix. A 10 mM potassium ferricyanide solution was added to a solution of $HTHP^{T12C}$ and mildly mixed for 2h at room temperature. The disulfide dimer of $HTHP^{T12C}$ was purified with the Superdex 200 Increase 10/300 GL column (eluent: 100 mM potassium phosphate buffer at pH 7.0 and 4 ˚C). A DMSO solution of fluorescein-5-maleimide (2.3 mM, 50 μL) was added to the solution of $HTHP^{T12C}$ dimer (30 μM, 2.0 mL) and mildly mixed for 2h at 4 ˚C. Excess Flu derivative was removed with the Superdex 200 Increase 10/300 GL column (eluent: 100 mM potassium phosphate buffer at pH 7.0 and 4 ˚C). Reductive cleavage of the disulfide bond in the obtained dimer using 20 mM DTT in 100 mM potassium phosphate buffer at pH 7.0 and 50 ˚C,

yielded five Flu moieties-attached $HTHP^{T12C}$ each possessing one unreacted cysteine residue. The obtained protein (15 μM, 3.0 mL) in 100 mM potassium phosphate buffer at pH 7.0 and Texas Red C_2 maleimide in DMSO (2.0 mM, 12 μL) were mildly mixed to afford $HTHP^{T12C}$ which has five Flu moieties and one Tex moiety attached (Flu_5-Tex_1-$HTHP^{T12C}$). Flu_5-Tex_1-$HTHP^{T12C}$ was purified using the Superdex 200 Increase column 10/300 GL (eluent: 100 mM potassium phosphate buffer at pH 7.0 and 4 ˚C). The obtained protein was characterized by UV-vis spectroscopy and MALDI-TOF MS.

Preparation of fluorescein-attached apoHTHP, Texas Red-attached apoHTHP, and fluorescein- and Texas Red-attached apoHTHP

Removal of heme was performed using Teale's method[12] as follows: a solution of Flu- and/or Tex-attached HTHP (20 μM as a monomer) in 200 mM of L-histidine solution at 4 ˚C was acidified to pH 1.7 by addition of 1 M HCl_{aq}. Unbound heme was extracted with 2-butanone (5 times) and the solution was neutralized by dialysis with 100 mM potassium phosphate buffer at pH 7.0 and 4 ˚C (4 times). The obtained apo-form of each protein was lyophilized and stored under a nitrogen atmosphere at 4 ˚C.

Reconstitution of fluorescein-attached HTHP, Texas Red-attached HTHP, and fluorescein- and Texas Red-attached HTHP with ZnPP

One equivalent of ZnPP (0.6 mM, 3.3 μL) in DMSO was added to a solution of the apo-form of Flu- and/or Tex-attached HTHP (1.0 μM, 2.0 mL) in 100 mM potassium phosphate buffer at pH 7.0 and incubated for 2 h at 25 ˚C under a nitrogen atmosphere. Completion of reconstitution was confirmed by UV-vis spectroscopy.

Titration experiments of ZnPP to fluorescein-attached apoHTHP, Texas Red-attached apoHTHP, and fluorescein- and Texas Red-attached apoHTHP

Various equivalents of ZnPP in a DMSO solution were added to a cuvette containing a solution of the apo-form of Flu- and/or Tex-attached HTHP in 100 mM potassium phosphate buffer at pH 7.0 and 25 ˚C. UV-vis spectra were measured after standing for 2 h under a nitrogen atmosphere (Figure 2-6, 2-13c, and 2-18c).

References and notes

1 (a) G. D. Scholes, G. R. Fleming, A. Olaya-Castro and R. van Grondelle, *Nat. Chem.*, 2011, **3**, 763–774; (b) G. McDermott, S. M. Prince, A. A. Freer, A. M. Hawthornthwaite-Lawless, M. Z. Papiz, R. J. Cogdell and N. W. Isaacs, *Nature*, 1995, **374**, 517–521; (c) T. Pullerits and V. Sundström, *Acc. Chem. Res*., 1996, **29**, 381–389.

2 (a) R. van Grondelle and V. I. Novoderezhkin, *Phys. Chem. Chem. Phys.*, 2006, **8**, 793–807; (b) R. J. Cogdell, A. Gall and J. Köhler, *Quarterly Reviews of Biophysics*, 2006, **39**, 227–324.

3 (a) N. Nagata, Y. Kuramochi and Y. Kobuke, *J. Am. Chem. Soc.*, 2009, **131**, 10−11; (b) P. Parkinson, C. E. I. Knappke, N. Kamonsutthipaijit, K. Sirithip, J. D. Matichak, H. L. Anderson and L. M. Herz, *J. Am. Chem. Soc.*, 2014, **136**, 8217−8220; (c) N. Aratani, D. Kim and A. Osuka, *Acc. Chem. Res.*, 2009, **42**, 1922−1934; (d) P. D. Frischmann, K. Mahata and F. Würthner, *Chem. Soc. Rev*., 2013, **42**, 1847−1870; (e) R. Ziessel and A. Harriman, *Chem. Commun.*, 2011, **47**, 611–631; (f) M.-S. Choi, T. Yamazaki, I. Yamazaki, and T. Aida, *Angew. Chem. Int. Ed.*, 2004, **43**, 150–158; (g) S. Fukuzumi, K. Ohkubo and T. Suenobu, *Acc. Chem. Res.*, 2014, **47**, 1455–1464.

4 Y. Ishida, T. Shimada, D. Masui, H. Tachibana, H. Inoue and S. Takagi, *J. Am. Chem. Soc.*, 2011, **133**, 14280–14286.

5 (a) C. F. Calver, K. S. Schanze and G. Cosa, *ACS Nano*, 2016, **10**, 10598–10605; (b) Y. Sun, F. Guo, T. Zuo, J. Hua and G. Diao, *Nat. Commun.*, 2016, **7**, 12042; (c) P. Duan, N. Yanai, H. Nagatomi and N. Kimizuka, *J. Am. Chem. Soc.*, 2015, **137**, 1887–1894.

6 H. Son, S. Jin, S. Patwardhan, S. J. Wezenberg, N. C. Jeong, M. So, C. E. Wilmer, A. A. Sarjeant, G. C. Schatz, R. Q. Snurr, O. K. Farha, G. P. Wiederrecht and J. T. Hupp, *J. Am. Chem. Soc.*, 2013, **135**, 862−869.

7 (a) T. Miyatake and H. Tamiaki, *Coord. Chem. Rev.*, 2010, **254**, 2593–2602; (b) S. Sengupta and F. Würthner, *Acc. Chem. Res.*, 2013, **46**, 2498–2512; (c) M. R. Wasielewski, *Acc. Chem. Res.*, 2009, **42**, 1910–1921; (d) C. D. Bösch, S. M. Langenegger and R. Häner, *Angew. Chem. Int. Ed.*, 2016, **55**, 9961–9964_; (e) P.-Z. Chen, Y.-X. Weng, L.-Y. Niu, Y.-Z. Chen, L.-Z. Wu, C.-H. Tung and Q.-Z. Yang, *Angew. Chem. Int. Ed.*, 2016, **55,** 2759–2763; (f) T. S. Balaban, *Acc. Chem. Res.*, 2005, **38**, 612–623.

8 (a) P. K. Dutta, R. Varghese, J. Nangreave, S. Lin, H. Yan and Y. Liu, *J. Am. Chem. Soc.*, 2011, **133**, 11985–11993; (b) C. V. Kumar and M. R. Duff, *J. Am. Chem. Soc.*, 2009, **131**, 16024–16026.

9 (a) I. Cohen-Ofri, M. van Gastel, J. Grzyb, A. Brandis, I. Pinkas, W. Lubitz and D. Noy, *J. Am. Chem. Soc.*, 2011, **133**, 9526–9535; (b) T. Koshiyama, M. Shirai, T. Hikage, H. Tabe, K. Tanaka, S. Kitagawa and T. Ueno, *Angew. Chem. Int. Ed.*, 2011, **50**, 4849–4852; (c) J. W. Springer, P. S. Parkes-Loach, K. R. Reddy, M. Krayer, J. Jiao, G. M. Lee, D. M. Niedzwiedzki, M. A. Harris, C. Kirmaier, D. F. Bocian, J. S. Lindsey, D. Holten and P. A. Loach, *J. Am. Chem. Soc.*, 2012, **134**, 4589–4599; (d) A. Kuki and S. G. Boxer, *Biochemistry*, 1983, **22**, 2923–2933; (e) F. A. Tezcan, B. R. Crane, J. R. Winkler and H. B. Gray, *Proc. Natl. Acad. Sci. U. S. A.*, 2001, **98**, 5002–5006.

10 (a) R. A. Miller, A. D. Presley and M. B. Francis, *J. Am. Chem. Soc.*, 2007, **129**, 3104–3109; (b) L. S. Witus and M. B. Francis, *Acc. Chem. Res.*, 2011, **44**, 774–783; (c) M. Endo, M. Fujitsuka and T. Majima, *Chem. Eur. J.*, 2007, **13**, 8660–8666; (d) Y. S. Nam, T. Shin, H. Park, A. P. Magyar, K. Choi, G. Fantner, K. A. Nelson and A. M. Belcher, *J. Am. Chem. Soc.*, 2010, **132**, 1462–1463.

11 J.-H. Jeoung, D. A. Pippig, B. M. Martins, N. Wagener and H. Dobbek, *J. Mol. Biol.*, 2007, **368**, 1122–1131.

12 F. W. J. Teale, *Biochim. Biophys. Acta*, 1959, **35**, 543.

13 It is unsuitable to determine the energy transfer efficiency from Flu to ZnPP within Flu-rHTHP^{Cys} mutants by comparison of the absorption and excitation spectra because the fluorescence bands of Flu and ZnPP are found to overlap each other, and Φ_f of ZnPP is much smaller than that of Flu (Table 2-2).

14 J. R. Lakowicz, *Principles of Fluorescence Spectroscopy*, 2nd ed., Springer, New York, 1999.

15 As shown in Fig. 2-9, fluorescence bands of the attached Flu molecules in Flu-rHTHP^{Cys} mutants are overlapped with the fluorescence of ZnPP moieties around 600 nm. Thus, it is difficult to calculate the quenching efficiency values using areas of fluorescence band. The fluorescence bands of the Flu moiety of Flu-rHTHP^{Cys} mutants are fully consistent with the normalized fluorescence spectra of Flu-apoHTHP^{Cys} at the peak top, indicating that the area of fluorescence band has a linear relationship with the intensity. Hence, the peak top intensity was used instead of the area in equation (1) to calculate the quenching efficiency.

16 N. Marmé, J.-P. Knemeyer, M. Sauer and J. Wolfrum, *Bioconjugate Chem.*, 2003, **14**, 1133–1139.

17 G. Hungerford, J. Benesch, J. Mano and R. L. Reis, *Photochem. Photobiol. Sci.*, 2007, **6**, 152–158.

18 (a) A. J. Lee, A. A. Ensing, T. D. Krauss and K. L. Bren, *J. Am. Chem. Soc.*, 2010, **132**, 1752–1753; (b) R. M. Clegg, *Methods Enzymol.*, 1992, **211**, 353–388.

19 According to the spectra obtained by normalizing the area of the fluorescence profile with the fluorescence quantum yield for Tex-apoHTHP^{T12C} and rHTHP^{ZnPP}, the fluorescence intensity of ZnPP in the HTHP matrix is found to be 3% of Tex within Tex-apoHTHP^{T12C} at 615 nm. Hence, the contribution of the ZnPP fluorescence within Flu_5-Tex_1-rHTHP^{T12C} at 615 nm was negligible.

20 The $E_{Tex•ZnPP}$ value is evaluated by the fluorescence intensity changes of Tex with the following equation: $E_{Tex•ZnPP} = 1 - (I_{Tex•ZnPP} / I_{Tex})$, where $I_{Tex•ZnPP}$ and I_{Tex} are fluorescence intensity of Flu_5-Tex_1-rHTHP^{T12C} and Flu_5-Tex_1-apoHTHP^{T12C}, respectively (λ_{ex} = 593 nm, λ_{em} = 615 nm, Figure 2-19).

Chapter 3
Substitution of axial ligand from to enhance the peroxidase activity of HTHP

3-1. Introduction

Axially coordinated amino acid residues in the heme pocket of hemoprotein are a prime example of such protein matrix control.[1] In the case of horseradish peroxidase, the coordinated imidazole functional group of the histidine residue forms a hydrogen bond with an aspartic acid group to afford imidazolate-like coordination, which induces efficient formation of the high valent reactive intermediate, compound I species (Fe^{IV}-oxo porphyrin π-cation radical) in a reaction with hydrogen peroxide.[2] Cytochrome P450s, which are heme-dependent monooxygenases, employ cysteine as the axial ligand.[3] The strong push-effect and the radical character in the compound I species collectively enable highly efficient activation of inert C–H bonds. Tyrosine is axially coordinated to heme in catalase, which promotes the disproportionation of hydrogen peroxide.[4] The phenolate-type coordination to the heme provided by the tyrosine side chain also appears to provide a strong push-effect for the formation of a compound I species. Thus, the axial ligand is extremely important for regulating the reactivity of high-valent catalytic species and mutations focusing on axial ligands in hemoproteins have been investigated.[5]

Hexameric tyrosine-coordinated heme protein (HTHP) has a heme molecule in each subunit which is coordinated by Tyr45 as an axial ligand to form a five-coordinate structure. The peroxidase and catalase activities of HTHP are relatively low compared with typical peroxidase and catalase activities. In contrast to these enzymes, the heme in HTHP is highly exposed to solvent.[6] In chapter 3, the author focuses on proximal ligation of heme for modification of HTHP and demonstrate that substitution of the axial ligand from tyrosine to histidine enhances the peroxidase activity of HTHP (Figure 3-1).

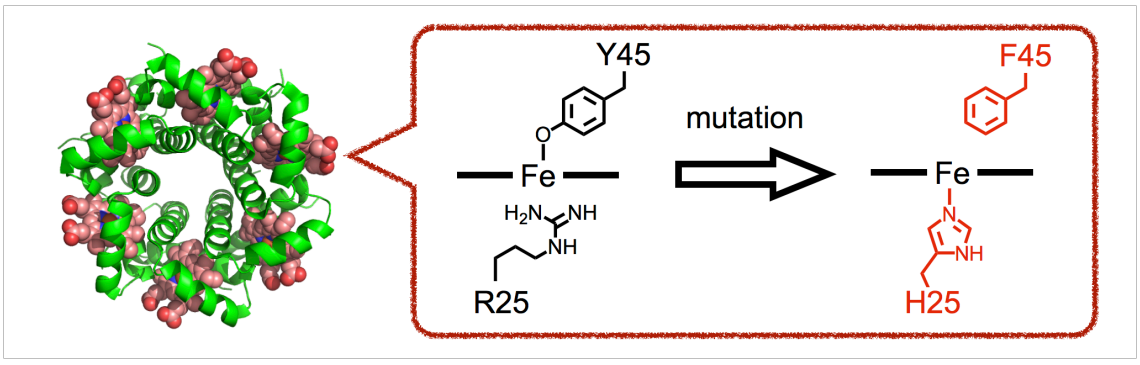

Figure 3-1. Schematic heme pocket structure of $HTHP^{WT}$ and $HTHP^{R25H/Y45F}$.

3-2. Results and discussion

Mutant design

The crystal structure of wild type HTHP ($HTHP^{WT}$) suggests that direct replacement of Tyr45, an axial ligand to the heme molecule in the protein, with His45 is inappropriate for constructing a His-coordinating hemoprotein because the distance between the heme Fe ion in heme and the α-carbon of the axially coordinated residue Tyr in the protein is significantly longer than the analogous distance observed in a series of His-coordinated hemoproteins. In contrast, it is found that Arg25 in the distal site of the heme pocket is relatively close to the heme iron: the distances from Cα (Tyr45) or Cα (Arg25) to Fe (heme) in $HTTP^{WT}$ are 8.5 and 5.8 Å, respectively (PDB ID: 2OYY[6]), whereas the distances from Cα (His93) or Cα (His64) to Fe (heme) in Mb are 6.6 and 8.6 Å, respectively (PDB ID: 1YMB[7]). Therefore, we prepared a double mutant HTHP ($HTHP^{R25H/Y45F}$) where Tyr45 and Arg25 were replaced with Phe45 and His25, respectively. As a result, the engineering allows swapping of proximal and distal sites in this hemoprotein as shown in Figure 3-1.

Purification and characterization of $HTHP^{R25H/Y45F}$

$HTHP^{R25H/Y45F}$ was expressed in a recombinant *E. coli* system and purified by ion exchange chromatography and SEC. The purity of $HTHP^{R25H/Y45F}$ isolated from cultured cells was confirmed by SDS-PAGE (Figure 3-2a). The band of $HTHP^{R25H/Y45F}$ was only at about 6 kDa, which is consistent with the molecular weight of the monomer of $HTHP^{R25H/Y45F}$. This is an expected result because $HTHP^{R25H/Y45F}$ disassembles to the apo-form monomer in the presence of SDS. ESI-TOF MS (Figure 3-2b) shows the desired mass numbers of the multiply ionized apo- and holo-forms of the monomer: found m/z = 2732.5 and 2938.3; calcd m/z = 2732.4 (z = 3+, apo-form) and 2938.2 (z = 3+, holo-form). The observed isotopic pattern of the apo-form (z = 3+) matched well with the simulated pattern. Dynamic light scattering measurements revealed a monodispersed species with a hydrodynamic diameter of 6.26 nm, which is consistent with the value expected from the reported crystal structure of $HTHP^{WT}$.[6] Support for the formation of the hexameric structure in solution is also provided by analytical SEC with several protein standards as shown in Figure 3-3: the elution volume of $HTHP^{R25H/Y45F}$ at 14.9 mL indicates a molecular weight of approximately 50 kDa. Furthermore, the SEC trace for $HTHP^{R25H/Y45F}$ monitored by measuring absorbance at 280 nm (for protein matrices) is clearly consistent with that monitored at 400 nm (for heme), indicating that the heme molecules are bound to the matrix of $HTHP^{R25H/Y45F}$.

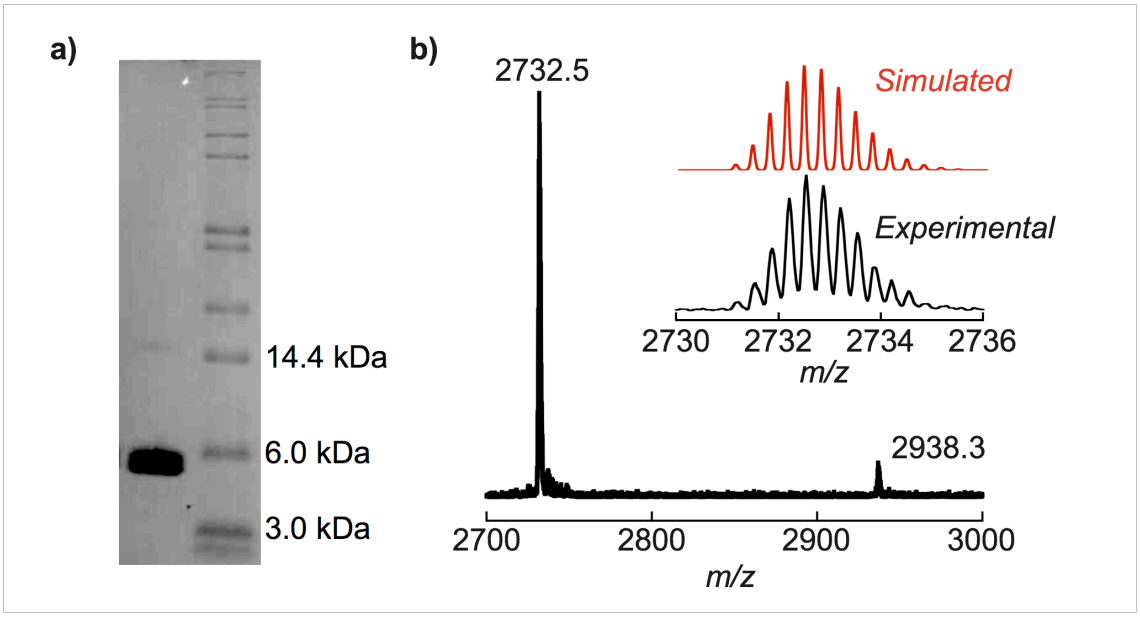

Figure 3-2. (a) SDS-PAGE electrophoretogram of HTHP$^{R25H/Y45F}$ (left lane) and several protein standard markers (right lane). (b) ESI-TOF mass spectrum of the monomer of HTHP$^{R25H/Y45F}$. The sample was dissolved in 10 mM NH_4OAc aqueous solution at pH 6.9. Multiply ionized species were observed: found *m/z* = 2732.5 and 2938.3; calcd *m/z* = 2732.4 (*z* = 3+, apo-form) and 2938.2 (*z* = 3+, holo-form). Inset: The simulated (red, upper) and experimental (black, lower) isotopic distribution patterns for $[C_{370}H_{582}N_{98}O_{112}]^{3+} + 3H^+$ (*z* = 3+, monomer of apo-form of HTHP$^{R25H/Y45F}$).

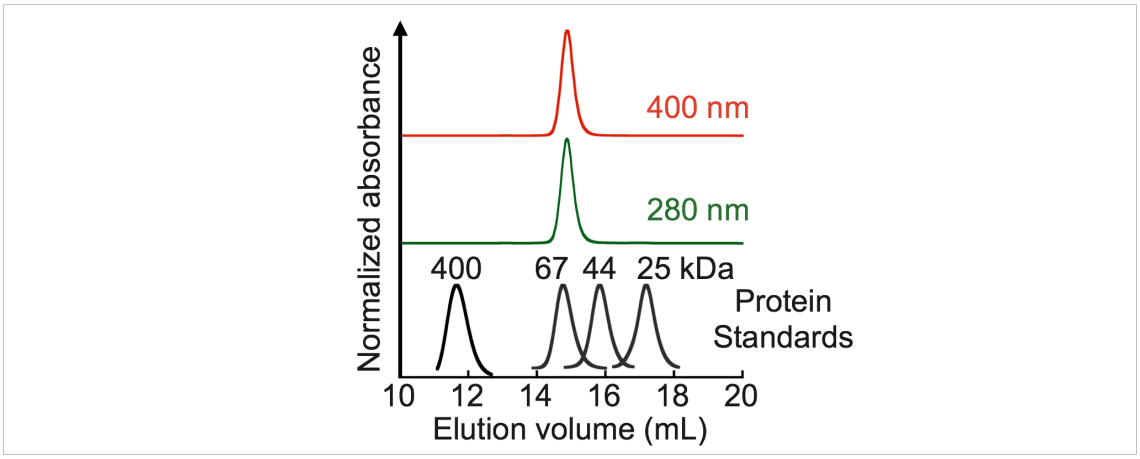

Figure 3-3. Analytical SEC traces of HTHP$^{R25H/Y45F}$ (red and green). The black traces were obtained by various protein standards. Red, green and black profiles were observed at 400, 280 and 280 nm, respectively.

UV-vis spectroscopic study

The UV-vis absorption spectra of several states of $HTHP^{R25H/Y45F}$ and $HTHP^{WT}$ are shown in Figure 3-4. The spectrum of as-isolated $HTHP^{R25H/Y45F}$ is almost identical to that of $HTHP^{WT}$, although the peak of the Q-band at 528 nm in $HTHP^{WT}$ is absent in the spectrum of $HTHP^{R25H/Y45F}$. Interestingly, a similar result has also been observed in the engineered heme-binding human serum albumin ($HSA^{I142H/Y161L}$) where the proximal and distal sites are swapped in a double mutation (Table 3-1).[5d,8] These findings support the evidence indicating that the heme pocket of $HTHP^{R25H/Y45F}$ provides a coordination environment which is similar to that of His-ligated heme-binding $HSA^{I142H/Y161L}$. Additionally, the characteristic features of the spectrum of $HTHP^{R25H/Y45F}$ are almost identical to those of wild type met-Mb with high-spin ferric heme, which has a His residue as an axial ligand. Reduction of $HTHP^{R25H/Y45F}$ upon addition of a small excess of $Na_2S_2O_4$ affords the characteristic red-shift of the Soret band (Figure. 3-4) which is seen for Mb and heme-binding $HSA^{I142H/Y161L}$, indicating the formation of deoxy $HTHP^{R25H/Y45F}$ which has a His-ligated five-coordinate structure.[8] Next, bubbling of CO into the sample of deoxy $HTHP^{R25H/Y45F}$ yields a sharp Soret band at 420 nm and two peaks in the Q-band region (Figuew 3-4 and Table 3-1). These are typical features of CO-ligated heme as seen in heme-binding $HSA^{I142H/Y161L}$ and Mb. The addition of potassium cyanide to ferric $HTHP^{R25H/Y45F}$ also produces clear spectral changes of the Soret and Q-band as shown in the formation of cyanide complex of met-Mb.[9] This behavior is sharply different from that observed for $HTHP^{WT}$: the wild type ferric protein with the Tyr ligand does not bind cyanide.[6] Taken together, these results indicate that the introduced His25 residue undoubtedly coordinates to the heme iron in the heme pocket of $HTHP^{R25H/Y45F}$, since $HTHP^{R25H/Y45F}$ does not have other accessible His residues in the protein matrix.

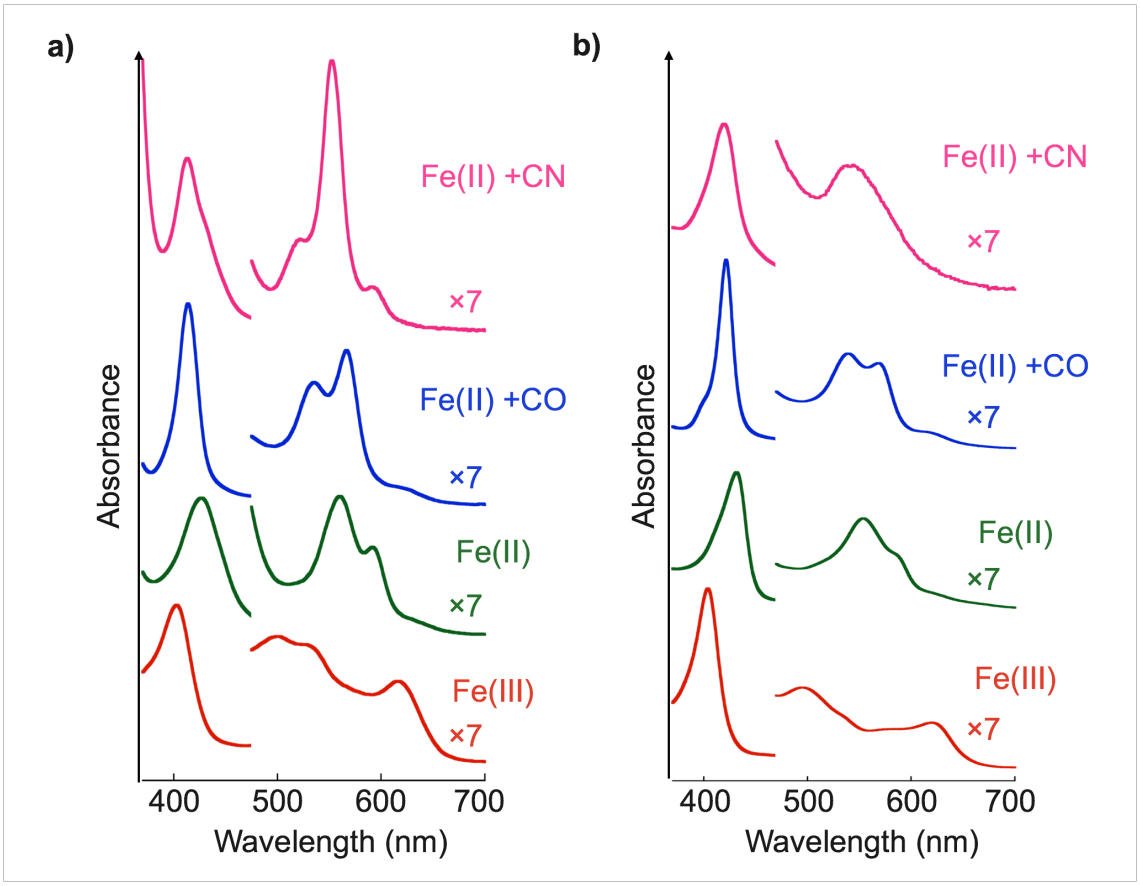

Figure 3-4. UV-vis absorption spectra of ferric, ferrous, CO- and CN-forms of (a) $HTHP^{WT}$ and (b) $HTHP^{R25H/Y45F}$.

Table 3-1. λ_{max} in the UV-vis absorption spectra of $HTHP^{WT}$, $HTHP^{R25H/Y45F}$ and reported hemoproteins

Protein	State	λ_{max} at Soret band (nm)	λ_{max} at Q-band (nm)
$HTHP^{WT}$	Fe^{3+}	402	501, 528, 616
	Fe^{2+}	431	560, 592
	Fe^{2+} + CO	420	535, 566
	Fe^{2+} + CN	413	523, 553, 591
$HTHP^{R25H/Y45F}$	Fe^{3+}	405	495, 620
	Fe^{2+}	432	554, 589(sh),
	Fe^{2+} + CO	421	539, 568, 615(sh)
	Fe^{3+} + CN	420	542
heme-binding HSA^{WT} [a]	Fe^{3+}	405	501, 534, 624
	Fe^{2+}	419	538, 559(sh), 570
	Fe^{2+} + CO	416	539, 568
heme-binding $HSA^{I142H/Y161L}$ [a]	Fe^{3+}	402	533, 620
	Fe^{2+}	426	531(sh), 559
	Fe^{2+} + CO	419	538, 565
Mb [a]	Fe^{3+}	409	503, 548(sh), 632
	Fe^{2+}	434	557
	Fe^{2+} + CO	423	541, 579

[a] Ref. 8

Reaction with cumene hydroperoxide

To evaluate the reaction behavior of ferric $HTHP^{R25H/Y45F}$ with hydroperoxide, the O–O bond cleavage of cumene hydroperoxide (CHPO) was investigated. In this reaction, it is known that two possible products, cumyl alcohol and acetophenone, are produced after protein-assisted heterolytic and homolytic cleavage of the O–O bond, respectively (Scheme 3-1). The product ratio (cumyl alcohol/acetophenone) provided by $HTHP^{R25H/Y45F}$ was determined to be 2.3 ± 0.3, whereas the ratio of Mb was reported to be 3.3.[10] The obtained lower ratio for $HTHP^{R25H/Y45F}$ indicates that approximately 1/3 heme-peroxide provides the oxoferryl species (Fe(IV)=O), compound II, via O–O bond homolysis. These findings suggest that the push-effect of the proximal His to the heme in

HTHP$^{R25H/Y45F}$ is lower than that of Mb. In contrast, it is found that HTHP^{WT} does not react with CHPO.

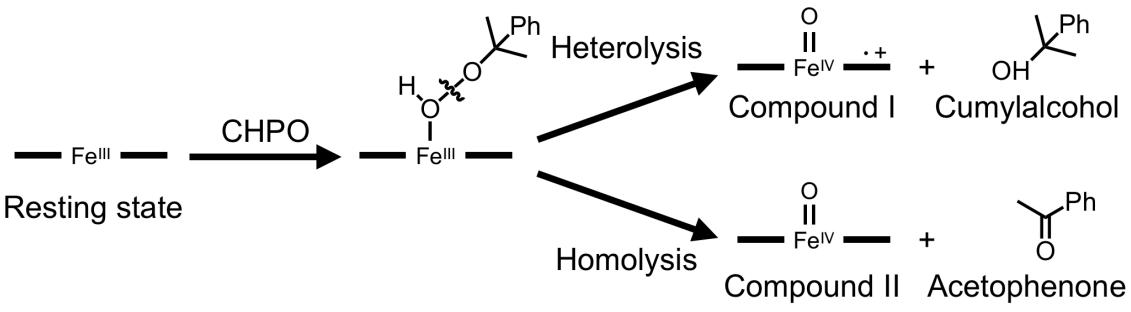

Scheme 3-1. Reaction of heme in HTHP with cumene hydroperoxide (CHPO).

Peroxidase activity of HTHP$^{R25H/Y45F}$

The steady-state kinetics of ABTS and guaiacol oxidation by HTHP$^{R25H/Y45F}$, and HTHP^{WT} horseradish peroxidase (HRP) were evaluated to understand the effects of the axial ligand substitution on peroxidase activity. After addition of H_2O_2 to a solution of HTHP$^{R25H/Y45F}$ or HTHP^{WT} containing the substrate, the absorbance changes derived from the resulting products were observed. The initial reaction rates (v) were used to determine the values of Michaelis-Menten kinetic parameters, k_{cat} and K_m (Figure 3-5, 3-7 and Table 3-2, 3-3).

The k_{cat} values of HTHP$^{R25H/Y45F}$ for ABTS and guaiacol oxidation (Scheme 3-1, 3-2) are 10- and 100-fold higher than those of HTHP^{WT}, respectively. It is possible that the improvement of the peroxidase activity is due to the substitution of the axial ligand. However, the k_{cat} value of HTHP$^{R25H/Y45F}$ was found to be much lower than that of HRP, primarily because HTHP$^{R25H/Y45F}$ lacks the imidazolate-formed proximal His and distal His supporting the H_2O_2 activation. The K_m values for the ABTS and guaiacol oxidation reactions with HTHP$^{R25H/Y45F}$ are only 3-fold lower and higher than those of HTHP^{WT}, respectively. The present modification of HTHP does not significantly affect the affinity between the substrates and protein. The values of overall catalytic efficiency, k_{cat}/K_m, of HTHP$^{R25H/Y45F}$ are 30-fold higher than that of HTHP^{WT} for both substrates, suggesting that the replacement of the tyrosine axial ligand with histidine clearly enhances peroxidase activity of HTHP^{WT}.

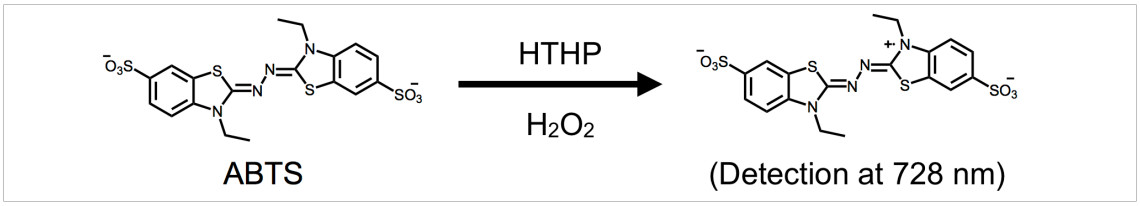

Scheme 3-2. H_2O_2-dependent ABTS oxidation mediated by HTHP.

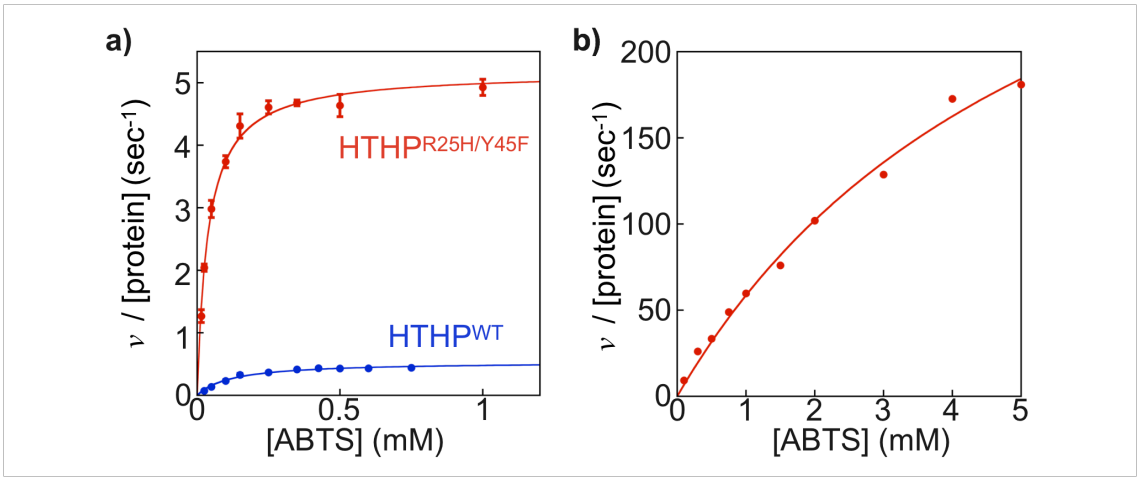

Figure 3-5. Michaelis-Menten plots for ABTS oxidations catalyzed by (a) HTHP$^{R25H/Y45F}$ (red) and HTHP^{WT} (blue) and (b) HRP. Conditions: [protein] = 1 μM, [H_2O_2] = 5 mM in 100 mM potassium phosphate buffer at pH 7.0 and 25 ˚C.

Table 3-2. Kinetic parameters of HTHP^{WT} and HTHP$^{R25H/Y45F}$ from the Michaelis-Menten equation for the oxidation of ABTS [a]

Protein	k_{cat} (s^{-1})	K_m (mM)	k_{cat}/K_m ($mM \cdot s^{-1}$)
HTHP^{WT}	0.54	0.12	4.5
HTHP$^{R25H/Y45F}$	5.2	3.8×10^{-2}	1.4×10^{2}
HRP	4.0×10^{2}	5.8	5.1×10^{3}

[a] Reaction conditions: [protein] = 1 μM, [H_2O_2] = 5 mM, [ABTS] = 0.05 to 1 mM in 100 mM potassium phosphate buffer at pH 7.0 and 25 ˚C.

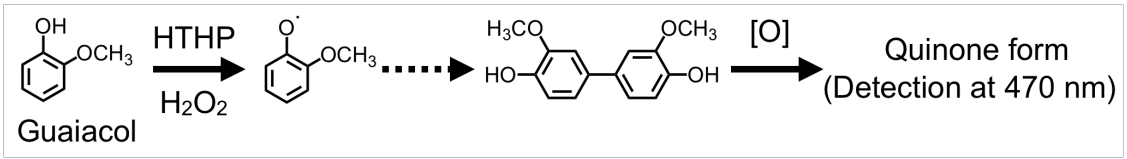

Scheme 3-3. H_2O_2-dependent guaiacol oxidation mediated by HTHP.

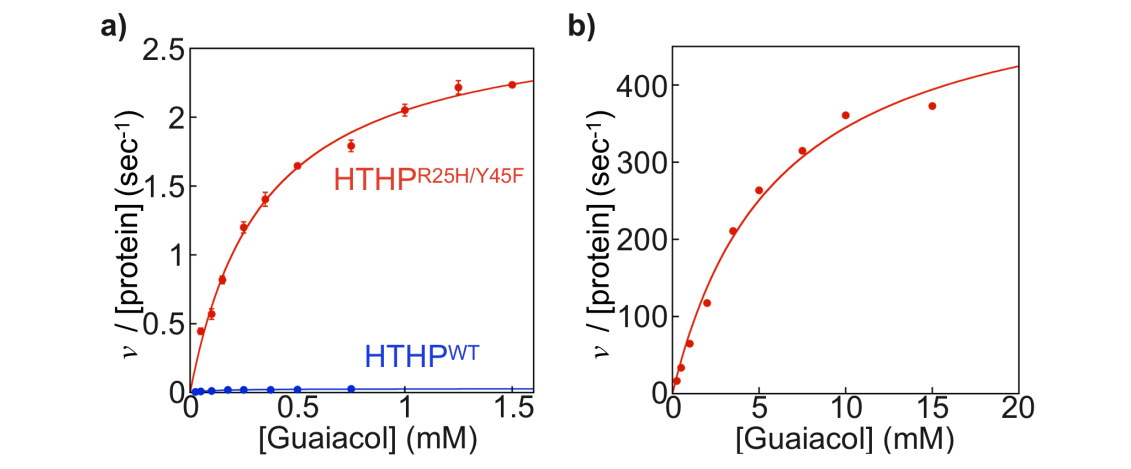

Figure 3-7. Michaelis-Menten plots for Guaiacol oxidations catalyzed by (a) $HTHP^{R25H/Y45F}$ (red) and $HTHP^{WT}$ (blue) and (b) HRP. Conditions: [protein] = 1 μM, [H_2O_2] = 5 mM in 100 mM potassium phosphate buffer at pH 7.0 and 25 ˚C.

Table 3-3. Kinetics parameters of $HTHP^{WT}$ and $HTHP^{R25H/Y45F}$ from the Michaelis-Menten equation for the oxidation of guaiacol [a]

Protein	k_{cat} (s^{-1})	K_m (mM)	k_{cat}/K_m ($mM \cdot s^{-1}$)
$HTHP^{WT}$	3.0×10^{-2}	0.11	0.27
$HTHP^{R25H/Y45F}$	2.8	0.34	8.1
HRP[b]	5.5×10^{2}	6.0	92

[a] Reaction conditions: [protein] = 1 μM, [H_2O_2] = 5 mM, [Guaiacol] = 0.05 to 1.5 mM in 100 mM potassium phosphate buffer at pH 7.0 and 25 ˚C.

Sulfoxidation activity of $HTHP^{R25H/Y45F}$

To evaluate the two-electron oxidation ability of $HTHP^{R25H/Y45F}$ and $HTHP^{WT}$, thioanisole was employed as a substrate for an H_2O_2-dependent sulfoxidation reaction (Scheme 3-4). The turnover

numbers of HTHP$^{R25H/Y45F}$ and HTHP^{WT} were found to be 43 and 23, respectively, at pH 7.0 (Table 3-4). Over-oxidation products such as sulfone were not detected after 12 h. These results indicate that axial-ligand substitution in HTHP is also effective for promotion of catalytic sulfoxidation.

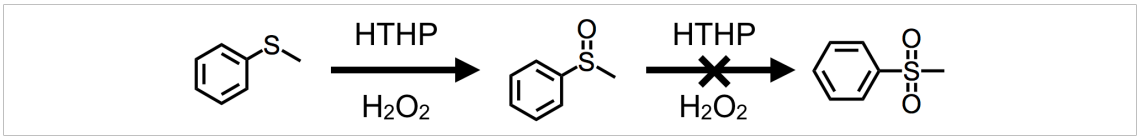

Scheme 3-4. H_2O_2-dependent thioanisole oxidation catalyzed by HTHP^{WT} and HTHP$^{R25H/Y45F}$.

Table 3-4. Turnover numbers for thioanisole sulfoxidation catalyzed by HTHP^{WT} and HTHP$^{R25H/Y45F}$

Protein	Turnover number
HTHP^{WT}	23
HTHP$^{R25H/Y45F}$	43

3-3. Summary

To convert an originally tyrosine-coordinated heme to histidine-coordinated heme in hexameric tyrosine-coordinated hemoprotein, HTHP, Tyr45, a residue coordinating to the heme cofactor, and Arg25 located in the distal site are replaced with Phe45 and His25, respectively in each of the subunits of the protein. The obtained HTHP mutant (HTHP$^{R25H/Y45F}$) maintains its stable hexameric structure with the altered ligation of each of the heme cofactors. Comparison of UV-vis absorption spectra of the ferric-, ferrous-, CO- and CN-forms of HTHP$^{R25H/Y45F}$ with those of several well-known His-ligated hemoproteins indicates that heme is coordinated by the His25 residue. Peroxidase activity of HTHP$^{R25H/Y45F}$ is found to follow Michaelis–Menten kinetics. The k_{cat} values of HTHP$^{R25H/Y45F}$ for H_2O_2-dependent oxidation of ABTS and guaiacol are 10- and 100-fold higher, respectively, than those of wild type HTHP (HTHP^{WT}). The k_{cat}/K_m values of HTHP$^{R25H/Y45F}$ for both substrates are increased 30-fold relative to that of HTHP^{WT}. Moreover, HTHP$^{R25H/Y45F}$ is capable of promoting catalytic sulfoxidation of thioanisole with H_2O_2 with a turnover number ca. 2-fold higher than that of HTHP^{WT}. The present findings demonstrate that proximal His ligation to the heme is significantly effective to increase the peroxidase activity in the HTHP matrix.

3-4. Experimental section

Instruments

UV-vis spectral measurements were carried out with a UV-2700 double-beam spectrophotometer (Shimadzu), a V-670 UV-vis-NIR spectrophotometer (JASCO) or a BioSpec-nano spectrophotometer (Shimadzu). ESI-TOF MS analysis was performed with a Bruker Daltonics micrOTOF-II mass spectrometer. The pH measurements were made with an F-52 Horiba pH meter. Size exclusion chromatography was performed using an ÄKTApurifier system equipped with a Superdex 200 Increase 10/300 GL column (GE Healthcare) at 4 ˚C. Dynamic light scattering was measured using a Malvern Zetasizer μV light scattering analyzer with an 830 nm laser at 25 ˚C. HPLC analysis was conducted with a Shimadzu HPLC Prominence system equipped with a YMC-Triart C18 column (150 × 4.6 mm I.D.). The measurements for evaluation of peroxidase activity were conducted with a rapid scan stopped-flow system (Unisoku) using a Xe or halogen light source. The GC/FID measurements were made with a Shimadzu GC-2010 gas chromatography system.

Materials

Ultrapure water (Milli-Q) was prepared using a Millipore Integral 3 apparatus. Other all chemicals were of the highest guaranteed grade commercially available and were used as received unless otherwise indicated. Mb and HRP were purchased from Sigma Aldrich and Wako, respectively.

Amino acid sequence of the monomers of HTHP^{WT} and HTHP$^{R25H/Y45F}$

HTHP^{WT};

SETWLPTLVTATPQEGFDLAVKLSRIAVKKTQPDAQVRDTLRAVYEKDANALIAVSAVVAT
HFQTIAAANDYWKD

HTHP$^{R25H/Y45F}$;

SETWLPTLVTATPQEGFDLAVKLSHIAVKKTQPDAQVRDTLRAVFEKDANALIAVSAVVAT
HFQTIAAANDYWKD

Expression and purification of HTHP$^{R25H/Y45F}$

The gene expression system for HTHP^{WT} was reported in chapter 1. Site-directed mutagenesis was performed using the polymerase chain reaction (PCR) and the LA PCR *in vitro* Mutagenesis Kit (Takara) according to the manufacturer's protocol. The HTHP gene cloned into pDEST14 was used

as a template to introduce mutations into the HTHP matrix with primers (5-5i). After PCR, the template DNA plasmids were digested with Dpn I (Thermo Fisher Scientific). *E. coli* DH5α competent cells were transformed with the PCR products. After cultivation, the plasmids were purified with PureLink™ Quick Plasmid Miniprep Kit (Thermo Fisher Scientific). The obtained plasmid was further used as a template for site-directed mutagenesis with the primers (ii). The desired plasmid containing the gene for the double mutant of HTHP (R25H/Y45F) was obtained using the same method.

DNA sequencing was performed to verify each correct mutation in the gene sequence.

The primer sequences used to generate the mutant were:

(i) R25H: (5'- GGCCGTGAAACTGTCGCACATTGCGGTCAAGAAAAC -3') and the complementary primer;

(ii) Y45F: (5'- GCGATACTCTCCGTGCTGTGTTCGAGAAAGATGCGAATGCGC
TG -3') and the complementary primer.

The resulting expression plasmid was used to transform *E. coli* BL21 (DE3). LB medium (4 L) containing ampicillin (400 mg) was inoculated with 50 mL of the culture (OD = 0.5) of the transformed cells. After the cells were grown aerobically with vigorous shaking at 37 ˚C until OD600 was reached ~0.5, isopropyl-β-D-1-thiogalactopyranoside (IPTG, final concentration: 1 mM) was added to the culture for induction of protein expression. The culture was continued at 37 ˚C overnight. The cells were harvested by centrifugation at 4000xg for 10 min. The harvested cells from 4 L of culture were re-suspended in ca. 50 mL of a 10 mM Tris-HCl buffer, pH 8.0, and lysed by freeze-thaw cycles with subsequent sonication for 30 sec x 10 times at 4 ˚C. The lysate was then centrifuged and the supernatant was collected. The solution was diluted 10-fold with 100 mM potassium phosphate buffer at pH 7.0 and loaded through a CM Fast Flow (GE Healthcare) cation-exchange column pre-equilibrated with 100 mM potassium phosphate buffer at pH 7.0. The flow-through solution was loaded onto a DEAE Fast Flow (GE Healthcare) anion-exchange column pre-equilibrated with 100 mM potassium phosphate buffer at pH 7.0. The fraction of the target protein was collected with a 100 mM potassium phosphate buffer at pH 7.0 containing 0.3 M NaCl. The obtained solution was concentrated using an Amicon stirred ultrafiltration cell with a 30-kDa molecular weight cut-off membrane (Millipore). The concentrated solution was passed through a Superdex 200 Increase 10/300 GL column with 100 mM potassium phosphate buffer at pH 6.0. The fractions with $R_z > 2$ (R_z is a ratio of absorbance values at 402 nm and 280 nm) were collected and loaded on a Hitrap Q HP 5 mL (GE Healthcare) anion-exchange column pre-equilibrated with 100 mM potassium phosphate buffer at pH 6.0. The fraction of the target protein was eluted with 100

mM potassium phosphate buffer at pH 6.0 containing 0.35 M NaCl. The obtained HTHP mutant ($HTHP^{R25H/Y45F}$) was characterized by SDS-PAGE (Figure 3-2a), ESI-TOF MS (Figure 3-2b), analytical size exclusion chromatography (Figure 3-3), and UV-vis spectroscopy (Figure 3-4a), and stored at –80 ˚C. The concentration of heme was determined by characteristic absorbance as a pyridine hemochrome complex (ε_{556} = 34.4 mM^{-1}•cm^{-1}). The extinction coefficient (ε_{405} = 111 mM^{-1}•cm^{-1}) of $HTHP^{R25H/Y45F}$ was determined from the plots of the absorbance at 405 nm of $HTHP^{R25H/Y45F}$ for the concentration of heme (Figure 3-8).

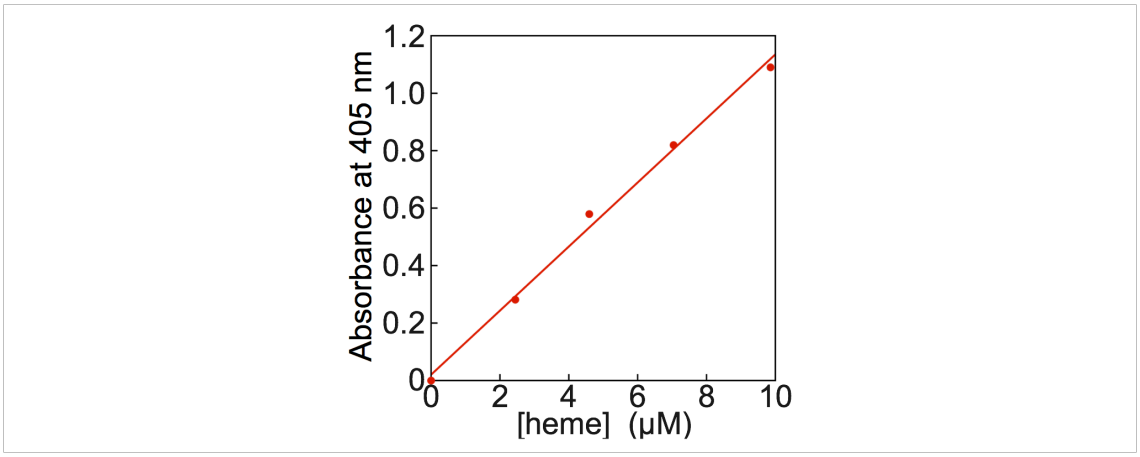

Figure 3-8. Plots of the absorbance of $HTHP^{R25H/Y45F}$ at 405 nm for the concentration of the heme molecule. The concentration of heme was determined using the pyridine hemochrome method.

Analytical size exclusion chromatography

For SEC analysis, 100 mM potassium phosphate buffer at pH 7.0 was used as an eluent. The analysis was performed at 4 ˚C and a flow rate of 0.5 $mL.min^{-1}$ with monitoring of the absorbance at 280 and 400 nm for detection. The Superdex 200 column was calibrated using the following reagents: ferritin (400 kDa), albumin (67 kDa), ovalbumin (40 kDa), and chymotrypsinogen (25 kDa).

Preparation of ferrous-, CO- and cyanide-forms of $HTHP^{WT}$ and $HTHP^{R25H/Y45F}$

To obtain the ferrous-forms of $HTHP^{WT}$ and $HTHP^{R25H/Y45F}$, a small excess amount of $Na_2S_2O_4$ was added to the protein solution. The CO-forms were prepared by bubbling the ferrous-form solutions with CO gas for 2 min. To solutions of ferrous-$HTHP^{WT}$ and ferric $HTHP^{R25H/Y45F}$ in 100 mM potassium phosphate buffer at pH 7.0 potassium cyanide solution was added (final concentration: 10 mM), giving cyanide-ferrous $HTHP^{WT}$ and cyanide-ferric $HTHP^{R25H/Y45F}$,

respectively.

Reaction of HTHP^{WT} and HTHP$^{R25H/Y45F}$ with cumene hydroperoxide

A cumene hydroperoxide, CHPO, solution was added to the protein solution ([protein] = 20 μM, [CHPO] = 2 mM, 100 μL) in 100 mM potassium phosphate buffer at pH 7.0 and 25 ºC for 2 h. The reaction mixture was filtered using a Millix®-GV filter (0.22 μm), and the filtrate was analyzed using an HPLC system equipped with a C18 column to determine the amounts of produced acetophenone and cumyl alcohol.

Peroxidase activity

A mixture of protein (2 μM) and substrate dissolved in 100 mM potassium phosphate buffer at pH 7.0 was incubated at 25 ˚C for 10 min. UV-vis spectral changes were recorded upon addition of H_2O_{2aq} (10 mM). The final concentrations of guaiacol or ABTS as a substrate were from 0.05 to 1.5 mM. After mixing the same volume (125 μL) of these two solutions, absorbance changes were recorded and the initial rates within 1 s were determined using the extinction coefficients of the oxidized products: ε_{470} = 26.6 mM^{-1}•cm^{-1} for guaiacol and ε_{728} = 15.0 mM^{-1}•cm^{-1} for ABTS. The plots of initial rates, v, per protein against substrate concentration were fitted with the following Michaelis–Menten equation to estimate the kinetic parameters for the oxidation reactions.

$$\frac{v}{[\text{protein}]} = \frac{k_{\text{cat}}[\text{substrate}]}{K_{\text{m}} + [\text{substrate}]}$$

Sulfoxidation of thioanisole

The reactions were carried out in 100 mM potassium phosphate buffer at pH 7.0 and 25 ºC. A buffer solution of protein and thioanisole was incubated prior to the addition of H_2O_2 to initiate the reaction. The final concentrations of each component was follows: [protein] = 10 μM, [thioanisole] = 2.0 mM and [H_2O_2] = 1 mM. After the reaction was complete at 12 h, benzyl alcohol as an internal standard and ether were added, and the reaction mixture was vigorously shaken using a vortex mixer to extract the organic materials. The separated organic phase was evaporated by N_2 gas flow, dissolved in CH_3CN and analyzed with a GC/FID system equipped with a DB-1 column.

3-5 References and notes

1. (a) J. H. Dawson, *Science*, 1988, **240**, 433–439. (b) T. L.Poulos, *J. Biol. Inorg. Chem.*, 1996, **1**, 356–359.
2. (a) H. B. Dunford and J. S. Stillman, *Coord. Chem. Rev.*, 1976, **19**, 187–251; (b) I. G, Berglund, H. G. Carlsson, T.A. Smith, H. Szöke, A. Henriksen and J. Hajdu, *Nature*, 2002, **417**. 463–468.
3. (a) R. P. Ortiz de Montellano, *Chem. Rev.*, 2010, **110**, 932–948; (b) G. I. Denisov, M. T. Makris, G. S. Sligar and I. Schlichting , *Chem. Rev.*, 2005, **105**, 2253−2277.
4. (a) M. Zamocky and F. Koller, *Progr. Biophys. Mol. Biol.*, 1999, **72**, 19–66; (b) I Fita and M. G. Rossmann, *J. Mol. Biol.*, 1985, **185**, 21–37.
5. (a) H. Sato, T. Hayashi, T. Ando, Y. Hisaeda, T. Ueno and Y. Watanabe, *J. Am. Chem. Soc.*, 2004, **126**, 436-437; (b) D. Barrick, *Biochemistry,* 1994, **33**, 6546–6554; (c) Onderko EL, Silakov A, Yosca TH and Green MT. *Nat. Chem.* 2017; **9**: 623–628; (d) T. Komatsu, N. Ohmichi, A. P. Zunszain, S. Curry and E. Tsuchida, *J. Am. Chem. Soc.*, 2004, **126**, 14304-14305; (e) K. Watanabe, N. Ishikawa and T. Komatsu, *Chem. Asian J.*, 2012, **7**, 2534–2537; (f) J. Sun, M. M. Fitzgerald, D. B. Goodin and T. M. Loehr, *J. Am. Chem. Soc.*, 1997, **119**, 2064–2065; (g) S. Adachi, S. Nagano, K. Ishimori, Y. Watanabe, I. Morishima, T. Egawa, T. Kitagawa and R. Makino, *Biochemistry*, 1993, **32**, 241–252 (h) J. Du, M. Sono and J. H. Dawson, *Coord. Chem. Rev.*, 2011, **255**, 700–716.
6. J. Jeoung, D. A. Pippig, B. M. Martins, N. Wagener and H. Dobbek, *J. Mol. Biol.,* 2007, **368**, 1122–1131.
7. S. V. Evans and G. D. Brayer, *J. Mol. Biol.*, 1990, **213**, 885–897.
8. T. Komatsu, N. Ohmichi, A. Nakagawa, P. A. Zunszain, S. Curry and E. Tsuchida, *J. Am. Chem. Soc.*, 2005, **127**, 15933–15942.
9. K. S. Reddy, T. Yonetan, A. Tsuneshige, B. Chance, B. Kushkuley, S. S. Stavrov and J. M. Vanderkooi, *Biochemistry,*1996, **35**, 5562–5570.
10. T. Matsui, S. Ozaki, E. Liong, G. N. Phillips Jr. and Y. Watanabe, *J. Biol. Chem.*, 1999, **274**, 2838–2844.

Conclusions

The author demonstrated the modification of hexameric tyrosine-coordinated heme protein (HTHP) since it has a relatively small, rigid, highly thermal stability and ring-shaped hexameric structure with tyrosine-coordinated heme molecules. Each heme molecule is fixed in the heme-binding site of each subunit with same orientation and shortest distance between the heme iron centers in HTHP is 1.8 nm. Inspired by a sophisticated array of chlorophyll photosensitizers in the light harvesting system of purple bacteria, the protein matrix of HTHP was utilized for the scaffold to assemble the photosensitizers. In addition, the tyrosine coordination was converted to histidine coordination toward a new-type of hexameric hemoprotein with the different axial ligand of heme.

In chapter 1, the author investigated the construction and evaluation of an artificial light harvesting system with HTHP as a scaffold. The heme cofactor in HTHP was successfully replaced with porphyrinoid photosensitizers, Zn protoporphyrin IX (ZnPP) and Zn Chlorin e6 (ZnCe6). The obtained photosensitizer array was characterized by UV-vis and CD spectroscopy. The energy migration within these Zn-cofactor-substituted HTHPs was evaluated by titration measurement with a fluorescence quencher. The fluorescence quenching efficiencies of the assembled ZnPP and ZnCe6 molecules are 2.3 and 2.6 fold-higher than those of the partially photosensitizer-inserted proteins, respectively. In the present system, the orientations of assembled photosensitizers are fixed at the same situations and insertion of other porphyrinoid photosensitizer is applicable to be assembled within a HTHP scaffold. This model contributes to constructing the efficient artificial light harvesting system and photo-catalysts.

In chapter 2, the author prepared an array of multiple photosensitizers to HTHP scaffold. In this system, six ZnPP molecules were arrayed at the heme-binding sites of HTHP by supramolecular interaction and five fluorescein (Flu) molecules and one Texas Red (Tex) molecule as donor and acceptor photosensitizers, respectively, were covalently conjugated on the HTHP matrix. One advantage of this system is to allow the convenient attachment of two- or three-types of the different photosensitizers into the protein scaffold. In Flu- and Tex-attached HTHPs reconstituted with ZnPP, the energy transfer efficiencies from Flu to ZnPP and from ZnPP to Tex were determined to

be 64% and 35%, respectively. In the case of three photosensitizers assembled system, the evaluation of successive energy transfer from five Flu molecules to one Tex molecule via ZnPP indicates the collection of the photo-excited energy at the Tex molecule from Flu and ZnPP molecules. Thus, the HTHP-based artificial light harvesting system modified with multiple photosensitizers contributes to making a new strategy for generating a much effective artificial light harvesting system for collection of excited solar energy with a wide range of visible light at a reaction center.

In chapter 3, the modification of the proximal heme-ligand of HTHP was demonstrated to increase the peroxidase activity. Tyr45, a residue originally coordinating to the heme cofactor, and Arg25 locating in the distal site are substituted with Phe45 and His25, respectively, to produce a HTHP mutant, $HTHP^{R25H/Y45F}$. $HTHP^{R25H/Y45F}$ maintained its stable hexameric structure with the altered ligation of each of the heme cofactors. UV-vis spectra of $HTHP^{R25H/Y45F}$ clearly support the fact of the His-coordination to the heme cofactor. The H_2O_2-dependent peroxidase activities of $HTHP^{R25H/Y45F}$ were evaluated with the Michaelis–Menten analysis. The k_{cat} values, the catalytic rate constant, of $HTHP^{R25H/Y45F}$ for ABTS and guaiacol oxidations are 10- and 100-fold higher than those of wide type HTHP, respectively. In the sulfoxidation reaction of thioanisole via a two-electron oxidation step, the turnover number of $HTHP^{R25H/Y45F}$ is ca. 2-fold larger than that of wild type HTHP. These results indicate that the HTHP engineering focusing on the axial ligand exchange is a versatile tool for development of new biocatalysts.

Taken together, the author successfully demonstrates that HTHP is modified by two approaches to construct artificial light harvesting systems and enhance the peroxidase activity. Especially, HTHP is a promising template toward an artificial light harvesting system due to six closely adjacent heme-binding sites and rigid HTHP matrix. Furthermore, the author believes that these findings lead to the constructions of photocatalyst system driven by the sun light energy and elucidation of the mechanism of native enzyme.

List of Publications for This Thesis

1. Energy migration within hexameric hemoprotein reconstituted with Zn porphyrinoid molecules
   Koji Oohora, Tsuyoshi Mashima, Kei Ohkubo, Shunichi Fukuzumi and Takashi Hayashi
   Chemical Communications, 2015, **51**, 11138–11140.

2. Successive energy transfer within multiple photosensitizers assembled in a hexameric hemoprotein scaffold
   Tsuyoshi Mashima, Koji Oohora and Takashi Hayashi
   Physical Chemistry Chemical Physics, 2018, **20**, 3200–3209.

3. Substitution of an amino acid residue axially coordinating to the heme molecule in hexameric tyrosine-coordinated hemoprotein to enhance peroxidase activity
   Tsuyoshi Mashima, Koji Oohora and Takashi Hayashi
   Journal of Porphyrins and Phthalocyanines, 2017, **21**, 824–831.

Acknowledgements

The study presented in this thesis has been carried out at Department of Applied Chemistry, Graduate School of Engineering. Osaka University from April 2013 to March 2018. The author would like to express his best gratitude to Professor Takashi Hayashi for his continuous guidance, kind suggestion, constant discussions and warm encouragement throughout this research. The author would like to deeply thank Dr. Koji Oohora for his valuable suggestions and helpful discussions.

The author also acknowledges to Professor Hidehiro Sakurai and Professor Tsuyoshi Inoue for reviewing this thesis and valuable comments.

The author expresses his great gratitude to Professor Shunichi Fukuzumi (Ewha Womans Univ., Meijo Univ.) and Professor Kei Ohkubo (Osaka Univ.) for transient absorption measurements with fs pulse laser and helpful discussion.

The author would like to express his great gratitude to Dr. Akira Onoda for his helpful suggestions and constant discussions. Acknowledgement is also made to all members at Professor Takashi Hayashi's group for their encouragements and friendship in the laboratory.

The author would like to express his great gratitude to his family for their assistance.

Finally, The author is grateful for financial supports by Japan Society of the Promotion Science (JSPS).

Tsuyoshi Mashima

January 2018